Ph.D. thesis

ENVIRONMENT GEOCHEMICAL AND RADIOMETRIC STUDY OF BUILDING MATERIAL AND ATTIC DUST SAMPLES AFFECTED BY INDUSTRIAL ACTIVITY IN HUNGARY

submitted to the

Environmental Geology Ph.D. Program, Doctoral School of Environmental Sciences,

Eötvös Loránd University

Author:

Péter Völgyesi

Lithosphere Fluid Research Laboratory, Department of Petrology and Geochemistry,

Eötvös Loránd University

Supervisor:

Csaba Szabó, Ph.D.

Lithosphere Fluid Research Laboratory, Department of Petrology and Geochemistry,

Eötvös Loránd University

Head of the Doctorate School of Environmental Sciences: Imre Jánosi, Prof.

Head of the Environmental Geology Ph.D. Program: Csaba Szabó, Ph.D.

Budapest

2015

ACKNOWLEDGEMENTS

This work was financially supported by:

- *the Ph.D. fellowship of Hungary to Péter Völgyesi, 2010-2013;*
- *the Habilitas program of the Hungarian Development Bank Plc. (MFB zRt.) to Péter Völgyesi, 2009-2010 & 2010-2011;*
- *the DBU (Deutsche Bundesstiftung Umwelt) Scholarship at the Technische Universität Bergakademie Freiberg, 05.09.2013-28.02.2014.*

I am grateful to:

- *my supervisor Csaba Szabó (Eötvös University) for all the help and support he has given me since I joined his Laboratory on 19 July, 2008;*
- *my consultants: Győző Jordán (Szent István University) and Zoltán Kis (Centre for Energy Research) for their help, discussions, professionalism, and for providing the background information on the urban geochemical and gamma-spectrometric investigations; Jörg Matschullat (TU, Freiberg, Germany) for supervising me and my research for the duration of the DBU Scholarship in Freiberg;*
- *Imre Salma and Péter Zagyvai for their constructive comments in the prereview of the thesis;*
- *the following people for helping me in the analytical work: András Bartha (Szent István University, Hungary) in ICP-OES analysis, Ákos Horváth (Eötvös University), Ottó Csorba† (Eötvös University), Gyula Pávó (Eötvös University), János Somlai (University of Pannonia), Gábor Kocsy (Radosys Ltd. and OSSKI), Zsolt Bendő (Eötvös University) and László Szentmiklósi (Centre for Energy Research) in analyses relating to radiation measurements;*
- *former and present indoor members of the Lithosphere Fluid Research Lab (Eötvös University), especially to Dániel Breitner, Károly Hidas, Zoltán Konc, Márton Berta, Dóra Zacháry, Csilla Király, Beatrix Udvardi and Viktória Forray;*
- *Ábel Szabó for all technical assistances;*
- *Mária Szabó, Ádám Kiss, Gyula Záray, Tamás G. Weiszburg, Ildikó Mocsy and Zsuzsanna Angyal;*
- *the owners of all the houses from which we measured and sampled building material or attic dust samples, especially: Dezső Csóka, Lívia Kulcsár, Erzsébet Johannidesz, Oszkár Illési, Sándor Lévai, Antal Imréné and Klára Kovácsné;*
- *Angéla Baross-Szőnyi (LRG, ELTE) for her help, conversations and cakes;*
- *Andrea Förherczné, Henrik Kulla and Éva Bíró for helping in administration issues;*
- *Hédi, Zsuzsi and Kata for having been a doctorate student with you;*
- *Paul Thatcher and Gábor Fehérvári for the English review;*
- *Éva Kovács-Széles and my colleagues at the Centre for Energy Research for their patience;*
- *István Gábor Hatvani for all things in the last 10 years;*
- *my Friends, especially for all the Fridays gone because of 'lads'-Thursdays'.*
- *my Family, Apa, Gabiéni, Ildi, Kacsa, Gabsiék for being always beside me, tolerant and supporting me with their love.*

Dedicated to the memory of my mother dr. Edit Dömöcsök

Table of contents

List of figures:

List of tables:

List of appendices:

1. General introduction and objectives

As the majority of mankind lives in urban areas (Lyons and Harmon, 2012), these regions, mainly cities and their related industries, have a huge impact on the natural environment. For instance, they change the character of the landscape and soil, produce by-products and greenhouse gases, cause atmospheric pollution, and modify the (bio)geochemical cycle of the elements (Lyons and Harmon, 2012). The scientific field dealing with the analysis of the urban environment, is called 'urban geochemistry'. Although the excessive release of toxic and potentially toxic elements into the urban environment was first recognized in the 1950s, the term of urban (environmental) geochemistry was first used by Thornton in 1991 (Thornton, 1991). According to the definition of Siegel (2002), 'Urban environmental geochemistry can be defined as a field of scientific study that uses the chemistry of the solid earth, its aqueous and gaseous components, and life forms to examine the physical, chemical, and biological conditions of an urbanized environment.' Early studies assessed only Pb-contamination; however, due to the growing need to understand the processes operating in urban environments, and thanks to the development of analytical techniques, other potentially toxic elements (e.g. Cd, Cu, Ni, Zn) began to be studied simultaneously. Nowadays it is possible to analyze almost the whole periodic table in urban environments using water, sediment, soil, air, dust, etc. samples.

In Hungary the operation of coal mines and later on coal-fired power stations provided the opportunity for other industries using coal as either combustion material or the electrical power generated, to locate in the vicinity and begin production (e.g. the aluminium industry, steel works, glassworks, smelters, etc.; Gajzágó, 1962; Kozma, 1996). The post-war Hungarian centrally directed economy led to heavy industry producing large amounts of waste and emitting pollutants into the atmosphere in serious amounts, directly resulting in severe pollution. Many industrial sites in Hungary (e.g. Ajka, Dunaújváros, Komló, Ózd, Miskolc, Salgótarján, see Figure 1), which are currently closed-down or have technologically changed, were in operation all over the country. Our urban geochemical knowledge of these industrial sites in Hungary right up to the present day remains very scant. The amount and location of waste dumps in the country can indeed serve as a documentary indicator of these industrial activities. Nowadays, around five to six thousand mining objects (waste dumps) exist in Hungary, of which only 20% are already naturally or artificially recultivated. The amount of material in these waste dumps is estimated at around 835 Mt (Gáspár, 2005).

Many settlements were built and developed together with the growing local industry; hence, in several cases, the industrial site is effectively identical with the built-up area, directly affecting the living environment of the community. A typical example is Ajka, where, for instance, sites of the aluminium industry, coal mining, a coal-fired power plant, the glass industry, and waste dumps are found within the city limits (Gajzágó, 1962; Kozma, 1996; Figure 1).

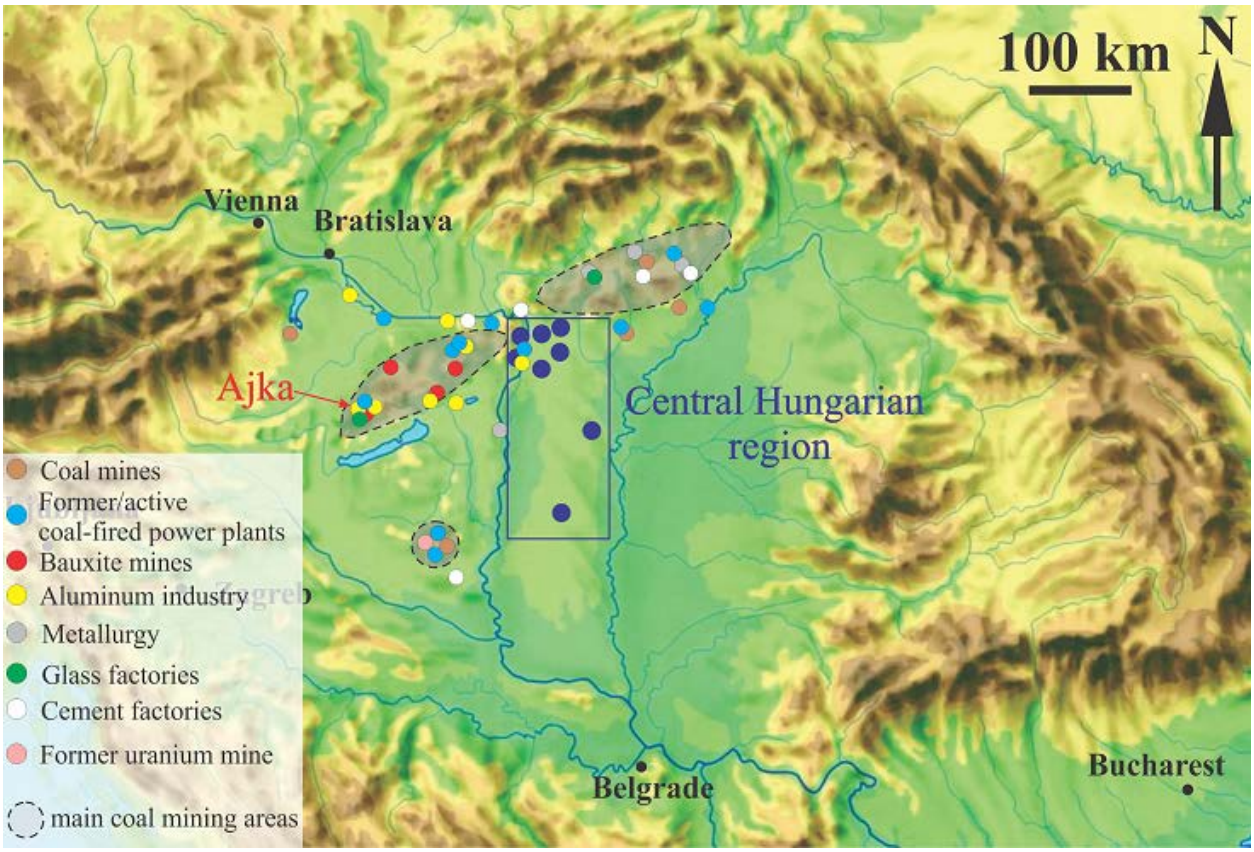

Figure 1. Main industrial sites in Hungary. Former (closed, converted to gas or biomass) and active coal-fired power plants, bauxite mining and the aluminium industry, metallurgy (including the steel industry) and the cement industry are marked with different colored symbols. The main coal mining areas are indicated with light grayshading. Building material (Central Hungarian region and Ajka) and attic dust sampling locations (Ajka) are also marked.

The emitted and deposited particles and the by-products of industrial production processes can cause environmental and health problems due to the mobilization of the toxic elements, for instance, as attached to dust particles or diluted in groundwater (Lyons and Harmon, 2012), and due to the usage of these by-products as construction or building materials (Kovler et al., 2002; Somlai et al., 2006).

The by-products of industrial activities (e.g. coal slag and fly ash, originating from coal-fired power plants) were often used in construction technologies as building materials on their own or as additives to building materials (Bijen, 1996; Quispe et al., 2012; Siddique, 2010). In Hungary,

from a radiological point of view, one of the most important issues is the utilization of the different types of coal slags and fly ashes because they can contain relatively high levels of naturally occurring radionuclides, which increase the indoor radiation exposure of residents (Somlai et al., 2006; Szabó et al., 2013; Völgyesi et al., 2014a). Internal exposure arises due to the inhalation of radon (^{222}Rn) and thoron (^{220}Rn) progenies, which are exhaled from the building materials as one of the main sources of radon, and accumulate in indoor air (e.g. Abo-Elmagd et al., 2010; Szabó et al., 2013). Indoor external exposure arises due to gamma radiation, mainly from the decay (or decay products) of three radionuclides: ^{226}Ra[1], ^{232}Th[2] and ^{40}K. These radionuclides are used in many qualification indices of building materials and soils in order to compare different samples and to determine the potential effect of these materials on human health (e.g. Beretka and Mathew, 1985; EC, 1999; Hamilton, 1971; Szabó et al., 2013). Therefore, the precise quantification of these radionuclides is necessary. A widely used method in the determination of the activity concentration of these nuclides is the gamma-ray spectrometry. Gamma-ray spectrometry is a non-destructive method which has been used for decades in the field of environmental studies, nuclear technology, food qualification, activation analysis, archaeology, nuclear physics, etc. (e.g. Bódizs, 2006; Gilmore, 2008). The gamma-ray spectrometric investigation was divided into two parts: as a first step the qualification of several Hungarian building materials was performed. The second part of this research was the development of an appropriate measuring system with which the accurate determination of ^{226}Ra can be proven.

Building materials from different areas within the central region of Hungary and Ajka (Figure 1) were studied. The measurements, including in situ and laboratory tests, were carried out basically due to requests of the inhabitants. As part of the laboratory work, activity concentrations of ^{226}Ra, ^{232}Th, and ^{40}K in building materials were measured at the Department of Atomic Physics of Eötvös University, Budapest. The goal of this research was to qualify the materials with international qualification indices and to compare the results to reference data and those of similar studies. Where the materials were used in bulk, the absorbed dose rate and annual effective dose estimations were also performed.

[1] In the ^{238}U decay chain, the segment starting from radium (^{226}Ra) is radiologically the most important, therefore, reference indices are often made to radium instead of uranium.
[2] ^{232}Th has very weak gamma lines, hence, it is often determined by measuring its decay products (e.g. ^{228}Ac).

In the gamma-ray spectrometric analysis of environmental samples (e.g. rock, soil and building material) the abundance of uranium isotopes is might be presumed to be the natural values (i.e. 0.72% for ^{235}U and 99.27% for ^{238}U). Moreover, the presence of secular equilibrium in the ^{238}U decay chain is often only assumed, without verification, which can result in several errors in the activity concentration calculations of the radionuclides. The different geochemical behaviors of the radionuclides (Huy and Luyen, 2004; Papp et al., 1997), the escape of the gaseous element radon (Rn) within the decay chains (Benke and Kearfott, 2000; Manolopoulou et al., 2003), and anthropogenic processes (e.g. burning process in the furnaces of coal-fired power plants, Papastefanou, 2010; Somlai et al., 1997) can all influence the existence of secular equilibrium. In the course of our measurements at the Eötvös University (Department of Atomic Physics), we observed these problems, and therefore aimed to develop a measuring system suitable for accurate radium determination. Coal slag represents a particularly significant group of the environmentally hazardous materials as also seemingly a suitable sample medium for study using gamma-ray spectrometry (Völgyesi et al., 2014a). Therefore, my main aim was to develop a measurement system where the use of the peak with the energy of 186 keV for ^{226}Ra determination can be assessed, and the uranium isotopic ratio and secular equilibrium between ^{226}Ra and ^{238}U can be studied. In order to achieve this, a low background chamber, a radon-tight sample holder and absolute full energy peak efficiency calculation in close, extended sample-detector geometry were needed. The necessary experiments and analyses were carried out in collaboration with the Nuclear Analytical and Radiography Laboratory of Centre for Energy Research, Hungarian Academy of Sciences.

Solid pollutants (e.g. fly ash from power plants and different types of dust particles) transported by wind could enter houses and contaminate the whole living area (Davis and Gulson, 2005). This pathway is one of the most prevalent routes for toxic element mobilization around industrial areas. The relevance of such airborne pollution has long been recognized, and has recently received renewed attention (Duong and Lee, 2009; Sammut et al., 2010; Wong et al., 2006).

The city of Ajka, a presumably contaminated settlement in the western part of Hungary (Figure 1), is an important industrial location, therefore it was chosen for a detailed urban geochemical study. Industrial activity in Ajka started in the late 19th century. The dam of the Ajka red mud tailings pond broke in 04 October 2010, causing catastrophic contamination in the region,

which even reached the level of international significance (e.g. Gelencsér et al., 2011). Based on the assumption that undisturbed dust, accumulating in old houses, contains ambient anthropogenic airborne contaminants, this part of the research estimates the long-term contamination load, and establishes the spatial airborne pollutant distribution using attic dust samples. Emphasis is placed on potentially toxic elements (As, Cd, Cu, Hg, Ni, Pb and Zn) as specified in the ATSDR Substance Priority List (ATSDR, 2011). This study aims to determine the geochemical behavior of these elements in the multi-source industrial area using chemical and statistical analysis. Beside the comparison of attic dust samples with a soil study and other urban geochemical studies, an estimate of metal sorption on Fe-oxy-hydroxide phases was also performed, with a subsequent correlation analysis.

As a summary, my Ph.D. research aimed to investigate if industrial activities in the past still influence our indoor environment and to emphasize the relevance of urban geochemical studies in Hungary.

2. Origin of natural radiation and its connection to building materials

2.1. Main sources of ionizing radiation

Exposure of the population to radioactivity can arise from both natural and artificial sources (Figure 2). As a global average, only ~0.6 mSv (range 0–20 mSv) of the annual effective dose of the populations' radiation exposure originates from man-made sources in developing and developed countries (Figure 2). Of these values, ~98% may be assigned to radiotherapy and medical diagnostics, with the remaining ~2% arriving from atmospheric nuclear weapons tests, nuclear accidents and nuclear energy production. It should be noted that the amount of the effective dose due to artificial sources is highly dependent on the level of the health care system in a given country (Fehér and Deme, 2010; Figure 2).

The greater proportion of the exposure originates from natural sources, e.g. high-energy cosmic rays, cosmic radiation induced radionuclides, known as cosmogenic isotopes, and radioactive nuclides deriving from the Earth's crust (terrestrial radionuclides). However, the radiation exposure can vary over a wide range (1–10 mSv y^{-1}; Figure 2); its worldwide average value from natural sources is 2.4 mSv y^{-1} (UNSCEAR, 2000; Figure 2). The various sources are represented in the following proportions: 0.39 mSv y^{-1} from cosmic radiation, including cosmogenic isotopes, 0.48 mSv y^{-1} from external terrestrial radionuclides, 1.26 mSv y^{-1} from the inhalation of terrestrial radionuclides, and 0.29 mSv y^{-1} from the ingestion of terrestrial radionuclides (Fehér & Deme, 2010; Figure 2). The effective dose from terrestrial radionuclides is highly dependent on the local geological background and the building materials used in the indoor environment (UNSCEAR, 2000). Cosmic radiation contributes only to external radiation due to its scattered secondary cosmic radiation, whereas cosmogenic isotopes and terrestrial radionuclides can cause both external and internal exposure to humans via alpha, beta and gamma radiation (UNSCEAR, 2000). The most widespread radionuclides in the environment are the nuclides of the uranium and thorium decay series, and ^{40}K. As the half-lives of ^{40}K, ^{238}U and ^{232}Th are comparable to the Earth's age, they, and their decay products, exist in every environmental medium.

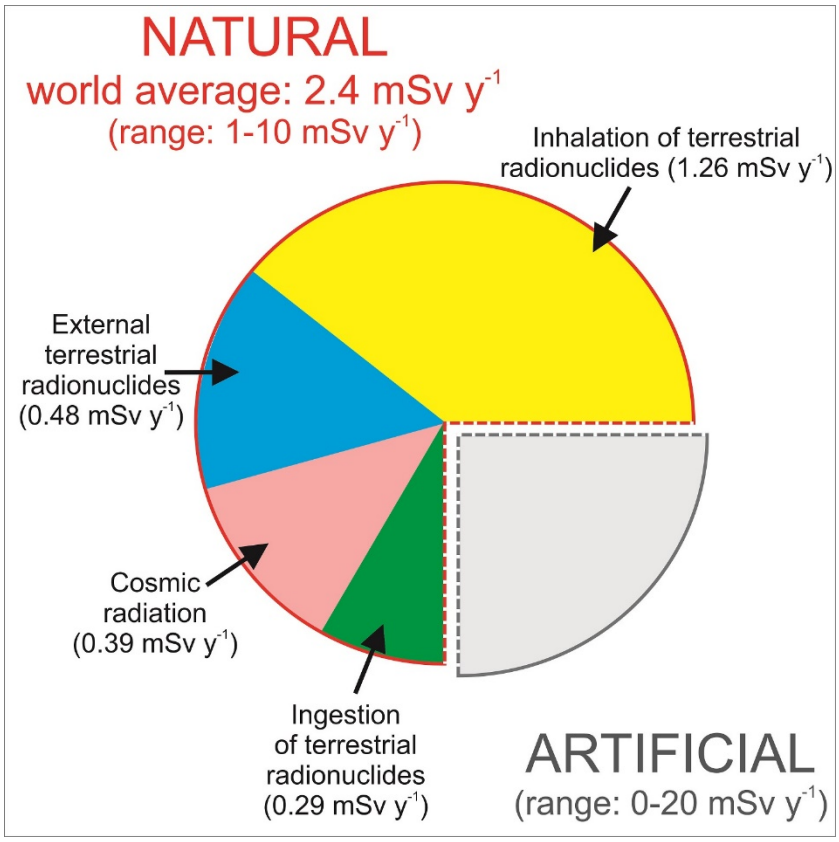

Figure 2. Exposure of the population to radioactivity from natural and artificial sources (Fehér and Deme, 2010).

2.2. Main properties of terrestrial radionuclides present in building materials

Based on the fact that, among other terrestrial radionuclides, ^{238}U, ^{226}Ra, ^{232}Th and ^{40}K contribute the most significant portion to the average annual effective dose received by humans, the separate introduction of these radionuclides is necessary. Their main properties are summarized in Tables 1–4.

Table 1. Main properties of uranium. Most of the data were summarized based on the database published by Salminen et al. (2005) and references therein.

Element	**U (uranium)**
Atomic number	92
Main oxidation states	+2, +3, +4, +5, +6
Main isotopes	^{238}U, ^{235}U
Geochemical property	lithophile
Main minerals	uraninite (UO_2), coffinite ($USiO_4$), brannerite ($(U,Ca,Ce)(Ti,Fe)_2O_6$) and carnotite ($K_2(UO_2)_2(VO_4)_2\,3H_2O$)
Median upper continental crust (mgkg^{-1})	2.7
Median topsoil (mg kg $^{-1}$)	2.0
Chemistry Uranium has three naturally occurring isotopes, the most abundant being ^{238}U (natural abundance: 99.27%), the next ^{235}U (0.72%), and the least frequent ^{234}U (0.001%). This latter is a decay product in the ^{238}U decay series with a half-life of approximately 10^5 years. Uranium-238 and ^{235}U have their own decay series, and their half-lives are comparable with the age of the Earth, 4.46×10^9 years and 7.03×10^8 years, respectively (Figure 3). The mobility of U in soil is governed by the formation of the hydrated cation UO_2^{2+}, which is responsible for its solubility over a wide range of soil pH. In aqueous systems, uranium is generally more soluble in oxidized, alkaline and carbonate-rich water than under acidic, reduced conditions (Salminen et al., 2005). Uranium is readily soluble in the strongly acid, oxidized water associated often with mine drainage. Under such conditions, the main species in solution is the uranyl cation UO_2^{2+}. Under reducing conditions, the insoluble U^{4+} oxide UO_2 and mixed oxides, such as U_3O_8 are formed. Dissolved uranium tends to form strong associations with organic matter such as humic and fulvic acids, iron oxides and with dissolved phosphates (Salminen et al., 2005). Where dissolved silica is present, U may precipitate as coffinite (Coles et al., 1978; Karangelos et al., 2004).	
Anthropogenic sources	Mining and milling, nuclear effluents, phosphate fertilizers and coal combustion.
Health	Uranium is a non-essential element. It is chemotoxic, radiotoxic and a carcinogen. Long-term exposure to uranium radionuclides can result in medical conditions such as kidney disease and the development of cancer (Salminen et al., 2005).
Notes	Due to the reductive conditions, uranium can be trapped in coal forming geological environments, resulting in a high radionuclide concentration for coals.

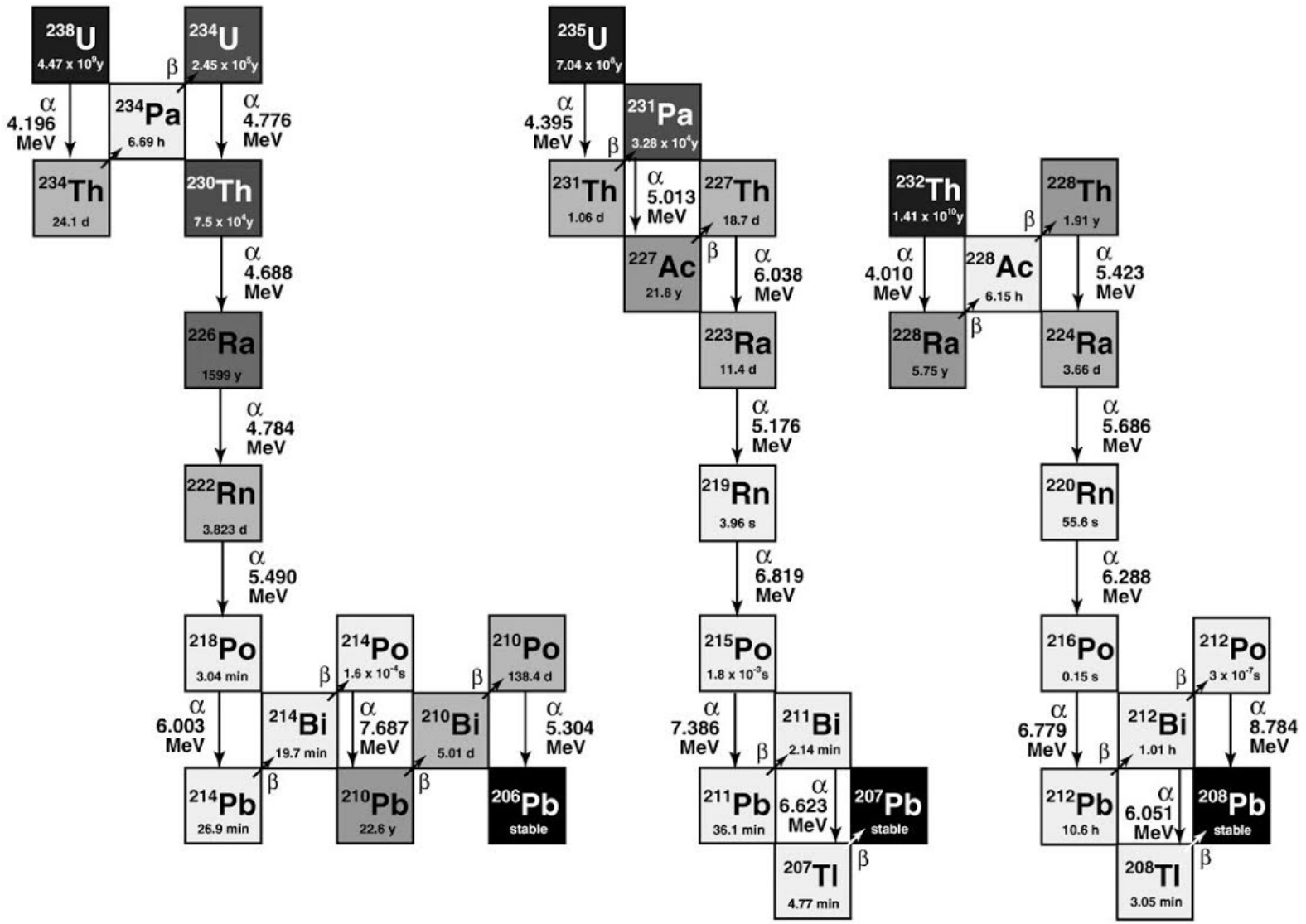

Figure 3. Natural decay series of ^{238}U, ^{235}U and ^{232}Th showing the half-lives (given exact number and tone), the decay type and energy of each isotope (Link 1).

Table 2. Main properties of thorium. Most of the data were summarized based on the database published by Salminen et al. (2005) and references therein.

Element	**Th (thorium)**
Atomic number	90
Main oxidation state	+4
Main isotope	^{232}Th
Geochemical property	lithophile
Main minerals	monazite ((Ce,La,Nd,Th)(PO_4,SiO_4)), thorite ($ThSiO_4$), thorianite (ThO_2)
Median upper continental crust (mg kg $^{-1}$)	10. 5
Median topsoil cc.(mg kg $^{-1}$)	7.24
Chemistry Thorium has low mobility under all environmental conditions, mainly due to the high stability of the insoluble oxide ThO_2 and the strongly resistant nature of its carrier minerals such as monazite and zircon. The mobility of Th in soil, like that of U, is governed by the formation of the hydrated cation Th^{4+}, which is responsible for its solubility over a large scale of soil pH. Organic acids increase the solubility of Th in soil, but its mobility may be limited due to the formation of slightly soluble precipitates (e.g. phosphates, oxides) and by adsorption on clay minerals and organic matter. Unlike uranium, thorium cannot be oxidized to a stable cation equivalent to the highly mobile uranyl ion UO_2^{2+}. The soluble species $Th(SO_4)^{2+}$ may form below pH 3, and under oxidizing conditions, like acid mine water. Any Th released into solution will be rapidly sorbed by clay minerals and hydrolyzed to the hydrous oxide $Th(OH)_4$, which will be intimately associated with the clay-mineral fraction, unless it can be mobilized by other inorganic or organic ligands.	
Anthropogenic sources	Fertilizers, uranium mining and processing, and coal combustion.
Health	Thorium has no known biological function. It is chemotoxic, radiotoxic and a carcinogen. In the environment, Th behaves similarly to the rare earth elements (REE), especially Ce, substituting Ca in bones and teeth. Long-term exposure to thorium increases the chances of developing lung diseases and lung, pancreas and bone cancer.
Notes	As in case of the uranium, thorium has also a radon decay product, called thoron (^{220}Rn, Figure 3). Indoor thoron can be an important source of exposure only under some rare conditions, where the building materials contain high concentrations of thorium (EC, 1999; Szabó et al., 2014).

Table 3. Main properties of ^{40}K. Most of the data were summarized based on the database published by Salminen et al. (2005) and references therein.

Radionuclide	**^{40}K (potassium-40)**
Atomic number	19
Main oxidation state	+1
Geochemical property	lithophile and biophile
Main minerals	clay minerals, micas and K-feldspar
Abundance	Potassium is the eighth most abundant element in the Earth's crust with a concentration of ~ 2%. Potassium-40 isotopic abundance among all potassium isotopes is 0.0117%.
Average activity concentration in soil	The activity concentration of ^{40}K in soil is an order of magnitude higher than that of ^{238}U or ^{232}Th. Its average activity concentration in Hungarian soils is 370 Bq kg^{-1}, its world average 420 Bq kg^{-1} (Fehér & Deme, 2010; UNSCEAR, 2000).
Chemistry	K^+ is very soluble and its mobility depends on the incorporation to clay minerals' lattices due to its large size, its absorption capacity is much higher than that of Na^+, and because K is an important element in biosphere it is readily taken up by plants. Potassium-40 is a widespread terrestrial radionuclide with a half-life of 1.28×10^9 years.
Anthropogenic sources	Fertilizers
Health	While stable potassium is an essential element, ^{40}K substitutes potassium which means it is present in all living organs which metabolize K.
Notes	In soils, the K^+ ions are fixed in 2:1 type clay mineral interlayers such as in the illite group (Szabó, 2014). Potassium-40 is present in living organisms due to substitution of stable potassium. It decays via β-radiation to ^{40}Ca (89%) or with electron capture to ^{40}Ar (11%). The decay to ^{40}Ar is always followed by a measurable gamma ray at 1460.8 keV.

Table 4. Main properties of ^{226}Ra. Most of the data were summarized based on the database published by Salminen et al. (2005) and references therein.

Radionuclide	**^{226}Ra (radium)**
Atomic number	88
Main oxidation state	+2
Geochemical property	lithophile
Main minerals	radiobarite ((BaRa) SO_4), uranium and thorium minerals: e.g. monazite ((Ce,La,Nd,Th)(PO_4,SiO_4)), thorite ($ThSiO_4$), thorianite (ThO_2), brannerite ((U,Ca,Ce)(Ti,Fe)$_2O_6$) and carnotite ($K_2(UO_2)_2(VO_4)_2$ $3H_2O$)
Average activity concentration in soil	The average ^{226}Ra content of soils in Hungary and the world are 33 Bq kg^{-1} and 32 Bq kg^{-1}, respectively.
Chemistry Radium is ubiquitous in all environmental compartments and the decay segment beginning with ^{226}Ra is radiologically the most important. Uranium and thorium's geochemistry highly determines the mineral occurrence of radium. It exists as Ra^{2+} in the environment and forms strong complexes in natural waters, and can be present in $RaSO_4$ at a pH of between 2 and 12, and in $RaCO_3$ at about pH 12 and above (Takeno, 2005).	
Anthropogenic sources	Fertilizers, uranium mining and processing, and coal combustion.
Health	Its health effects are high radiotoxicity due to absorption into bone structure (Mauring and Gäfvert, 2013).
Notes	Ra-226 has a half-life of 1601 years, and it decays to ^{222}Rn via the emission of an α particle. It also has a gamma line at 186.2 keV. However, on account of this line, ^{235}U needs to be taken into consideration as an interfering isotope for precise determination.

Additionally, a discussion of the characteristics of radon (Rn) is indispensable to an understanding of the processes for measuring radium and secular equilibrium in the ^{238}U decay chain. Radon is a naturally occurring radioactive element responsible for more than 50% of the population's annual effective dose (Figures 2 and 3). It has three isotopes, which can be found in all radioactive decay chains (Figure 3): (i) ^{220}Rn, known as thoron, which occurs in the ^{232}Th decay chain, (ii) ^{219}Rn (actinon), a decay product of ^{235}U, and (iii) the most abundant, ^{222}Rn (radon), a progeny of ^{238}U. Radon is a noble gas, and it is the decay product of Ra, which is present in all environmental media. Following the decay of radium, when an α particle is emitted, radon recoils in the opposite direction (Appendix 1). In soil, rock and building material radon can recoil into the pore volume, into another particle, or remain in the same grain (Tanner, 1980). When radon enters the pore volume via recoil or via diffusion, this process is called emanation. The process, when the emanated radon reaches the free air above its media through diffusion is called exhalation. The recoil length of radon is typically 30-50 nm in solid materials, 95 nm in water and 64000 nm in air (Porstendörfer, 1994; Tanner 1964 and 1980). Radon decays with α-decay to polonium, and its further progenies are bismuth, thallium and lead (Figure 3). These isotopes emit α particles, β particles and easily-measurable gamma radiation (Figure 3). The main parameters affecting radon migration in environmental media are the radium activity concentration, the emanation factor, porosity, permeability, moisture content and grain-size distribution. Emanation is usually expressed as the activity of radon isotopes leaving a unit mass (Bq kg^{-1} s^{-1}), or a unit volume (Bq m^{-3} s^{-1}) of the sample solid material in a unit time. It should be noted that radon causes many challenges for the determination of radon decay products in a sample holder by gamma-ray spectrometry because radon can escape from the sample holder, which distorts the presence of secular equilibrium of the decay chain (Figure 3; Manolopoulou et al., 2003).

2.3. Dose and health effects

Ionizing radiation can cause direct and indirect damage to biological systems. Direct damage means that the molecule exposed to radiation is harmed. Direct damage in a living cell could mean the damage of the DNA molecule and the different membrane structures. Indirect damage might occur is consequence of formation of reactive free radicals in water due to radiolysis. These radicals can transport the absorbed energy of radiation far from the place of origin. The resulting cell damage can lead to metabolism perturbations, in serious cases to chromosome aberrations and cellular proliferation (James, 1988; Jostes, 1996; Szerbin, 1994).

The biological reactions and effects in a living organism stand in close connection to the energy (namely the dose) absorbed by the cells and tissues. Radioactive dose has two types of effects on living organisms, deterministic and stochastic effects. The deterministic effect has a threshold value above which the severity of the effect caused by radiation is proportional to the dose. In case of stochastic effects, there is no threshold level for the effect, but its probability is proportional to the dose. Dose definitions can be found in Köteles (1994). In case of low doses (<10–100 mSv effective dose) the effect can only be studied by statistical methods (ICRP, 1987; Köteles, 1994; Szerbin, 1994). However, so far the relationship between these low doses and the probability of any adverse consequences on health is not well known. Many different models exist among which the LNT (linear non-threshold) model is the generally accepted (ICRP 1990, 2005, 2007, 2008) in radiation protection systems.

Estimating the radioactive exposure of human populations is an important part of any research dealing with the potential hazards of radioactivity. In indoor environments both external and internal radiation sources occur. As people spend most of their time (~80%) indoors, the study of indoor exposure takes on an even greater importance. The average indoor-to-outdoor ratio is 1.4 (UNSCEAR, 2000), meaning that the effective dose received indoors from terrestrial radiation is 40% higher than in outdoor circumstances. In order to decrease the population's indoor radioactive exposure, the maximum permissible radioactive isotope concentration of building materials is regulated in many countries by international hazard indices.

2.4. Overview of the coal combustion by-products in Hungarian building materials

There are many areas in the world where building materials with high radioisotope content were used, mainly owing to the addition of anthropogenic materials (Karangelos et al., 2004). The most commonly used materials are phosphogypsum, coal slag, fly ash and blast furnace slag (EC, 1999; Hull and Burnett, 1996; Jobbágy, 2007; Nuccetelli et al., 2015; Olszewski et al., 2015; Somlai et al., 1997). The radioactivity of these materials always depends on the geochemical and geological circumstances and the industrial procedure undergone.

Coal slag and fly ash are used widely in many countries as building materials or additives to building materials (e.g. Beretka and Mathew, 1985; Karangelos et al., 2004; Kovler et al., 2002; Kumar et al., 1999; Somlai et al., 2006). Their usage was introduced mainly after World War II in international construction technologies (e.g. Bijen, 1996; Quispe et al., 2012; Siddique, 2010).

In Hungary, the activity concentration of ^{238}U (and consequently the radium ^{226}Ra) in coal is highly variable, exceeding up to ten or twenty times the world average value (Bódizs et al., 1993). Particularly the coal beds in the Transdanubian Central Range contain high amounts of isotopes from the ^{238}U decay series (Somlai et al., 2006). A statutory act put in place in 1960 by the Ministry of Construction of Hungary banned the use of coal slag containing high level of radium as building materials in the Transdanubian Central Range (Németh et al., 2000; Somlai, et al., 1996; Figure 1). Even so, different types of coal slags have not ceased to be utilized as building materials on private and at public construction sites. Coal slag was particularly used as insulation material or to fill up the space above or between beams, but it was also used in building material blocks all over the country. The other application of these slags is the usage as ground leveling material outdoors, e.g. in wet places with higher groundwater level, sports grounds and courts, and parks (Dezső et al., 1997; Somlai et al., 1998; Zacháry et al., submitted). As the transportation routes of raw materials are unknown in the country, materials with elevated radionuclide concentrations can be present in areas where normally the average radionuclide concentration is equal to the background values.

2.5. Background information on the relevance of the methodology improvement

2.5.1. Secular equilibrium in the radioactive decay chain and its relevance

The verification of the existence of radioactive equilibrium represents a gigantic challenge in the exact determination of radionuclides in the uranium decay chain, particularly for the determination and the comparison of uranium, radium and radon daughters using gamma-ray spectrometry. In a non-disturbed decay chain, where the half-life of a parent nuclide is much longer than that of its decay products (T1>>T2, Figure 4), after a given period the secular equilibrium is established. The period is normally more than five times the half-life of the decay products, when the activity of the daughter elements is identical to the activity of parent nuclide with more than 3% accuracy. Natural and artificial processes can influence the existence of secular equilibrium (see Chapter 1). Most surface and near-surface geological environments are subject to the mobility of nuclides due to either physical or chemical processes (Rosholt, 1957). As an example, a slightly modified equilibrium can exist between ^{226}Ra and ^{238}U because separation may occur between its parent ^{230}Th and ^{234}U and because ^{226}Ra has greater mobility in the environment

(UNSCEAR, 2000, Table 4). In some cases radionuclides in coal used as combustion material are already in slight disequilibrium, which will be further altered following the burning process in a power-plant. Therefore, coal combustion by-products form a special group for secular equilibrium studies by gamma-ray spectrometry. For these studies, further criteria (e.g. uranium isotopic ratio, radon leakage) should be analyzed before the proper results are presented.

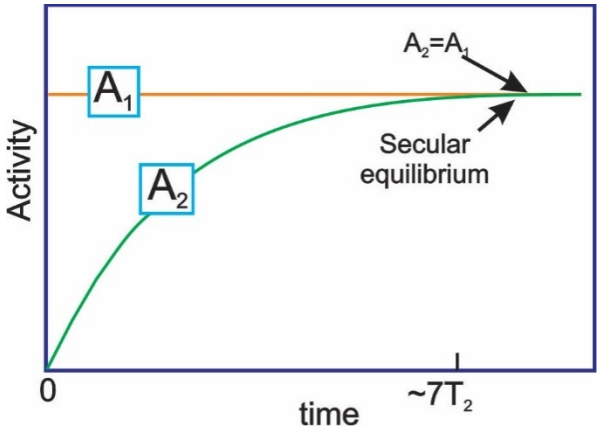

Figure 4. Demonstration of secular equilibrium between two isotopes, where A_1 is the activity of the parent nuclide, and A_2 is the activity of the short-lived daughter nuclide. $\sim 7T_2$ represents the time (7-times the half-life of the daughter nuclide) which needs to pass to reach secular equilibrium (Redrawn from: Link 2; Link 3).

2.5.2. A suitable measuring system

To be able to measure low activity environmental samples, the use of a low-background chamber is required. The development and testing of a radon-leakage-free sample container is also necessary. Moreover, the so-called efficiency transfer method for extended samples in close-in geometry should be applied for the results obtained from the measuring system.

In the literature, there are many papers dealing with radon leakage. Some of them resort to the use of sealed metal vessels (Papp et al., 1997) and the vacuum-close method (Mauring and Gäfvert, 2013), whereas others propose the use of a mixture of the sample and charcoal (Manolopoulou et al., 2003). Since the uncertainty of these measurements is usually accepted at the level of a few percent, a simpler, more easily useable and re-sealable HDPE[3] container was considered as sufficient. The literature data for the permeability of radon gas through a polyethylene layer (Arafa, 2002; Ashry et al., 2011) and the workability of the material made it a good candidate for usage.

[3]High-density polyethylene

In direct gamma-ray spectrometry, there are basically two ways to measure the activity concentration of nuclides in the sample, the relative and absolute methods. The basic principle of the relative method is the comparison of counting rates measured for a given spectrum peak of the unknown sample to that of a reference sample with known activity concentration. The method works well if both samples contain the same radionuclides, and their matrices are the same, or at least, quite similar, so that the self-attenuation effects would not change the measured intensities to differing degrees. In this way, one can avoid the laborious determination of the valid absolute full-energy peak (FEP) efficiency, which is needed for the absolute measurements. In our case, as we wanted to measure the radioactivity of building materials, it soon turned out that the absolute method has to be applied. The reason for this was that certified soil samples spiked with the nuclides of interest were not available and the densities of the unknown building material samples were different, therefore the application of the relative method described above was not feasible.

Preliminary measurements showed that the radioactivity level of the samples was rather low and, therefore, a close sample-detector geometry was advantageous in maximizing the counting rates. The absolute FEP efficiency values had to be determined at various energies for extended sources in close sample-detector geometry. A possible technique for this is the use of a method called efficiency transfer (Moens et al., 1981; Moens et al., 1982).

2.5.3. The accurate determination of ^{226}Ra and validation of the 186 keV peak

Because ^{226}Ra is one of the most prominent isotopes in the ^{238}U decay chain, and the value of its activity concentration is used by many international qualification indices (e.g. Ra_{eq}, I, H_{ex} [4]; EC, 1999), its fast, easy and precise gamma-ray spectrometric determination is indispensable. There are two different methods used to determine the ^{226}Ra content of a sample measured by gamma-ray spectrometry. One is an indirect method involving measuring the gamma-lines of the radon daughters ^{214}Pb and ^{214}Bi following a waiting period (>19 days, i.e. five times the half-life of radon) in a sample holder (Jia and Jia, 2012). It is important to use radon-tight sample holders and assume that the isotope to be measured is homogeneously distributed (Manolopoulou et al., 2003; Mauring and Gäfvert, 2013). This is a widely used technique to determine the ^{226}Ra content of a sample (e.g. Daza et al., 2001; De Corte et al., 2005; Huy and Luyen, 2004; Manolopoulou et al., 2003), but it requires complicated sample preparation. The other method is the direct use of

[4]Radium equivalent index, Activity concentration index, External hazard index

the186.2 keV line of ^{226}Ra (e.g. Johnston and Martin, 1997; Köhler et al., 2000). This can be applied without any pre-treatment of the sample, and there is no need for the tight sealing of the sample container. However, as mentioned above, there is a problem with using the intensity of the 186 keV peak since there is significant interference from an unresolved 185.7 keV gamma ray following the α decay of ^{235}U. To be able to take into consideration the non-negligible interfering effect of ^{235}U at this energy, the method requires:

(i) knowledge of the activity ratio (or equivalently the isotopic abundance ratio) between the uranium isotopes (^{235}U and ^{238}U) and
(ii) proof of the ^{238}U–^{226}Ra secular equilibrium.

The ^{238}U activity concentration can be measured directly with gamma-ray spectrometry on the 1001.2 keV line from its daughter nuclide ^{234m}Pa. Although this line has a weak intensity, it can be successfully used when a sophisticated measurement with very low background (Kis et al., 2013), relatively high uranium content (>100 Bq kg^{-1}, Papachristodoulou et al., 2003) and long acquisition time (measured in days) of the spectrum is used. Comparing the result of this peak to that of the radon daughters (^{214}Pb and ^{214}Bi), the ^{238}U–^{226}Ra secular equilibrium and, hence, the applicability of the 186 keV peak for radium determination can be proven. After the verification of the assumptions, the usage of the 186 keV line provides the quick and accurate radium determination of the samples. Taking into account the proportion of ^{235}U, the use of the 186 keV method was considered to be more effective instead of using other gamma lines (e.g. 143 keV, 163 keV and 205 keV) of ^{235}U due to their relative weak emission probabilities (10.9%, 5.0% and 5.0%; Link 4) and the possible interferences (Yücel, 2009).

3. General overview of attic dust analysis

This part of my thesis includes a typical Central-Eastern European industrial area, the city of Ajka (Western Hungary). Industrial activity in Ajka started in the late 19th century. Lignite mining, a lignite-fired power plant, the aluminium industry and numerous waste heaps act as sources of multiple contamination in the area.

Trace element contamination in the urban environment may increase human exposure via inhalation, ingestion and dermal contact (Ferreira-Baptista and De Miguel, 2005; Mielke et al., 1999; Saeedi et al., 2012; Wong et al., 2006). It is well documented that particles (<PM 10) are easily enriched in potentially toxic elements since their large surface area in relation to volume acts as a scavenger for volatile elements such as As, Hg and Cd. When inhaled, such particles may penetrate into the alveolar regions of the lungs and cause chronic health issues (Bhanarkar et al., 2008; Campa and Castanas, 2008; Goodarzi, 2006; Sysalova and Szakova, 2006). Atmospheric particles originate both from natural (e.g. erosion, dust storm, volcanoes) and anthropogenic sources (e.g. fuel combustion, mining, metal industry, traffic, coal-fired power plants; Banerjee, 2003; Cizdziel and Hodge, 2000; Goodarzi, 2006). Many of these particles contain trace elements, acids, biogenic material and other organic and inorganic compounds (Al-Khasman, 2004; Charlesworth and Lees, 1999; Cizdziel and Hodge, 2000; Gosar and Miler, 2011; Wong et al., 2006).

Urban soil studies to investigate the impact of industrial activity on the environment are widespread (Ajmone-Marsan et al., 2008; Ferreira da Silva et al., 2004; Ljung et al., 2006; Ottesen et al., 2008; Wong et al., 2006). Another medium is settling dust such as street and road dusts (Ferreira-Baptista and De Miguel, 2005; Saeedi et al., 2012; Zheng et al., 2010). Their respective analysis is a useful tool to identify sources of potentially toxic components and to study their mobility (Banerjee, 2003; Duong and Lee, 2009; Lu et al., 2009a, b; Zhang et al., 2012). However, such dusts do not remain in place for a long time because they can easily be re-suspended into the atmosphere or will be washed away by precipitation (De Miguel et al., 1999; Ferreira-Baptista and De Miguel, 2005).

Airborne pollutants can enter houses through doors, windows, vents and cracks, and may contaminate entire living areas (Cizdziel and Hodge, 2000). Beside the radioactive hazard of building materials, the study of indoor dust has attracted increasing attention over the past decades. House dust can be used to calculate the occupants' indoor exposure to toxic elements (Gulson et

al., 1995; Hogervorst et al., 2007; Hunt et al., 2012; Meyer et al., 1999; Mølhave et al., 2000). Normal house dust analyses may only serve to illuminate the recent history of exposure, since household cleaning gets rid of atmospheric dust from the past, thus disabling the assessment of the long-term contamination load. This is usually not the case with attic dust, where particle accumulation may remain undisturbed; making it a useful medium for the assessment of long-term airborne contamination (Cizdziel and Hodge, 2000). Attic dust is derived primarily from aerosol deposition of external sources, including industrial emissions and soil dusts, and to a much lesser extent from household activities (Balabanova et al., 2011).

Attic dust sampling is therefore a reliable method to map contamination loads around industrial areas (Balabanova et al., 2011; Davis and Gulson, 2005; Gosar et al., 2006). Respective analytical work was first presented by Cizdziel et al. (1998), analyzing ^{137}Cs and ^{239}Pu near the Nevada nuclear test site. Cizdziel and Hodge (2000) studied 17 urban attic dust samples and found Pb, Zn, Cd, Sb and Sn in concentrations exceeding the natural background. Ilacqua et al. (2003) measured Pb-concentrations and found a positive correlation with the history of leaded gasoline consumption. Davis and Gulson (2005) found Cd, Cu, Pb, Sb, and Zn levels to be consistently higher in industrial settings as compared to other places in Sydney (Australia). The attic dust method has been widely used in Slovenia to trace the Hg-halo of the Idrija area (Gosar and Sajn, 2001; Gosar et al., 2006), to study chemical elements and historical anthropogenic loads in Meza Valley (Sajn et al., 2000; Sajn, 2002; Sajn, 2006) and Celje area (Sajn, 2001; Sajn, 2005; Žibret, 2013), and to study the influence of ironworks in Slovenia, Bosnia and Herzegovina (Alijagić and Sajn, 2006). A study by Tye et al. (2006) on tree barks and attic dust samples in three villages in Eastern England around a former tin smelter showed high enrichment factors for Sn, Cd, Pb and Sb, which were likely to have derived from non-soil sources. Hensley et al. (2007) sampled attic dust in eleven houses in the vicinity of a former wood treatment facility in southern Alabama, USA and analyzed the dioxin/furan, PAH, As, Cu and Cr contents of the samples. Balabanova et al. (2011) collected attic dust samples from 29 different houses, built between 1920 and 1970 in a copper mining area of eastern Macedonia, and analyzed 19 elements. The authors identified three element groups by means of factor analysis as two natural groups and one anthropogenic group. These results suggest that undisturbed attic dusts can act as archives of atmospheric dust by preferentially trapping and preserving airborne particulate matter (Cizdziel and Hodge, 2000). All

these publications considered, attic dust is a new urban geochemical method for the analysis of potential pollution in Hungarian urban areas (Völgyesi et al, 2014b).

3.1. Main properties of the toxic elements analyzed

In this chapter the main properties of toxic elements (As, Cd, Cu, Hg, Ni, Pb and Zn) based on ATSDR list (ATSDR, 2011) are presented. These elements do not decay or disappear from the environment, therefore causing a unique challenge for urban geochemistry. Some of these metals are absolutely unimportant for living biota and some micrograms can cause toxicity; some of them are essential in a given range, but cause symptoms of deficience below or toxicity above it. To avoid the long and wearisome introduction of these elements, the main information is summarized separately in the Appendix 2–8.

4. Materials for studies

4.1 Sampling strategy of building materials

The sampling strategy developed in the course of my research focused on houses where in most cases the owners requested our laboratory to measure the level of indoor radioactivity because they had heard about the harmful effects of coal slag- and fly ash-bearing materials. The campaign consisted of a quick (1–3 days) radon measurement by using active radon detectors (AlphaGUARD or RAD7), gamma dose rate determination with a portable FH40 GL10 device and, where possible, building material sampling. Unfortunately, the collection of building materials was not possible in all the studied houses, but in houses under renovation it was easily carried out. In this thesis only those houses are discussed from which building material samples were available. To compare the results of coal combustion by-products, other building materials (brick, the concrete from blocks of flats) were also sampled. The amount of coal slag samples was supplemented by the attic dust sampling campaign in Ajka (Figure 5). Although it was not an original aim, coal slag samples were collected at the attics, too, as the coals of this region (Transdanubian Central Range) contain elevated levels of radionuclides (Chapter 2.4). As a result of the sampling campaigns 29 building materials were sampled, of which 25 contained by-products of coal combustion. As was previously highlighted, the coal slag samples in Hungary are considered as samples with higher Ra-content (>100 Bq kg^{-1}), and provide the opportunity of using them as test samples in the study of the existence of secular equilibrium and the validation of the 186 keV peak for accurate ^{226}Ra determination (Figure 5).

Hence, two sample groups were distinguished. The first group consists of building material samples collected from the Central Region of Hungary (Figures 1 and 5). These materials were qualified with gamma-ray spectrometry analysis by measuring the ^{232}Th, ^{226}Ra and ^{40}K activity concentrations at the Eötvös University, Department of Atomic Physics. The second group contains 9 coal slag samples from the Central Region of Hungary (n=4) and Ajka (n=5) with high radium activity concentrations (>100 Bq kg^{-1}) and was used for testing a measuring system at the Centre for Energy Research, Hungarian Academy of Sciences. Samples from Ajka were also qualified based on the same methodology used for the samples from the Central Region of Hungary. Additionally, for radon leakage test of the sample holders a soil sample from Kővágószőlős (sample code: KSZPF1, Nagy et al., 2009) with very high radium activity concentration (>8000 Bq kg^{-1}) and radon emanation was used (Figure 1).

4. 2. Study area of building materials

Beside the request of inhabitants, another requirement from our side was the relatively short distance of a studied house from Budapest (actually from the Campus), which is easily reachable by car or by public transport for reasons of cost-effectiveness. The building material samples consisted of brick (B) samples (n=2), concrete (from blocks of flats) (CBF) samples (n=2), coal slag (CS) samples (n=15), coal slag concrete (CSC) samples (n=3) and gas silicate (GS) samples (n=6) with fly ash as additive and (n=1) without fly ash (Figure 5). These were collected from nine locations (Budapest, Dunaharaszti, Gödöllő, Kecskemét, Kiskunhalas, Kistarcsa, Sülysáp, Százhalombatta) in the Central Hungarian Region (CHR), and additional coal slag samples originating from Ajka city (Figure 5). In the case of coal slag and gas silicates, the additives or the whole material had undergone heat treatment during production, which causes changes in its internal structure, and hence can influence radon and thoron exhalation (Sas et al., 2012). Moreover, it can result in the enrichment of radionuclides (TENORM[5]). Most samples were used in bulk amounts, whereas the coal slag samples were only used restrictedly (i.e. used for under-floor filling below the parquet or in the attics above the ceiling).

The sampled coal slags collected in Ajka were all the by-products of locally mined coal with elevated radioactive isotope content and burned in the local coal-fired power plant or other local furnaces (Somlai et al., 2006, personal communication of Oszkár Illési, 2011). Therefore, the origin of the source material of these samples was easily definable. For the coal slag samples from Budapest, the source material origin is unknown because it is assumed that coals from several sources all around the country were transported to the capital for burning. The composition and origin of coal or coal slag in the coal slag concretes is also unknown. Regarding fly-ash bearing materials, the gas silicates were produced in Kazinczbarcika and in Gyöngyösvisonta (Link 5). The fly ash used as additives in these materials is the by-product of the coal burned in the coal-fired power plant, the coal having been mined in the North Hungarian Mountains (Figure 1). Due to the same technological procedure, one gas silicate sample is also called a gas silicate, but does not contain fly ash, only sand as additive.

[5]Technologically enhanced naturally occuring radioactive material

The samples were labeled based on type (e.g. B, CBF, CS) and origin (CHR, Ajka), and an additional number if necessary (e.g. a coal slag sample from Central Hungarian Region is labelled as CS_CHR_4).

Figure 5. Locations of building material and attic dust samples used for the studies. Different types of building materials are indicated by different colors, and those materials containing power plant by-products are indicated by a star. The location of Ajka is indicated by a purple dot. Purple arrows refer to sites of attic dust analysis, red arrows indicate methodology improvement through the use coal slag samples, and blue arrows indicate building material classification. n=number of samples, ICP-OES=inductively coupled plazma-optical emission spectrometry, AAS=atom absorption spectrometry, Bq/kg=Becquerel/kilogramm, Ra_{eq}=radium equivalent, I=activity concentration index.

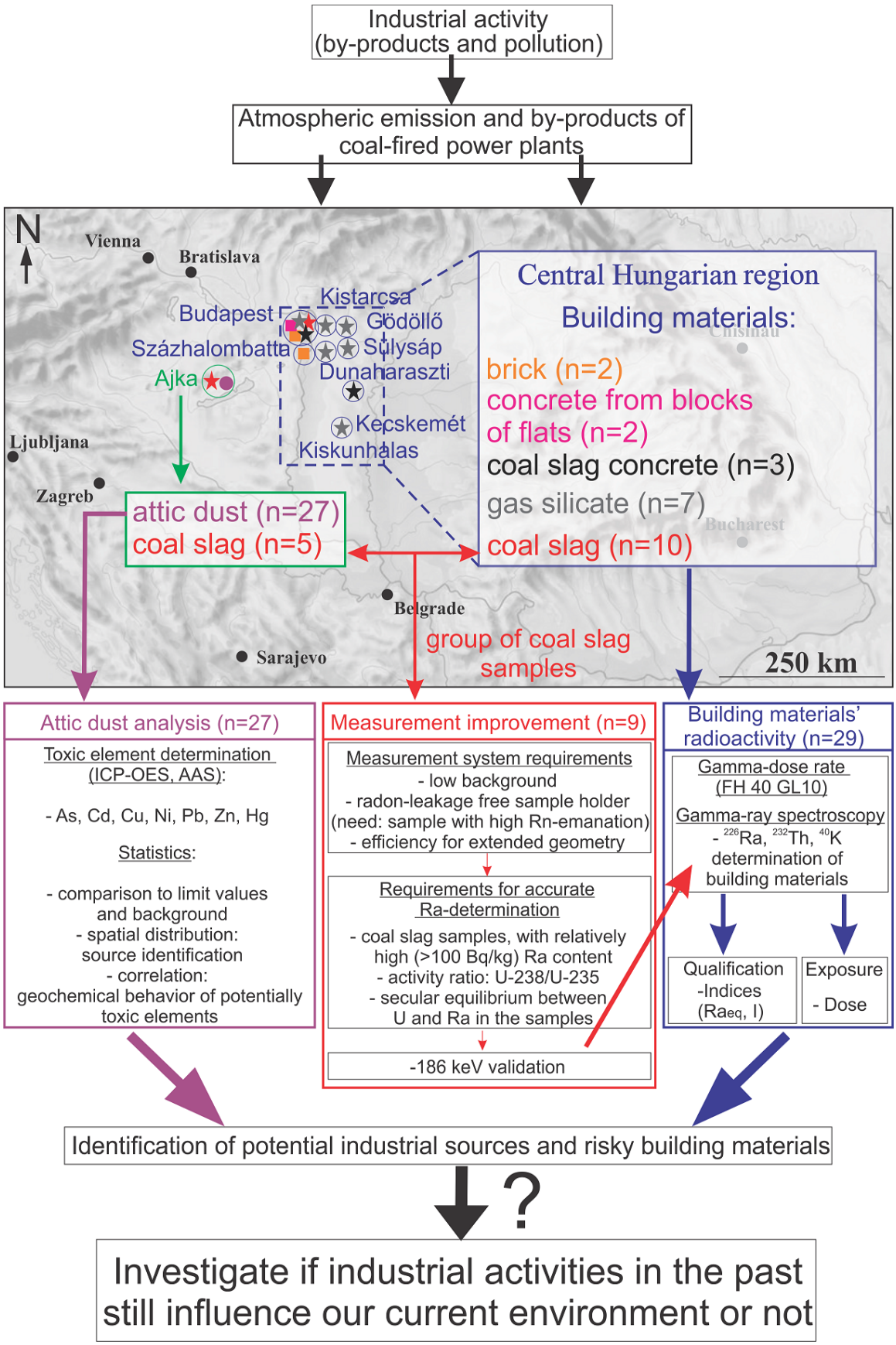
Industrial activity
(by-products and pollution)
Atmospheric emission and by-products of coal-fired power plants
N
Vienna
Bratislava
Budapest
Százhalombatta
Ajka
Kistarcsa
Gödöllő
Sülysáp
Dunaharaszti
Kecskemét
Kiskunhalas
Ljubljana
Zagreb
Belgrade
Sarajevo
Chisinau
Bucharest
Central Hungarian region
Building materials:
brick (n=2)
concrete from blocks of flats (n=2)
coal slag concrete (n=3)
gas silicate (n=7)
coal slag (n=10)
attic dust (n=27)
coal slag (n=5)
group of coal slag samples
250 km
Attic dust analysis (n=27)
Toxic element determination (ICP-OES, AAS):
- As, Cd, Cu, Ni, Pb, Zn, Hg
Statistics:
- comparison to limit values and background
- spatial distribution: source identification
- correlation: geochemical behavior of potentially toxic elements
Measurement improvement (n=9)
Measurement system requirements
- low background
- radon-leakage free sample holder (need: sample with high Rn-emanation)
- efficiency for extended geometry
Requirements for accurate Ra-determination
- coal slag samples, with relatively high (>100 Bq/kg) Ra content
- activity ratio: U-238/U-235
- secular equilibrium between U and Ra in the samples
-186 keV validation
Building materials' radioactivity (n=29)
Gamma-dose rate (FH 40 GL10)
Gamma-ray spectroscopy
- 226Ra, 232Th, 40K determination of building materials
Qualification -Indices (Raeq, I)
Exposure
- Dose
Identification of potential industrial sources and risky building materials
?
Investigate if industrial activities in the past still influence our current environment or not

4.3. Sampling strategy of attic dusts

Sampling was conducted following an attic dust sampling guidance protocol based on international methods and experience (Cizdziel and Hodge, 2000; Davis and Gulson, 2005; Ilacqua et al., 2003; Sajn, 2005; Salminen et al., 2005). A special field sheet was elaborated for the most effective and detailed collection of information regarding the sampling sites (Appendix 9). The sampling was carried out in the summer of 2011 in 27 houses in Ajka and its vicinity, including industrial areas, urban dwelling locations and the taking of background samples (27 attic dust samples including 3 duplicate samples; Figures 6 and 7). The sampling strategy followed a grid-based, stratified random sampling design. The 48 km^2 project area was covered by a 1x1 km grid. In each cell, one house located closest to a randomly generated point in the cell was selected for attic dust collection. A further selection criterion, superimposed on the grid design, was related to the position of the alumina and power plant industrial areas, of the lignite mines, and of the red mud tailings reservoirs (Figure 7). To obtain representative geochemical background samples, material was collected from the up-wind direction (NW). Grid cells remote from potential contamination sources were not sampled to increase sampling effectiveness. Four ash samples were collected from the waste dump of the power plant, three samples from the waste heaps in the lignite mining area, and ten red mud samples close to the mud tailings pond two days after the catastrophe on 06 October 2010, to study the possible effect of the main contamination sources of the lignite mines, the lignite-fired power plant and the alumina industry (Figure 7).

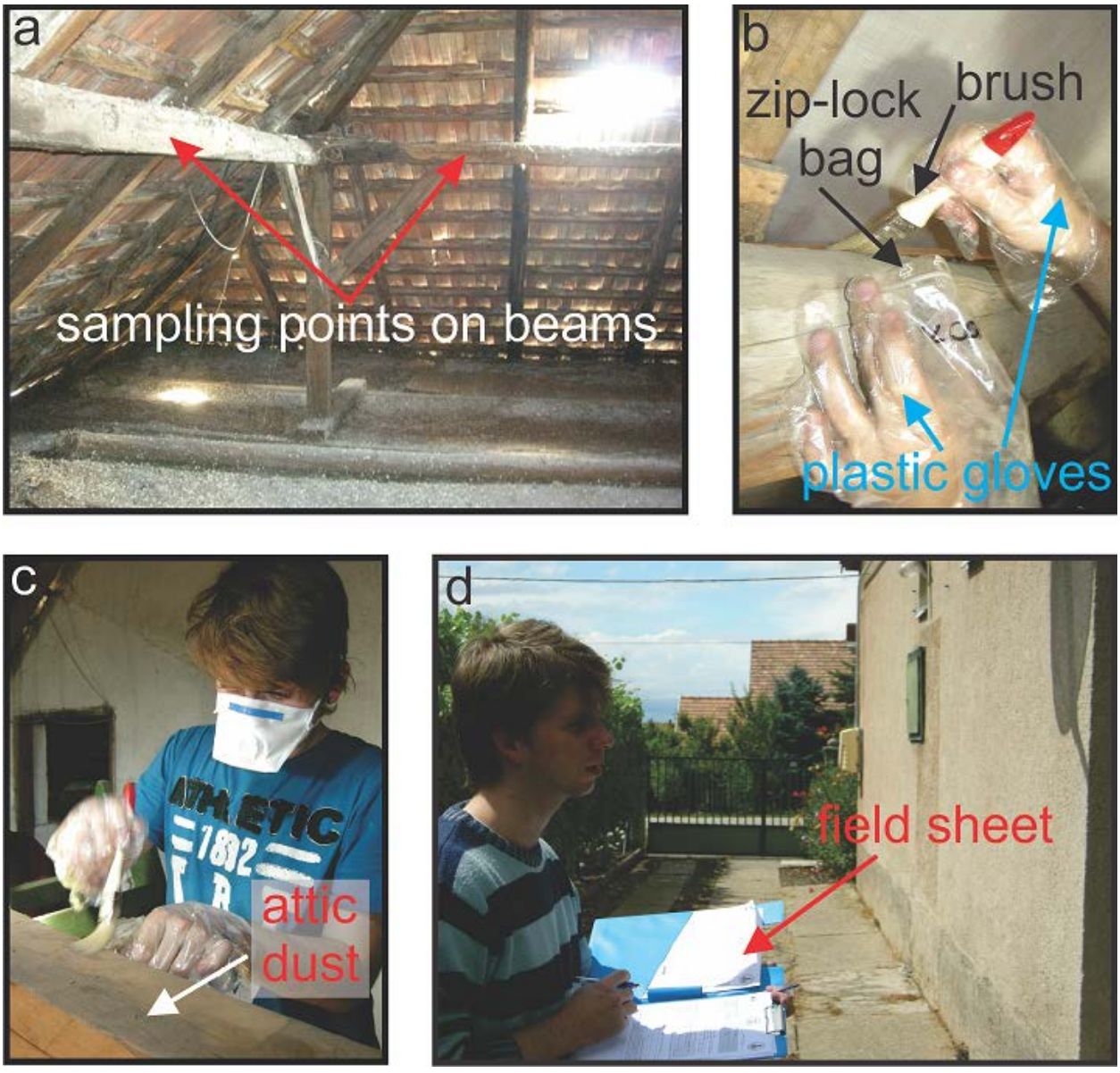

Figure 6. Attic dust sampling in Ajka, 03 July 2011.

Houses with attics left unchanged for at least the past 30 years were considered representative for long-term contamination. All attics were checked for disturbances by human activity. Attic floors were not sampled. Samples were collected away from the attic entrance and at the highest possible point of the attic to minimize possible disturbing effects of resident activities (Figure 6a). Two to thirty grams of dust, composed of 3 sub-samples, were manually swept into zip-lock plastic bags (in most cases from the surface of beams), using fine disposable brushes and plastic gloves (Figure 6a, b, c). Along with photographic documentation, sampling conditions, building orientation, GPS coordinates, roof type and house characteristics such as construction

material and paintwork condition, renovation history, together with surrounding characteristics such as local development history, landscape and land-use were recorded (Figure 6d, Appendix 9). Close communication and then collaboration with the local community was essential for a successful sampling campaign.

4.4. Study area of attic dusts

Ajka has a total area of 95 km^2 and more than 29.000 inhabitants (Figure 7). The surrounding lithology is characterized by Triassic limestone and dolomites together with Cretaceous limestone. The Cenozoic cover is composed of Eocene marl and limestone, Miocene-Pliocene sediments and basalts, while Quaternary loess and gravel represent the most abundant sediments. The Cretaceous formation bears lignite deposits that formerly made Ajka an important mining town in Hungary (Császár, 2005). The prevailing soil types of the region are brown forest soils, meadow soils and rendzina. The studied area is located in the Geochemical Landscape Region 2 of Hungary, characterized by an association of Ca^{2+}, Mg^{2+}, Sr^{2+}, CO_3^{2-}, SO_4^{2-}, PO_4^{3-}; typical for carbonate rock terrains (Ódor et al., 1996). The region has a typical wet continental climate with an annual average temperature of 11 °C and 660 mm of average annual precipitation. The prevailing wind direction is north-west (Link 6).

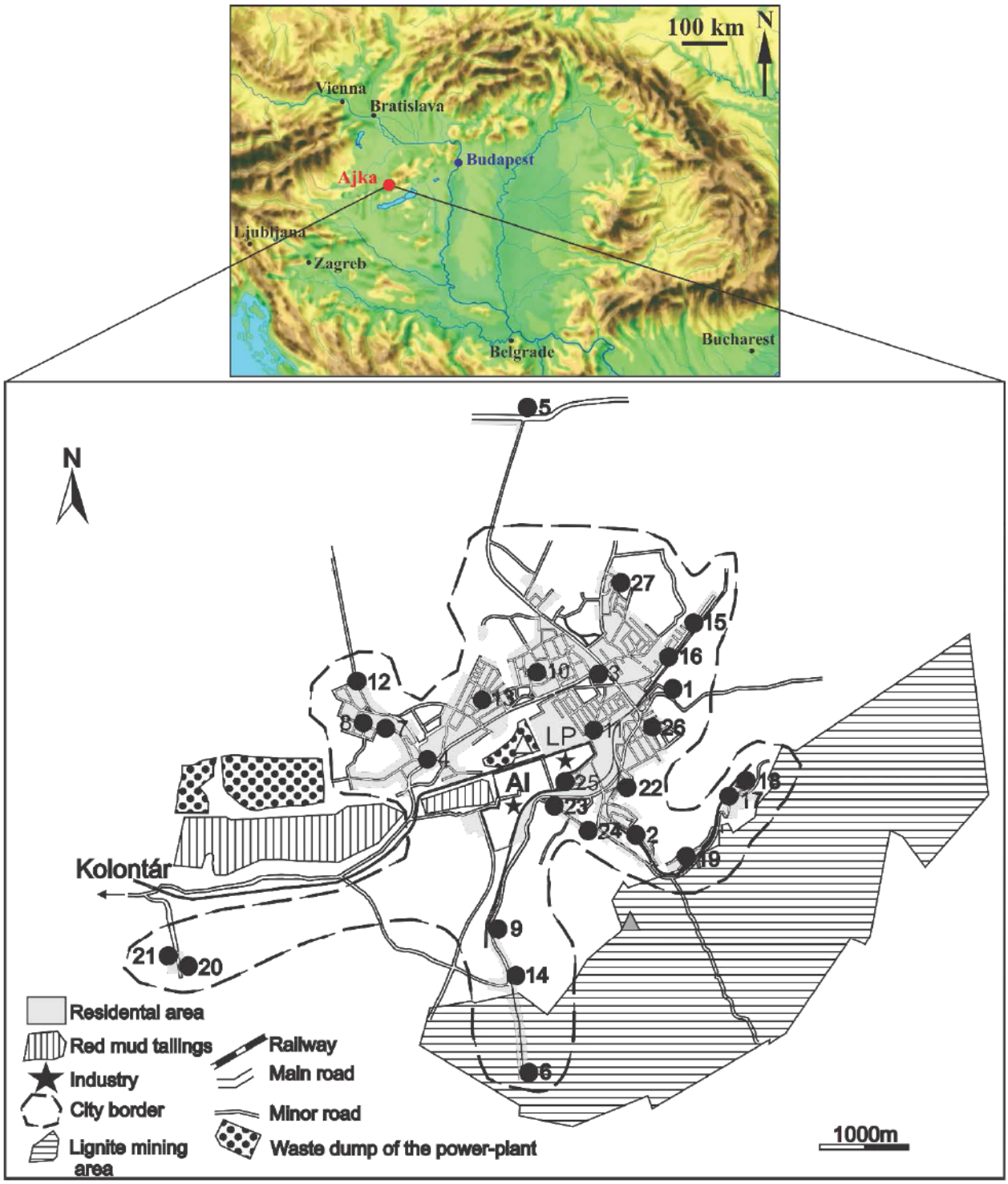

Figure 7. The Ajka study area. AI: aluminum industry, LP: lignite-fired power plant, horizontally lined field: Csinger-valley lignite mining area; vertically lined field: red mud tailings; dotted field: waste dumps of the lignite-fired power plant; dashed-line: border of residential area; gray field: residential area; fine lines: minor roads; heavy lines: major roads; black and white lines: railways; numbered black dots: sample locations with sample codes. Blank triangle: sampling site from the waste dump of the power plant, gray triangle: sampling sites from the waste heaps of the lignite mining area. Inset: location of the study area in the Transdanubian Central Range (Hungary).

Industry has played a significant role in history of Ajka, starting with the discovery of lignite in the second part of the 19th century. The lignite mines are located in the south-eastern part of town (Figure 7). They produced a total of 88 million tons of lignite up to 2004, when the last mine was shut down (Kozma, 1996). Several large mine waste heaps accumulated that burned spontaneously until their complete remediation after mine closure. The so-called 'little power plant' was built up in 1912 in the mining area and operated until 1945, providing energy for the mines and for a krypton factory. The annual lignite combustion of the power plant never exceeded 15.000–20.000 tons. The present 'large power plant' was constructed next to the alumina industry in the 1940s (Figure 7). It burnt almost exclusively Ajka lignite (93% of all coal and lignite in the period 1975–1997; Kozma, 1996). Efficient fly ash retention equipment was installed in the mid 1980s, resulting in its retention efficiency increasing from 94% (1985) to 99.85% (1995; Papp et al., 2002). The total amount of fly ash emitted from the beginning of the operation to 1997 can be estimated to be about 900.000–950.000 tons (Papp et al., 2002). Today the power plant burns the mixture of biomass and import coal.

The nearby manganese mine at Úrkút, and bauxite opencast and underground mining to the southwest of Ajka supported the massive industrial development and the operation of both a large-scale alumina factory and an aluminum smelter from the 1940s (Figure 7). Typical annual alumina production was 485.000 tons and the annual aluminum production was 22.000 tons until production stopped for economic reasons in the early 1990s. The alumina factory is still active and produces special hydrate and alumina products in addition to synthetic zeolites and high-purity gallium as by-products (Link 7).

5. Methods

In the next paragraphs the qualification calculations, the methodology improvement of a low-background counting chamber used for building materials and the attic dust analysis will be presented separately.

5.1. Methodology used for radionuclide determination and qualification of building materials

5.1.1 In situ gamma dose rates

A portable FH40 GL10 (Thermo Scientific, 2007) detector was used to determine the in situ gamma dose rate in the studied buildings. The device detects the gamma dose rate from 10 nSv h^{-1} up to 1Sv h^{-1} using a proportional counter in the 30 keV–4.4 MeV energy range. The device is designed to meet the energy response behavior of the SI-units ambient dose equivalent and ambient dose equivalent rate according to Report 39 of the International Commission on Radiation Units and Measurements (ICRU, 1985). Measured values are shown on a clear, backlit LCD display in the units of nSv h^{-1}. Dose rate values were measured at ground level and at a height of 1m at several points in the studied house.

5.1.2. ^{226}Ra, ^{232}Th and ^{40}K determination and qualification of building materials

5.1.2.1. The measuring system

Activity concentrations of ^{226}Ra, ^{232}Th and ^{40}K in the building material samples were analyzed by gamma-ray spectrometry using a GC1520- 7500SL HPGe detector in the Department of Atomic Physics, Eötvös University, Budapest. Detector shielding of 10cm thick lead was applied to reduce the background radiation. The detector was cooled to the liquid nitrogen temperature and coupled to a PC-based 4 K multichannel analyzer. The energy resolution of the detector is 2.0 keV at 1332.5 keV (^{60}Co peak) and its relative efficiency is 15% (Link 8). All of the building material samples were dried in lab air till constant mass and then different amounts (due to the quantitative limitations in sampling) were powdered. This made it possible to place them into cylindrical Al-containers to get a standard geometry varying only in the sample height. Gamma rays from powdered and weighed samples filled and sealed into Al-containers were measured for a minimum of 16 h. The detection efficiency for gamma-photons of characteristic energies was determined by Monte Carlo simulation (Link 9). It ranges from 0.45% to 9%

depending on photon-energy, geometry, density and average element composition of the sample, with general uncertainty of <2%. For efficiency determination, a theoretical elemental composition of an average andesite rock was assumed due to the relatively high SiO_2 content of the samples. Absolute transition probabilities came from the NuDat2.5 database (Link 10). The ^{226}Ra was measured by its 186.2 keV line, taking into account that it overlaps the 185.7 keV line of ^{235}U. In this case, both the natural isotopic abundance between ^{238}U (99.3%) and ^{235}U (0.7%), and the secular equilibrium between $^{238}U$and ^{226}Ra were assumed leading to a ratio of 58.3%–41.7% (Ebaid et al., 2005) in the counts of the appearing peak of ^{226}Ra and ^{235}U, respectively. These reasonable assumptions had to be applied in the calculations because the use of the peaks of radon decay products was considered disadvantageous in this experimental setup (Szabó et al., 2013). The reason was that radon exhaling from the sample fills the free volume of the Al-container and progenies attach to the inner wall, also where no sample is present in the upper parts of the volume. Hence, the detection efficiency of their gamma photons is unidentifiable. This effect can be avoided only if the sample fills the whole volume of the container which was difficult to achieve, due to large differences in the available sample amount and the level of activity. Moreover, despite sealing, some radon leakage can also occur, reducing the count number of radon decay product peaks. Hence, the 186.2 keV line with the corrections detailed above was considered to provide the most reliable results for the ^{226}Ra activity concentrations of the studied samples. These assumptions inspired us to develop a measurement improvement in which all these factors could be tested and considered for accurate radium determination. The activity concentration of ^{232}Th was determined by using the interference free ^{228}Ac peak at 911.2 keV, whereas ^{40}K was measured by its own peak at 1460.8 keV, respectively.

5.1.2.2. Calculations used for building material qualification

To qualify building materials, different indices are applied in the literature based on activity concentrations of ^{226}Ra, ^{232}Th and ^{40}K, and they have been widely used in recent publications for presenting the radioactive hazards of building materials (e.g. Al-Sulaiti et al., 2011; Damla et al., 2011; Moura et al., 2011). The most frequently used radium equivalent index is given in the following expression (Eq. 1; Beretka and Mathew, 1985; Hamilton, 1971):

$$Ra_{eq} = C_{226Ra} + \frac{10}{7} C_{232Th} + \frac{10}{130} C_{40K} \quad \textit{(Equation 1)}$$

where Ra_{eq} is the radium equivalent index (Bq kg^{-1}), C_{226Ra} is the activity concentration of ^{226}Ra, C_{232Th} is that of ^{232}Th and C_{40K} is that of ^{40}K (Bq kg^{-1}).

The requirement is that the value of Ra_{eq} in building materials be less than the limit value of 370 Bq kg^{-1} (OECD, 1979) for safe use (i.e. to keep the external dose below 1.5 mSv y^{-1}). Other limits are the following: 740 Bq kg^{-1} for industrial use, 2200 Bq kg^{-1} for roads and railways, 3700 Bq kg^{-1} for landfill materials, and the use of materials with Ra_{eq} > 3700 Bq kg^{-1} for any construction is forbidden (Somlai et al., 1996).

The unitless activity concentration index recommended by the RP 112 (EC, 1999) was used for building material qualification. This index is derived to indicate whether the annual dose due to the excess external gamma radiation in a building may exceed 1 mSv y^{-1}. This dose criterion was applied based on Trevisi et al. (2012), who showed that the adoption of 0.3 mSv y^{-1} is probably too ambitious a health goal since too many materials exceed the value. A background cosmic and terrestrial dose rate of 50 nGy h^{-1} has been used in deriving the index, which is defined in the following way (Eq. 3). The limitation for materials used in bulk amounts (e.g. concrete and brick) is $I \leq 1$, whereas $I \leq 6$ is applied for materials with restricted usage (e.g. tiles, boards, coal slag samples).

$$I = \frac{C_{226Ra}}{300\ Bq\ kg^{-1}} + \frac{C_{232Th}}{200\ Bq\ kg^{-1}} + \frac{C_{40K}}{3000\ Bq\ kg^{-1}} \leq 1 \quad \textit{(Equation 2)}$$

where I is the activity concentration index, C_{226Ra} is the activity concentration of ^{226}Ra, C_{232Th} is that of ^{232}Th and C_{40K} is that of ^{40}K (Bq kg^{-1}).

According to the RP112 (EC, 1999), the absorbed dose rate in a room with dimensions of 4×5×2.8 m^3, a wall thickness of 20 cm and a wall density of 2.350 kg m^{-3} (concrete) can be calculated by using Eq. 3. A background cosmic and terrestrial dose rate of 50 nGy h^{-1} is taken into account like in the case of the activity concentration index (EC, 1999):

$$D_a = aC_{226Ra} + bC_{232Th} + cC_{40K} \quad \textit{(Equation 3)}$$

where D_a is the absorbed dose rate (nGy h^{-1}) and a, b and c are the dose rates per unit activity concentrations of ^{226}Ra, ^{232}Th and ^{40}K [(nGy h^{-1}) (Bq $kg^{-1})^{-1}$], respectively. The values of a, b and c were taken to be 0.92, 1.1 and 0.08, respectively.

The external, annual effective dose can be estimated using the following formula (Eq. 4.):

$$D_e = 10^{-6} OFD_a \qquad \textit{(Equation 4)}$$

where De is the calculated annual effective dose (mSv y^{-1}), O is the annual indoor occupancy time (0.8×24 h×365.25 d=7012.8 h y^{-1}) and F is the dose conversion factor, 0.7 Sv Gy^{-1} (EC, 1999).

To calculate the excess of building materials to the external dose received outdoors one can subtract the assumed 50 nGy h^{-1} background radiation (EC, 1999) from the result provided by Eq. 3. and Eq. 4.

5.2. Description of the methodology improvement

5.2.1. A low-background detection system

After the demand for measurement improvement emerged, low-level radioactivity measurements began in 2011 at the Nuclear Analysis and Radiography Laboratory (NARL) of the Centre for Energy Research, Hungarian Academy of Sciences, Budapest. The low-background detection system called 'DÖME' (from its Hungarian name '**Dö**gnehéz **M**érő**e**szköz' meaning in English 'Extremely Heavy Measurement Instrument') in Figure 8 is an adequate tool for the study of samples with low radioactivity levels (e.g. originating from environmental studies). It is made of 8 t of pre-WW II iron[6] to mitigate the background effect due to artificial radionuclides. It has internal dimensions of 800×800×800 mm^3 (Figure 8). The 150 mm thick iron wall is covered inside with a graded shielding consisted of lead (5 mm) and copper (1.5 mm) layers. As a result of this passive shielding the overall background within the chamber is about 1.39 cps [7] over the energy range of 7–3150 keV, which compares to 211 cps outside the chamber (a reduction factor of 152). An n-type HPGe detector (Canberra GR1319) with a relative efficiency of 13% and a Canberra DSA-2000 data acquisition system with 16 K channels were used for measuring the gamma-ray spectra. The cylindrical detector has dimensions of 46 mm in diameter and 41 mm in

[6] The usage of a pre-WW II iron from the bombed Elizabeth-bridge of Budapest (1945) is advantageous because it was not influenced by the atomic bomb tests, hence, has lower background radiation.
[7] counts per second

length. The distance of its entrance surface from the 0.5 mm thin carbon epoxy endcap window is 5 mm. The energy resolution (full width at half maximum) is 1.53 and 1.99 keV at 662 and 1332 keV, respectively. The peak-to-Compton ratio is 42.8:1 at 1332 keV. Dead-time losses during the experiments never exceeded 0.05%. The measured spectra were evaluated by Hypermet-PC software developed by the NARL (Révay et al., 2005). The counting rates were calculated using the background corrected net peak area of the full energy peaks for the gamma energies of the nuclides to be determined.

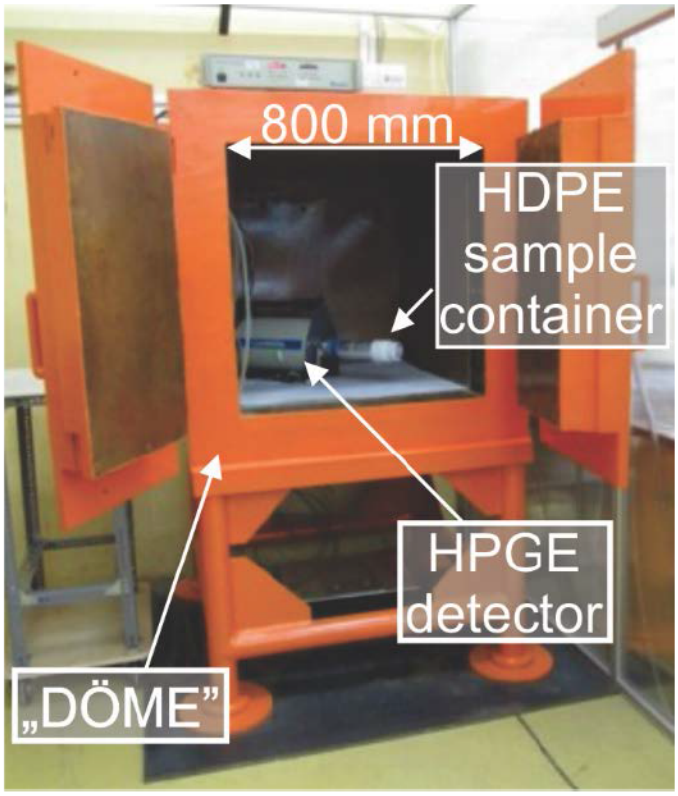

Figure 8.The low-background counting chamber 'DÖME' with the HPGe detector and the HDPE sample container in a close sample-detector setup in the neutron guide hall of the Budapest Neutron Centre, Center for Energy Research, Hungarian Academy of Sciences.

5.2.2. Sample container design

Radon (^{222}Rn) can easily escape from sample containers, distorting the secular equilibrium in the ^{238}U decay chain (Chapter 2.5.). Hence, a special theoretically radon-leakage-free sample container made of HDPE was developed because this material has advantageous mechanical and radon permeability features (Ashry et al., 2011). The four fabricated containers, with net volumes of 105 cm^3 each, enable the measurement of both liquid and solid samples. The inner diameter and height are 52 and 49.5 mm, respectively (Figure 9). To reduce the absorption of low-energy

photons, the wall thickness is 3.5 mm at the bottom, whereas it is 5 mm elsewhere. The container can be sealed using a lid with threads, which fastens a plug to the wall of the container (Figure 9). In order that radon and its daughters can be kept in equilibrium it is gas- and liquid-tight, sealed by means of a 2 mm thick Viton FPM 80 Standard fluorocarbon elastomer O-ring (Dupont, 2012, ERIKS, 2012) between the plug and the wall of the container (Figure 9).

5.2.3. Sample used for radon leakage test

In Kővágószőlős, sandstone debris in the upper layer (0–2 m) of the soil has high uranium content as a result of a uranium ore deposit located beneath the village. This area, having extremely high radon levels, was studied (Nagy et al., 2009) and a test soil sample (KSZPF1) with about 8000 Bq kg^{-1} ^{226}Ra-content was provided for our experimental work (Nagy et al., 2009). The radon production of this sample was assumed to be high enough to precisely verify a non-negligible radon leakage from the HDPE sample holder.

Figure 9. The sample container made of HDPE (High-density Polyethylene) and Viton O-ring.

The KSZPF1 test sample, weighing 158 g, was only dried and poured into the container. The container was filled up totally to maintain the constant geometry of the sample and to avoid the biasing effect of radon accumulation in empty space, which can change counting efficiency (Mauring and Gäfvert, 2013).

5.2.4. Testing the sample container for radon leakage

A saturation curve for the activity concentration in a sealed container should theoretically follow equation 5, with the same decay constant (λ) for ^{222}Rn and its daughters, because they are in secular equilibrium if there is no leakage from the container:

$$C = \left(C_{eq} - C_0\right) \cdot \left(1 - e^{-\lambda t}\right) + C_0 \qquad \textit{(Equation 5)}$$

here C, C_{eq} and C_0 stand for the activity concentration of the nuclides at time, at saturation and at the start of the measurement, respectively.

Fitting this function to the results of the saturation curve measurements of the sample described above, the value of the apparent decay constant can be obtained. Radon escape was tested by comparing the measured decay constant of the daughters (^{214}Pb, ^{214}Bi) to the value found in the literature of the ^{222}Rn decay constant for each energy, separately. A compartment model can be used to describe mathematically the processes as shown in Figure 10. The materials in the boxes[8] can be considered well mixed and the transport between them can be formulated by the decay constants and the possible leakage rate (red arrow, Figure 10). If there is leakage from the container, the measured apparent decay constant will be larger than the value in the literature, which is based solely on radioactive decay. In this case Eq. 6 gives the measurable decay constant:

$$\lambda_{measured}^{Rn-222} = \lambda_{decay}^{Rn-222} + \lambda_{leakage}^{Rn-222} \qquad \textit{(Equation 6)}$$

[8]Here, the material implies a radionuclide within a compartment (box). One compartment contains one radionuclide.

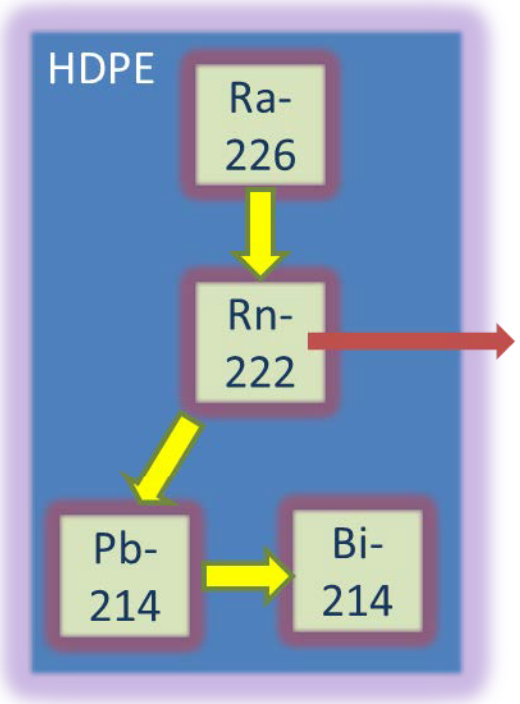

Figure 10. Compartment model of the measurable decay constant of ^{222}Rn in the case of possible leakage from the container. The red arrow represents ^{222}Rn leakage.

After sealing the container with the KSZPF1 test sample, every 6 h successive measurements were carried out for 18 days to record the saturation curves of the radon daughters' radiations at different energies (^{214}Pb: 295 keV, ^{214}Bi: 609 keV and 1764 keV).

5.2.5. Full-energy peak efficiency calibration for extended samples in close-in geometry

In the case of the absolute method (Chapter 2.5.2.), the reliable determination of the absolute FEP [9] efficiency is necessary for a sample in close-extended geometry. Unfortunately, the results of point source efficiency measurements in this close-in geometry are not applicable and, furthermore, the detection geometry will maximize the true coincidence counting (TCC)[10] effects. Therefore, correction factors were needed to obtain the true FEP efficiency values at the desired energies for the close-extended geometry. To obtain the corrected true FEP efficiency values, the

[9]Full energy peak
[10]True coincidence counting is a factor which must be considered in efficiency calculations when close-in geometry is used.

transfer method was employed using the EFFTRAN 1.2 code[11] (Vidmar, 2005, Vidmar et al., 2011). It transfers the FEP efficiency values from calibrated point source measurements (references) to the actual geometry using the results of a priori Monte Carlo simulations. If the Moens-theorem[12] (Moens et al, 1981; Moens et al., 1982) is valid then the FEP efficiency can be calculated according to Eq. 7:

$$\varepsilon = \varepsilon_{ref} \cdot \frac{\eta}{\eta_{ref}} \qquad \textit{(Equation 7)}$$

where ε and ε_{ref} are the FEP efficiencies for the extended and for the reference (e.g. point source) geometry, respectively, where ε_{ref} has to be measured. Symbols of η and η_{ref} are the so-called virtual total efficiencies, which come from a Monte Carlo detector model.

The parameters used in the transfer code are usually taken from the manufacturer's data sheet. A further advantage is that the code takes into account the self-attenuation[13] correction using as an input parameter the density of the actual sample. To obtain the FEP efficiency for the close-extended geometry, a three-step process was followed.

Due to the lack of a certified solution (which is itself an extended source) containing all the necessary single line nuclides for a reliable efficiency calibration, certified point sources available at the Nuclear Analysis and Radiography Laboratory were used. In the first step, a series of these certified point sources (^{60}Co, ^{133}Ba, ^{152}Eu, ^{207}Bi, ^{226}Ra, ^{241}Am) were measured at a distance of 167 mm from the detector endcap to obtain the FEP efficiency at the γ-ray energies of these sources. With this source-detector geometry the TCC events play practically no role, and this could be checked with the use of the EFFTRAN 1.2 code. As the second step, these results were used as input to the Hypermet-PC code to yield the reference FEP efficiency curve and its uncertainty at the decay energies of the nuclides in the natural decay chains. As the third step these latter were fed to EFFTRAN 1.2 to transfer the reference FEP efficiency to the close-extended geometry. This step takes account the self-attenuation correction and the TCC events. The calculated TCC correction factors, F_{COI} referring to close-in geometry are available from the code.

[11]EFFTRAN is the name of the program developed by Vidmar (2005) for gamma-ray spectrometry efficiency calculations.
[12]Moens-theorem: The theorem takes into account the distortion of true coincidence summing for the determination of full-energy peak efficiency.
[13]Self attenuation must be considered in calculations when extended samples are used.

The validation of the results by measuring the FEP efficiency using the same container in close-extended geometry filled with a water solution (Table 5) was also considered. Fortunately, a solution (ERX5-Ba, activity reference time: 17 July 2008, volume: 105.124 mL) contained some single line nuclides[14] (^{241}Am, ^{109}Cd, ^{57}Co, ^{137}Cs, ^{54}Mn) in measurable quantities was available in the Laboratory. The outer bottom surface of the container was 2.2 mm distant from the entrance window of the detector and the measurement time was 98.82 h. Here the F_{COI} correction factors should be equal to 1 for coincidence-free transitions, whereas they should be different from 1 for nuclides with a simple decay scheme. The ratio of the FEP efficiency values calculated by EFFTRAN 1.2 to the measured FEP efficiency values ($FEP_{measured}$) corrected only by the TCC correction (F_{COI}) factors ($FEP_{measured} \times F_{COI}$) gives a figure of merit for the accuracy of the transfer process calculation.

[14] It means a nuclide having only one decay line in the scheme; hence, it is not influenced by true coincidence.

Table 5. A water solution of nuclides with a single line, coincidence-free transition (^{54}Mn, ^{57}Co, ^{109}Cd, ^{137}Cs, ^{241}Am) or a simple decay scheme (^{60}Co, ^{133}Ba).

Nuclide	energy (keV)	intensity	abs. unc. of intensity	$T_{1/2}$ (sec)	abs. unc. of $T_{1/2}$ (sec)	nominal activity (Bq/100 mL)	rel. unc. of activity (%)
single line							
^{241}Am	59	0.3592	1.70E-03	1.37E+10	1.89E+07	248.30	0.30
^{109}Cd	88	0.03626	2.60E-04	3.99E+07	1.04E+05	171.70	0.90
^{57}Co	122	0.8551	6.00E-04	2.35E+07	5.18E+03	68.00	0.40
^{137}Cs	661	0.8499	2.00E-03	9.49E+08	9.47E+05	251.20	0.60
^{54}Mn	834	0.999746	1.10E-05	2.70E+07	5.18E+03	46.80	0.60
not single line							
^{133}Ba	276	0.0716	5.00E-04	3.32E+08	1.58E+06	64.80	2.00
^{133}Ba	302	0.1834	1.30E-03	3.32E+08	1.58E+06	64.80	2.00
^{133}Ba	356	0.6205	1.90E-03	3.32E+08	1.58E+06	64.80	2.00
^{133}Ba	383	0.0894	6.00E-04	3.32E+08	1.58E+06	64.80	2.00
^{60}Co	1173	0.9985	3.00E-04	1.66E+08	1.21E+04	374.40	0.40
^{60}Co	1332	0.99826	6.00E-06	1.66E+08	1.21E+04	374.40	0.40

The activity reference time of the water solution ERX5-Ba,: 17 July 2008, volume: 105.124 mL
keV: kiloelectron Volt
$T_{1/2}$: half-life of the nuclides
abs. unc.: absolute uncertainity
rel. unc.: relative uncertainity
single line: a nuclide having only one decay sheme, hence, it is not influenced by true coincidence

5.3. Validation of the 186 keV peak for accurate ^{226}Ra determination

After the low-level counting system (Chapter 5.2.1.), the HDPE sample containers (Chapter 5.2.2–5.2.4.) and the FEP efficiency for extended sources (Chapter 5.2.5.) had been tested and calculated, the measurement system developed was considered appropriate for the investigation of the secular equilibrium and uranium isotopic ratio and for the validation of the 186 keV peak for acccurate ^{226}Ra detemination in the nine coal slag samples.

5.3.1. Preparation of coal slag samples

The coal slag samples, weighing between 81 and 127 g were air-dried. The variation in the masses was due to some differences in grain sizes. They were poured into radon-leakage-free HDPE containers (Kis et al., 2013) and sealed for at least 24 days in order to reach secular equilibrium between the radium and its progenies, ^{214}Pb and ^{214}Bi (Figure 9). The sample containers were fully filled to maintain a constant geometry.

5.3.2. Calculations used for the validation

Ebaid (2010) carried out the determination of the ^{235}U activity concentration from the 186 keV peak which has an interference with ^{226}Ra (Appendix 10). Based on the measured spectral data, the activity concentration of ^{235}U was calculated using the following equation (Eq. 8):

$$A_{U-235} = 1.75\left(\frac{CR_{Total\,(186.1keV)}}{\varepsilon_{186keV}}\right) - 0.063(A_{Ra-226}) \qquad \textit{(Equation 8)}$$

where $A_{Ra\text{-}226}$ is calculated using its daughters (Eq. 9):

$$A_{Ra-226} = \frac{CR_{Pb-214,Bi-214}}{\varepsilon_{Pb-214,Bi-214} \times I_{Pb-214,Bi-214}} \qquad \textit{(Equation 9)}$$

where:

$A_{U\text{-}235}$ and $A_{Ra\text{-}226}$ are the activity concentrations of ^{235}U and ^{226}Ra in Bq kg^{-1};

CR is the counting rate in full-energy peak, count s^{-1} (cps);

ε is the detection efficiency at energy ε_i, taking into consideration true coincidence summing effects;

I_i is the emission probability (intensity) of the gamma line of energy ε_i.

These results directly provide the ^{226}Ra activity concentration value since we have avoided any radon leakage. This methodology enables the determination of ^{235}U activity concentration

from Eq. 8. To determine the ^{238}U activity concentration, we used the line following the decay of ^{234m}Pa with an energy of 1001.2 keV (Eq.10):

$$A_{U-238} = \frac{CR_{Pam(1001\,keV)}}{\varepsilon_{Pam(1001\,keV)} \times I_{Pam(1001\,keV)}} \qquad \textit{(Equation 10)}$$

Hence, the uranium activity ratio and the isotopic ratio can be calculated according to Eq. 11 using the ratio of Eq. 8 and Eq. 10:

$$\frac{A_{U-235}}{A_{U-238}} = \frac{eq.8}{eq.10} \qquad \frac{N_{U-235}}{N_{U-238}} = \frac{A_{U-235}}{A_{U-238}} \frac{\lambda_{238}}{\lambda_{235}} \qquad \textit{(Equation 11)}$$

where N and λ are the number of atoms and the decay constant of the isotopes, respectively.

Determining the uranium activity ratio in the above way requires time (~30 days), due to the necessary condition of reaching secular equilibrium between ^{226}Ra and its progenies. However, the measurement time for ^{226}Ra could be shortened for the rest of the samples if it can be proven, for a group of the similar samples, that there is secular equilibrium between ^{238}U and ^{226}Ra. Furthermore, if it can be verified that the use of the 186 keV peak for a fast radium determination is reliable, this then means the results of the fast (radium measured from its 186 keV peak) and slow (radium measured from the result of the radon decay-products) methods are in good agreement. In this case, there is no need to seal the sample holder and wait for about 30 days, but the measurement can be begun immediately after filling the sample holder.

To test for secular equilibrium in the ^{238}U decay chain, the ^{226}Ra activity concentration was calculated from the radon daughter peaks (Eq. 9) and then compared to the ^{238}U results obtained from the 1001.2 keV peak following ^{234m}Pa decay (Eq. 10). If the activity concentrations gained are equal, then secular equilibrium has been established, and instead of the activity concentration of ^{226}Ra, the activity concentration of ^{238}U can be used in the formula (Eq. 8). To follow this, one can start with Eq. 12, which says that the total count rate of the 186 keV peak is composed of the counts of ^{235}U and ^{226}Ra:

$$CR_{U-235,186keV} = CR_{total,186keV} - CR_{Ra-226,186keV} \qquad \textit{(Equation 12)}$$

and dividing it by $CR_{Ra\text{-}226}$ gives Eq. 13:

$$\frac{CR_{U-235,186keV}}{CR_{Ra-226,186keV}} = \frac{CR_{total,186keV}}{CR_{Ra-226,186keV}} - 1 \qquad \textit{(Equation 13)}$$

The ratio of the count rates of ^{235}U and ^{226}Ra in the total count rate of the 186 keV peak is also described by Eq. 14:

$$\frac{CR_{U-235,186keV}}{CR_{Ra-226,186keV}} = \frac{A_{U-235} I_{U-235,186keV} \varepsilon_{186keV}}{A_{Ra-226} I_{Ra-226,186keV} \varepsilon_{186keV}} \qquad \textit{(Equation 14)}$$

From Eq. 13 and 14:

$$CR_{Ra-226,186keV} = \frac{CR_{total,186keV}}{\frac{A_{U-235}}{A_{Ra-226}} \times \frac{I_{U-235,186keV}}{I_{Ra-226,186keV}} + 1} = \frac{CR_{total,186keV}}{\frac{A_{U-235}}{A_{U-238}} \times \frac{I_{U-235,186keV}}{I_{Ra-226,186keV}} + 1} \qquad \textit{(Equation 15)}$$

Using Eq. 15 has the advantage that one can use the activity concentration ratio between uranium isotopes, which has previously been determined. Thus, the 186 keV peak can be used for the determination of the ^{226}Ra activity concentration using Eq. 15 because the invariability of the uranium activity ratio determined previously is assumed.

If abundances are not disturbed then, based on Ebaid et al. (2005), the activity concentration ratio ($A_{U\text{-}235}/A_{U\text{-}238}$) is 0.0462. Furthermore, if ^{226}Ra and ^{238}U are in secular equilibrium then the proportions of the count rates in the unresolved doublet peak at 186 keV peak for ^{226}Ra and ^{235}U are 58.3% and 41.7%, respectively. Based on the calculations these proportions and the applicability of the 186 keV peak for radium determination could be verified.

The nuclear data used for the activity concentration determinations are seen in Appendix 10 (Bé et al., 2013, Janis, 2013). The most intense and easily measured lines of ^{234m}Pa, ^{226}Ra, ^{214}Pb and ^{214}Bi isotopes were used, preferring those which are interference free. If there was a non-negligible spectral interference then its effect was taken into account. Only those lines of ^{214}Pb and ^{214}Bi were used in the calculations which gave a calculated standard deviation uncertainty in the activity concentration value of ≤5%. This constraint resulted in a different number of lines being used from sample to sample, according to the counting rate levels and the acquisition time lengths. The true coincidence correction factors valid for the given gamma transitions were taken from the module of EFFTRAN 1.2 for each sample, separately.

5.4. Methods used for the analysis of attic dust samples

5.4.1. Laboratory method

Aqua regia extraction was applied in an open vessel system to dissolve the material at the Laboratory of the Hungary Geological Institute. An amount of 0.25 g of powdered substance (grain size <0.063 mm) was selected from each sample and 5 ml aqua regia (3:1=HCl:HNO_3) was added (Bertalan et al., 2003). The aliquots were boiled in a water bath for c. 1 hour. Thereafter, 3 ml HCl and distilled water were added to a total of 50 ml (concentration of 5 g/l). Arsenic, Cd, Cu, Ni, Pb and Zn, and major element concentrations were quantified by ICP-OES (JobinYvon Horiba Ultima 2C). Mercury was quantified by AAS with the direct combustion method (AMA-254 Advanced Mercury Analyser, Altec Ltd.). The samples were heated in an oxygen stream to 800–850 °C. Mercury is released from the sample within a few seconds at this temperature, and an Au-amalgamator collects the Hg in its vapor phase. Oxides produced during the disintegration were sorbed to the catalyst. Mercury is thereafter liberated from the surface of the amalgamator at 900–950 °C and the produced Hg-vapor can be detected with the cold vapor atomic absorption method (CV-AAS), thus avoiding matrix effects. Analytical quality was checked using certified reference materials (GBW 07109-GBW07114, Wepal, IAEA 356 and Mostar). The coefficient of variation for reference materials was always below 10%. Laboratory duplicates confirmed that the uncertainty remained in the 10% range.

5.4.2. Statistical data analysis

Robust statistics were used in this study since geochemical data series often display non-normality, heterogeneity and outliers. Tukey (1977) resistant five-letter summary statistics, containing the minimum, lower quartile, median, upper quartile and the maximum values, were calculated and displayed using box-and-whiskers plots (e.g. Table 19 and Figure 16). To compare the overall variability of trace elements in the samples, their relative variability, represented by values of robust inter-quartile range per median (IQR/Md), were compared. The Range/Md measure was used to characterize extreme concentrations related to point-source contamination.

Assuming that natural dust contains wind-blown soil and surface rock particles (Gosar et al., 2006), the mineralogical and chemical composition of dust trapped in attics should reflect local and regional rock, soil and sediment geochemistry. Lacking regional dust survey results, it is reasonable to compare the measured attic dust composition to available geochemical soil and

sediment background data. Taking into account the size of the studied area (48 km^2), data were compared first on a regional scale with the Hungarian regional geochemical background (hereinafter referred to as HRGB) values (Ódor et al., 1996) and also with the more expanded European mean topsoil levels (FOREGS atlas, Salminen et al., 2005). Enrichment factors were computed by dividing the element concentration in the dust sample by the HRGB level (EF, $Md_{element}$/Regional background $value_{element}$), available from the stream sediment-based Hungarian Geochemical Atlas (Ódor et al., 1996). Stream sediments collected at the catchment outlet location represent the eroded upstream rock, soils and sediments of the upper crust (Darnley et al., 1995). However, special attention needs to be given to data interpretation, when comparing geochemical composition of different geological materials.

There are no environmental limitations for airborne dust. In my thesis , the Hungarian national pollution limit values for geological materials (soil and sediments; Joint Government decree, 6/2009) were used for a preliminary health risk assessment, assuming that wind-blown dust collected in attics primarily originate from soil and airborne anthropogenic particles (Zacháry et al., 2012). The data were also tested for heterogeneity. Sub-populations were identified using the natural brake method, based on cumulative histogram analysis according to Reimann et al. (2008). The natural brake is an inflexion point in the cumulative distribution function, which corresponds to the local minimum in the frequency histogram (multi-modal histogram; e.g. Figure 16).

Assuming that a homogeneous distribution represents a single stochastic process such as anthropogenic trace metal contamination from a single source or the natural geochemical background, each identified sub-population may reveal a geochemical process in the univariate data space. Separation of sub-populations was confirmed at the 95% confidence level by the Mann-Whitney (Wilcoxon) homogeneity test (Mann and Whitney, 1947) based on the comparison of medians. Outlying values were determined by the Tukey (1977) inner-fence criterion. These values represent sudden and unusual events, essential to identify elements as a contaminant at point sources. The Tukey (1977) inner-fence criterion was used for outlier definition. The summary statistics were calculated separately for the original data series and the identified sub-populations. The statistical analyses were performed using the Statgraphics Centurion XV software.

Attic dust concentration groups were plotted on maps to assess the spatial distribution of contaminated dust and its possible association with industrial sources. A further spatial

characterization of the trace elements, using contour maps, was generated with the linear and accurate Triangular Irregular Network (TIN) interpolation method (Guibas and Stolfi, 1985). A grid size of 25 m was used, based on the shortest distance between the closest two samples. Successive moving average smoothing was applied to generalize the TIN model and to capture the major spatial trends of attic dust contamination distribution. The single high values were removed from the interpolation procedure. Local maxima and minima in the interpolated surfaces were accepted only if they were defined by at least two samples. Thus, local extremeties, represented by a single outlying value, did not affect the smoothed interpolated contamination trend surface maps.

5.5. Correlation analysis used for both sampling materials.

The relationships between the measured parameters were studied with Pearson's correlation coefficient (Pearson, 1896), using the robust interactive outlier rejection regression method. No more than 10% of bivariate outliers were rejected in all cases. All correlations were checked visually using the regression bivariate scatter plots and all the correlations discussed were significant at the 95% confidence level. Correlations, possibly induced by the action of a background variable, were checked by means of partial correlations.

6. Methodology for improving the accuracy of ^{226}Ra determination of building material samples

6.1. Results of the HDPE sample holder test and the FEP efficiency transfer

Taking into account that accurate radium determination and the qualification of building materials are the main aims of the research, measurement improvement is described earlier in the thesis. However, measurements at Eötvös University (Department of Atomic Physics) were performed earlier in time and inspired the measurement improvement at the Centre for Energy Research, Hungarian Academy of Sciences.

To determine the decay constant of the saturation curve, a regression model ('saturation curve fitting'; Eq. 5) was fitted on three different strong gamma lines of radon daughters from the KSZPF1 test soil sample (Figure 11and Table 6). The result of the regression model represents the presence of any possible radon leakage from the sample holder.

Table 6 The results of the curve fitting for three different strong lines of the daughters of ^{222}Rn.

Statistics for the decay constant (n=3; DF=2; p=0.05; Student-t)	Arithmetic mean	295 keV	609 keV	1764 keV
$\lambda_{measured}$ (min^{-1})	1.257E-04	1.239E-04	1.265E-04	1.261E-04
std. err.	7.895E-07	2.360E-06	2.120E-06	5.270E-06
λ + (2.92 × std. err.)*	1.280E-04			

*: 95% confidence limit on $\lambda_{measured}$
λ: decay constant
keV: kiloelectron Volt

After the fitting of the parameters of Eq. 1 (Chapter 5.2.4.) to determine the decay constant of the saturation curve, the 1σ value of the arithmetic mean of the three λ values is given as a standard error. Because the sample size (n=3, is the three different strong lines of radon daughters; Table 6) is rather low, the confidence interval at p=0.05 level (only 5% probability for an error of the first kind) could be calculated on the Student-t distribution.

Because leakage can only increase the value of the apparent decay constant, I considered the one-sided t-distribution with a degree of freedom (DF) of 2. Hence, the multiplication factor in the hypothesis test is 2.92 instead of the usual 1.96, which latter is based on a Gaussian distribution for large sample size.

The value of the decay constant for ^{222}Rn radioactive decay in the literature is $\lambda_{decay} = 1.259 \times 10^{-4} \pm 2.635 \times 10^{-8}$ min^{-1} (Bé et al., 2013). Based on this value, the leakage effect

can be assessed. If, for example, the leakage rate was 1.83% of the radioactive decay constant then the measured decay constant $\lambda_{measured}$ would be equal to 1.280×10^{-4} min^{-1}. Having compared this value to the confidence interval ($\lambda + 2.92 \times$ std. err. $= 1.280 \times 10^{-4}$ min^{-1}) from Table 6, one can state the following. Assuming that the null hypothesis (i.e. there is no radon leakage from HDPE holder) is true, then the probability of obtaining a result for the radon leakage rate being larger than the 1.83% of the radioactive decay constant of ^{222}Rn is less than 5%. Therefore, the assumption that the HDPE container is well-sealed against radon leakage is justified.

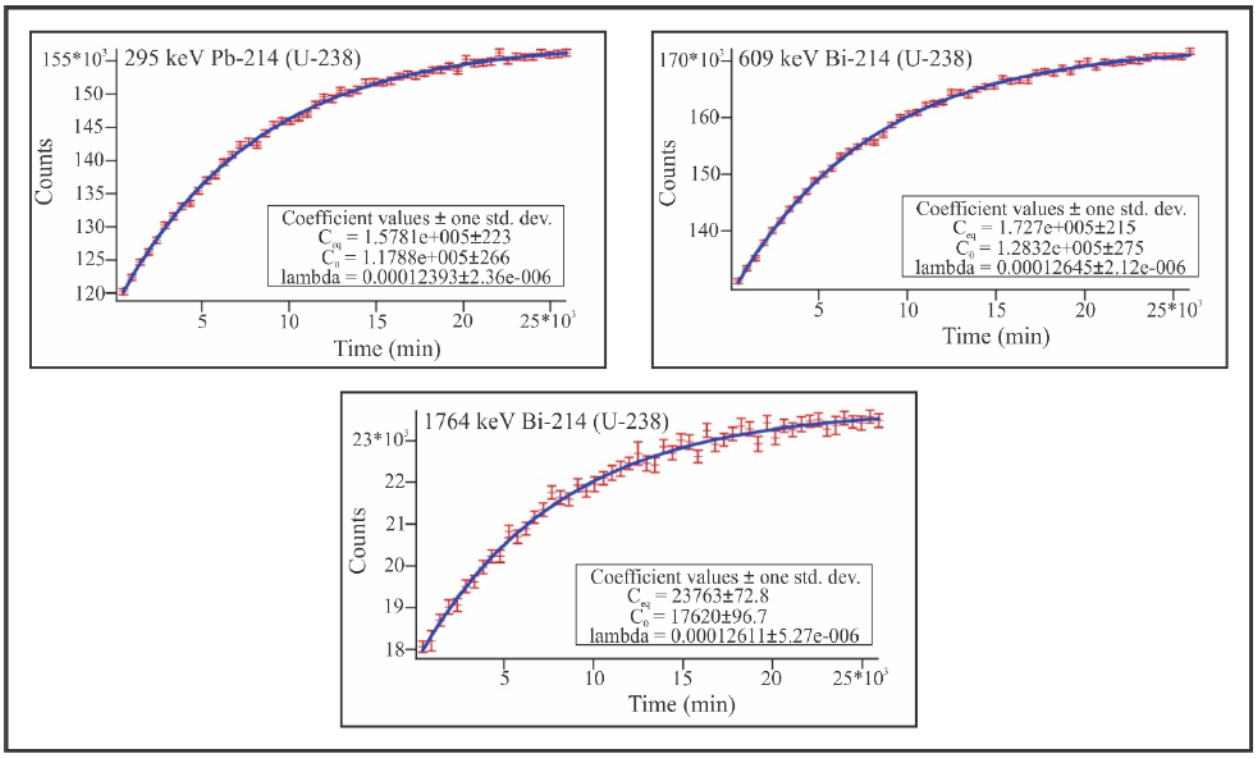

Figure 11. Result of the curve fitting (Eq. 1) of three strong lines of radon decay products, a, 295 keV; b, 609 keV; c, 1764 keV.

After following the three-step process outlined in Chapter *5.2.2.*, one obtains the FEP efficiency curves in Figure 12 for the close extended geometry (Sample) and the reference geometry of the point sources (Standard) at 167 mm distance from the HPGe detector as results from the calculations of EFFTRAN 1.2 code. These results are now free of the biasing of true coincidence summing effects. In this validation calculation, the HDPE sample container was filled with water of a density of 1 g cm^{-3}. As expected, the close-in geometry yields significantly higher FEP efficiency. The validation of the process is carried out based on the data in Table 7. Here the FEP efficiency values coming from EFFTRAN 1.2 are compared to those values from the measurement of a standard water solution. The FEP efficiency values from the standard solution

were corrected for the true coincidence summing effects by multiplying those with the F_{COI} values (see Chapter 5.2.5). The ratio of the efficiency values determined in these two different ways (EFFTRAN/measured) is around 1, signaling a good agreement (Table 7).

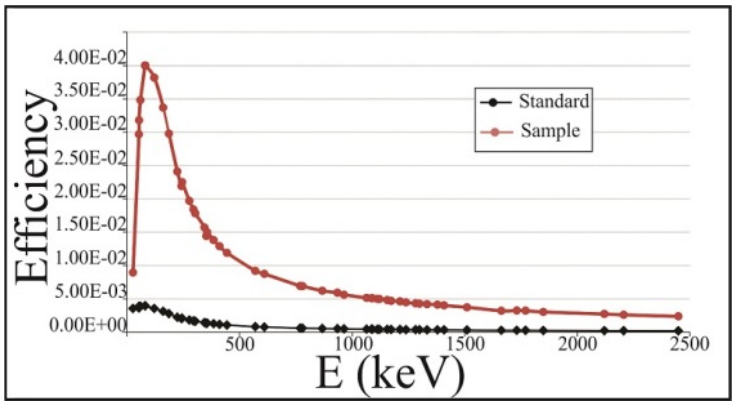

Figure 12. The results of the EFFTRAN 1.2 code after following the three step process, showing the FEP efficiency curves for the water solution sample in close extended geometry (Sample) and the reference geometry of the point sources (Standard) at 167 mm from the HPGe detector.

Table 7. Comparison of the efficiency values from the measurement of a standard water solution (ERX5-Ba, activity reference time: 17 July 2008, volume: 105.12 4mL, source-detector distance: 2.2 mm, measurement time: 98.82 h) with the FEP efficiency values from the EFFTRAN 1.2, (Kis et al., 2013).

Nuclide	energy (keV)	peak area (counts)	rel. unc (%)	efficiency measured	rel. unc (%)	F_{COI}	F_{COI}_corr. efficiency	efficiency EFFTRAN	unc. of eff. EFFTRAN	EFFTRAN / measured	rel. unc (%)
single line											
^{241}Am	59	1364633	0.1	4.12E-02	1.53	1	4.12E-02	4.26E-02	5.71E-03	1.035	13.49
^{109}Cd	88	16792	1.5	4.30E-02	3.22	1	4.30E-02	4.38E-02	4.12E-03	1.019	9.95
^{57}Co	122	40262	0.7	3.97E-02	0.83	1	3.97E-02	4.00E-02	3.35E-03	1.008	8.41
^{137}Cs	661	562084	0.2	7.59E-03	0.64	1	7.59E-03	8.07E-03	5.62E-04	1.063	6.99
^{54}Mn	834	7508	2.1	6.19E-03	2.18	1	6.19E-03	6.51E-03	4.45E-04	1.051	7.18
not single line											
^{133}Ba	276	21634	1.0	1.55E-02	2.26	1.29	2.00E-02	2.02E-02	1.44E-03	1.011	7.49
^{133}Ba	302	51368	0.5	1.44E-02	2.09	1.24	1.78E-02	1.83E-02	1.27E-03	1.027	7.26
^{133}Ba	356	151564	0.3	1.25E-02	2.05	1.17	1.47E-02	1.54E-02	1.05E-03	1.051	7.11
^{133}Ba	383	23700	1.0	1.36E-02	2.26	1.04	1.41E-02	1.41E-02	9.57E-04	0.998	7.16
^{60}Co	1173	393318	0.2	4.34E-03	0.45	1.05	4.55E-03	4.79E-03	3.10E-04	1.052	6.49
^{60}Co	1332	349602	0.2	3.86E-03	0.45	1.05	4.05E-03	4.27E-03	2.84E-04	1.055	6.66

keV: kiloelectron Volt
rel. unc.: relative uncertainity
eff.: efficiency
single line: a nuclide having only one decay sheme, hence, it is not influenced by true coincidence

6.2. Discussion of the HDPE sample holder test and the FEP efficiency transfer

The experimental application of a growth curve method, measuring radon gas in a sample holder, was performed by Szabó (2014) and Sakoda et al. (2008), in which radon emanation and potential radon leakage from sample holders, using radon monitors, was tested. The long-term (~18 days) acquisition of gamma lines following the decay of radon progenies to study the radon leakage of sample holder is novel (Figure 11). Note, a sample with very high radium content (>8000 Bq kg^{-1}) and high radon emanation rate was essential for this analysis.

The simplicity and practicability of the sealing method has a clear advantage compared to other methods. The methods providing similar tightness to this demanded sealing which uses either vacuum packaging in aluminum lined bags or adhesive that fuses the lid to the beaker (Mauring and Gäfvert, 2013). Manolopoulou et al. (2003) measured radon leakage from a Marinelli beaker by enclosing the samples in a small radon chamber (~0.1 m^3) and using Lucas cells for radon concentration monitoring. The use of samples mixed with charcoal would be a useful method given that they found only a very small amount of escaping radon using charcoal mixed with a phosphate fertilizer and soil sample. The use of Marinelli beakers can lead to better efficiency, but it requires greater sample sizes and increases the costs of these measurements (Manolopoulou et al., 2003).

It has also been proven that the use of the efficiency transfer method together with true coincidence correction for extended samples in close-in geometry provides the possibility of measuring samples with rather different geometry, material composition and density. The differences between the efficiency obtained by the EFFTRAN method and the measured solution, which are usually <5%, could be attributed to several effects:

(i) lack of an accurate knowledge of the detector dimensions;
(ii) a slight misalignment of the detector setup;
(iii) neglecting the low-energy X-rays, which can penetrate the detector material through the wall of the container, causing true coincidence events.

The necessity of coincidence-summing corrections for the full-energy peak efficiency values was highlighted also in García-Talavera et al. (2001) and Daza et al. (2001).

6.3. Results of the methodology improvement tested on coal slag samples

In the previous Chapters (6.1. and 6.2.), the applicability of the measurement system have been demonstrated. Thus, the coal slag samples from Ajka and Budapest (Figure 5) can be studied to evaluate the isotopic abundance, secular equilibrium and, as a result, the validation of the usage of 186 keV for quick and accurate radium determination.

6.3.1. Results of the uranium activity concentration ratio

The results of the activity concentration ratio (^{235}U and ^{238}U) measurements for the test coal slag samples (from Budapest and Ajka) are shown in Table 8. The weighted average activity ratio of all the 9 samples is 0.0466 ± 0.003, which may be further separated into samples from Budapest (average: 0.0496 ± 0.085) and from Ajka (0.0455 ± 0.0041).

Table 8. The results of the activity concentration ratio (^{235}U and ^{238}U) measurements for the studied samples.

Sample	Weight (g)	A_{U-235}	Unc. (%)	A_{U-238}	Unc. (%)	A_{U-235}/A_{U-238}	Unc. (%)	Unc.
T_CS_Bp_1	104.5	5	5	80	21	0.0569	22	0.0123
T_CS_Bp_2	81.6	25	5	522	6	0.0488	8	0.0037
T_CS_Bp_3	92.6	14	5	246	11	0.0560	12	0.0067
T_CS_Bp_4	105.7	11	5	256	10	0.0443	11	0.0048
CS_AJK_1	127.1	48	5	1045	5	0.0462	7	0.0032
CS_AJK_2	91.0	91	5	2181	5	0.0419	7	0.0029
CS_AJK_3	94.4	145	5	3155	5	0.0460	6	0.0030
CS_AJK_4	114.6	10	5	216	11	0.0483	12	0.0060
CS_AJK_5	85.5	66	5	1403	5	0.0471	7	0.0033
Weighted avg. Budapest						0.0496	17	0.0085
Weighted avg. Ajka						0.0455	9	0.0041
Weighted avg. all						0.0466	6	0.0030

unc: uncertainty
avg.: average
A: Activity concentration
Equations (1) and (3) were used for the calculations. The weighted averages were calculated as $\Sigma_i \text{value}_i/\sigma_i^2 / \Sigma_i 1/\sigma_i^2$, where value = A_{U-235}/A_{U-238} and σ = Unc. (%) of A_{U-235}/A_{U-238}
'T_CS' means test coal slag samples used only for the methodology improvement.

6.3.2 Results of ^{238}U-^{226}Ra secular equilibrium

Since the sample holders used were considered as radon-leakage-free (Chapter 6.1.) the activity concentrations of radon daughters provide reliable values for ^{226}Ra activity concentrations. It is seen that the ^{226}Ra/^{238}U values match, within the limits of uncertainties, except for one sample (CS_AJK_2). The other samples lie on the $f(x)=x$ line on Figure 13.

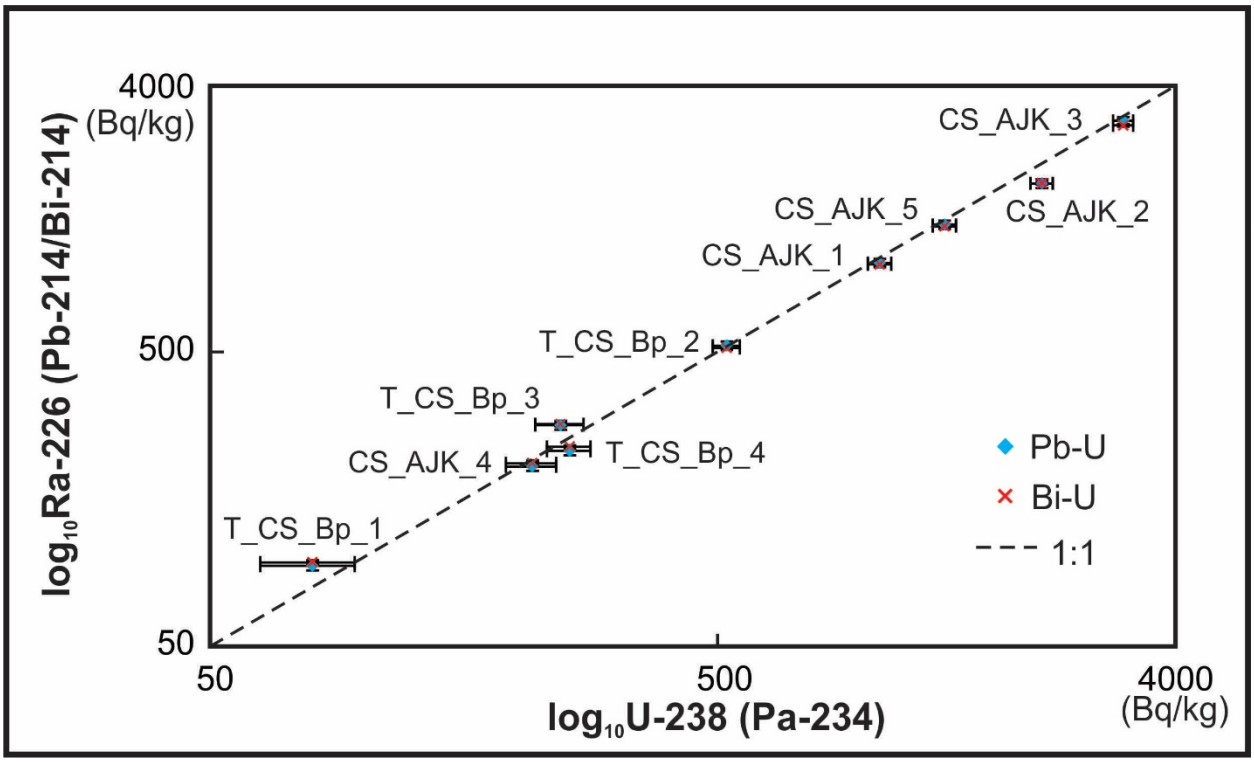

Figure 13. ^{238}U activity concentrations measured according to the 1001.2 keV peak of the ^{234m}Pa daughter vs. ^{226}Ra activity concentration measured by the peaks of radon daughters (^{214}Pb and ^{214}Bi). The Ajk2 sample displays a notable difference from the other samples. The dashed line is the $f(x)=x$ line. 'T_CS' means test coal slag samples, used only in the methodology improvement.

Based on the results presented above (Figure 13), the natural uranium isotopic abundance (Chapter 6.3.1. and Table 8) and the ^{238}U–^{226}Ra secular equilibrium are present in 8 coal slag samples (Figure 13 and Table 9) and, hence, their ^{226}Ra content can be determined using the 186 keV spectral peak with acceptable precision. To verify this, the estimated activity concentration of ^{226}Ra measured against its own contribution to the peak at 186.2 keV and the activity concentration of the ^{226}Ra calculated from the peaks of radon daughters were compared (Figure 14). Table 9 summarizes all measured data for detailed information.

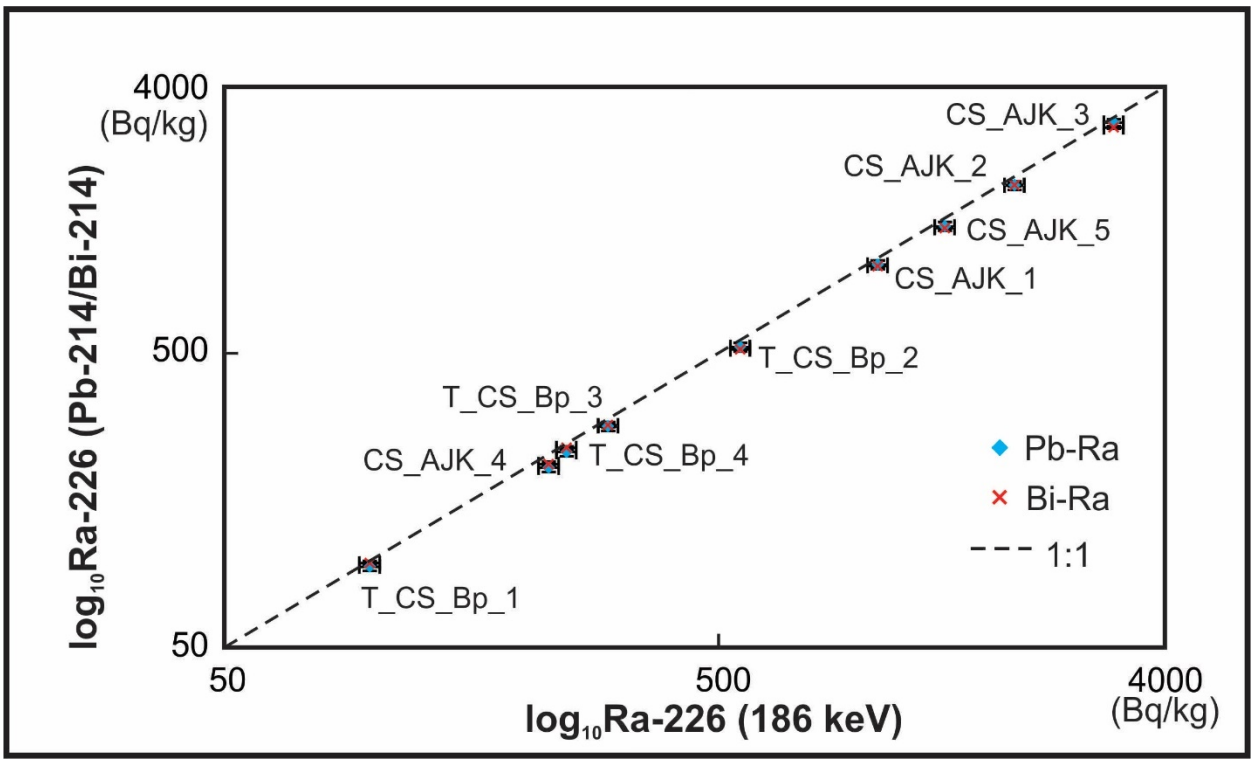

Figure 14. ^{226}Ra activity concentration measured by its own peak at 186 keV vs. ^{226}Ra activity concentration measured by the peaks of radon daughters (^{214}Pb and ^{214}Bi). The dashed line $f(x)=x$ line. 'T_CS' means test coal slag samples, used only in the methodology improvement.

Table 9. The ^{238}U and ^{226}Ra activity concentrations of the studied coal slag samples.

Sample	$A_{U\text{-}238}$ ^{234m}Pa, 1001 keV (Bq kg^{-1})	Unc. (Bq kg^{-1})	Unc. (%)	$A_{Ra\text{-}226}$ 186 keV (Bq kg^{-1})	Unc. (Bq kg^{-1})	Unc. (%)	$A_{Ra\text{-}226}$ ^{214}Pb (Bq kg^{-1})	Unc. (Bq kg^{-1})	Unc. (%)	$A_{Ra\text{-}226}$ ^{214}Bi (Bq kg^{-1})	Unc. (Bq kg^{-1})	Unc. (%)
T_CS_Bp_1	80	17	21	98	5	5	94	3	3	97	2	2
T_CS_Bp_2	522	32	6	553	25	5	525	18	3	515	5	1
T_CS_Bp_3	246	27	11	299	14	5	282	10	4	284	4	1
T_CS_Bp_4	256	25	10	246	11	4	231	8	3	238	3	1
CS_AJK_1	1045	55	5	1049	48	5	1001	34	3	990	10	1
CS_AJK_2	2181	112	5	1991	91	5	1862	63	3	1867	17	1
CS_AJK_3	3155	143	5	3152	144	5	3044	82	3	2933	26	1
CS_AJK_4	216	25	11	227	11	5	204	7	3	210	5	2
CS_AJK_5	1403	74	5	1435	66	5	1351	45	3	1333	13	1

Unc.: uncertainty
keV: kiloelectron Volt
'T_CS' means test coal slag samples, used only in the methodology improvement.

6.4. Discussion of the methodology improvement tested on coal slag samples

It turns out that the uranium activity ratio value 0.0462 given in the literature (Ebaid et al., 2005; Condomines et al., 2007) lies within the standard deviation of the measured average ratios. This normal value was not surprising because the uranium activity ratio is considered as a constant in environmental circumstances, which does not even change after burning the coal in power plant furnaces. Differences can be found in samples affected by anthropogenic activities (e.g. the nuclear industry, atomic wapons) and, therefore, used, for instance in nuclear forensic sciences to identify potential sources of uranium (Kristo and Tumey, 2013). Based on these, it can be concluded that the samples have the natural isotopic abundances for these two uranium isotopes and, hence, an overall activity concentration ratio is applied during the calculations.

Almost all samples are close to the $f(x)=x$ line (Figure 13), which clearly indicates that ^{238}U and ^{226}Ra are in secular equilibrium in the majority of the samples. As ^{226}Ra results determined from the 186 keV peak are similar to those from the ^{222}Rn daughters (Figure 14 and Table 9); ^{226}Ra activity concentration measured using the 186 keV peak also gives reliable values. If the data presented in Figures 13 and 14 are compared the CS_AJK_2 sample shows almost the same results in terms of the Ra measured from the 186 keV peak and from the radon daughters, suggesting an equilibrium in the radium and Rn daughters. In contrast, a difference is observed between the uranium and radon decay products. It verifies the disequilibrium between ^{238}U and ^{226}Ra in this sample.

The equilibrium between ^{226}Ra and ^{238}U in coal slag samples is rarely studied. An example is Karangelos et al. (2004), who showed equilibrium in bottom ash samples collected in a Greek CPP. The existence of secular equilibrium depends strongly on geochemical conditions, which can be explained in terms of the presence and mineralization of uranium in the coals and the geochemical behavior of elements in the ^{238}U decay chain. Radium and uranium can both associate organically and inorganically in coals (e.g. Coles et al., 1979; Eskenazy and Velichkov, 2012). Radium and uranium are organically bound with the humins, fulvo and humic acids or sorbed to the organic matter (Eskenazy and Velichkov, 2012). The inorganic association of radium includes surface adsorption to clay minerals and Fe-Al-hydroxides and co-precipitation with barite (Eskenazy and Velichkov, 2012).

Coal generally contains uranium in two different solid phases including uraninite (UO_2) and coffinite ($USiO_4$, Coles et al., 1978; Karangelos et al., 2004). It is widely known that uraninite

forms from soluble uranil carbonate after reduction and coffinite precipitates if sufficient silica is present in the solution during coal diagenesis. These geochemical processes and the conditions of the coal burning control the volatility of the uranium upon combustion. If the uranium is present mostly in the silicate phased coffinite it will remain in the coal slag after combustion. If it is associated with uraninite, which is easily volatilized under the oxidizing conditions during combustion, uranium will be present mostly in the fly ash fraction (Papastefanou, 2010). The so-called bimodal behavior of these nuclides in coals leads to the differing enrichment of the by-products (Coles et al., 1978; Coles et al., 1979; Karangelos et al., 2004; Manolopoulou and Papastefanou, 1992; Papastefanou, 2010). Radium-226, geochemically behaving in a similar way to the uranium in the process, will remain in the coal slag if it is associated with clays, inorganic compounds and the coffinite form of uranium in the coal. When ^{226}Ra associates with uraninite in the coal it can be volatilized as $Ra(OH)_2$ and enriched in the fly ash. Coles et al. (1978) observed a slight enrichment of ^{226}Ra in the fly ash fraction, where radium probably associated with uraninite. All these considerations indicate that in 8 of the 9 samples studied (except CS_AJK_2, Figure 13 and Table 9) the ^{238}U and ^{226}Ra were most probably in the same mineral phase in the coal burned in the Hungarian CPPs and, hence, there was no impetus to change the activity concentration ratio of these two isotopes. However, another possible explanation of the same behavior also exists, that the radium has not left the melted crystal phase during combustion and it remained in the glass phase of the coal slag together with uranium.

Some tiny discrepancies can be observed but none of the 8 samples shows any clear evidence of disequilibrium (Figure 13 and Table 9). Taking into account the uncertainty (statistical and systematic) of the results, a slightly modified equilibrium exists between the ^{238}U and ^{214}Bi even in the T_CS_Bp_3 and CS_Ajk_3 samples (Table 9).

A statistically significant difference was observed between the concentration of ^{222}Rn daughters and ^{238}U in the CS_AJK_2 sample (Figure 13 and Table 9). This might be due to the different geochemical behavior of the ^{238}U and ^{226}Ra isotopes during the carbonization process and during combustion (depending on the burning characteristics of the furnace), additionally, due to the chemical and physical properties of the coal (Coles et al., 1978; Karangelos et al., 2004). Some authors show that the equilibrium can be disturbed in coal before combustion (Coles et al., 1978; Eskenazy and Velichkov, 2012; Tadmor, 1986 and references therein). However, other works find a good secular equilibrium state in the coal used as fuel in the coal-fired power plant (e.g. Hedwall

and Erlandsson, 1996; Karangelos et al., 2004). According to Coles et al. (1978) and Karangelos et al. (2004), the secular equilibrium in the by-products is significantly disturbed rather by the end members of the ^{238}U decay chain.

It should be highlighted that coal slags represent a specific group of environmental samples for the study of secular equilibrium with anthropogenic influences, where, based on the hypothesis of the present work, the distortion of secular equilibrium between uranium and radium was assumed. As the results show, coal slags were considered as ideal subjects for be investigation, when the presence of secular equilibrium is sought. In other environmental samples, like samples in aquatic environment, uranium isotopes tend to remain in the dissolved phase, whereas thorium and, for example, lead isotopes are scavenged onto particles. This causes radioactive disequilibrium between the parent-daughter pairs (Th-Ra and Ra-Pb) and results selective incorporation in shells (Schmidt and Cochran, 2010). Water-rock interactions (Keith et al., 2007) and melting or crystallization processes may disturb the equilibrium between U, Th and Ra (Fabrizio et al., 2008, Hirosi et al., 2007). Radium-226 in the decay chain may have slightly different concentrations than ^{238}U because separation may occur between its parent ^{230}Th and uranium, and because radium has greater mobility in the environment (UNSCEAR, 2000). These examples indicate that a sufficient geochemical knowledge of the samples and their circumstances is inevitable.

Another positive feature of this material was that no radon diffusion and, hence, no inhomogeneity was observed within the sample holder, which phenomena is found to be widespread under such conditions. One possible explanation is that the unburned carbon behaved in the manner of activated charcoal in the sample holder and prevented radon diffusion and significant leakage. Based on Morawska and Phillips (1993), Breitner et al. (2010), Sakoda et al. (2010), the higher radium content does not necessarily cause higher emanation. If the radium is present in the crystal lattice the radon cannot escape. Radon emanation was found to be very low, despite the high radium content in coal slag samples analyzed by Somlai et al. (2006) and Jobbágy (2007). The biggest advantage of measuring coal slag samples is their relatively high radium activity concentration (>100 Bq kg^{-1}), which makes these measurement conditions more feasible.

6.5. Conclusion and further applications

In summary, if the uranium isotopic ratio is measured and the secular equilibrium state is proven for a group of samples, the 186keV spectral peak can be measured without a radon-tight sample holder and without the about 4 weeks waiting period for radium analysis of samples from the same source or with the same geochemical constitution. During the measurements at the Eötvös University (Department of Atomic Physics), the natural isotopic abundance between the uranium isotopes and the presence of the secular equilibrium between ^{238}U and ^{226}Ra were only assumed. The measurement system at the NARL enabled to verify these assumptions. Hence, the basic hypothesis, the measurement of radium content of the samples from the own peak of ^{226}Ra at 186 keV, is verified for the coal slag samples analyzed. Coal slag samples were considered the most likely candidates, due to the high radium content, but also the most sensitive, being possibly affected by secular disequilibrium, for study of the verification of 186 keV for accurate radium determination. Therefore, other building materials were not used in this methodology improvement. The reasons were the limited number and amount of these materials and the low radium activity concentration compared to coal slag samples. My experiment shows that the 186 keV peak can be successfully used, after corrections, to determine radium content of other building materials analyzed at Eötvös University, Department of Atomic Physics (all of coal slag concrete, brick, concrete from blocks of flats, gas silicate).

7. Results of radionuclide content and qualifications of building materials

7.1. In situ gamma dose rates

To give an overview of the gamma dose rates measured in the studied houses, their basic statistics should be first assessed (Table 10).

Table 10. Gamma dose rates (nSv h^{-1}) measured in the studied houses where the building materials were sampled. Results were measured at 0m and at 1 m height.

Material	Coal slag (n=15)		Gas silicate (n=6)		Coal slag concrete (n=3)		Brick (n=2)	
Height (m)	0	1	0	1	0	1	0	1
Average	195	180	126	120	152	156	145	147
Median	170	165	120	120	147	150	140	140
Minimum	73	110	80	70	120	120	70	80
Maximum	1000	500	200	180	230	260	230	250

The houses where coal slag or coal slag concrete was used have higher average concentrations (195 nSv h^{-1} and 152 nSv h^{-1} at 0 m, and 180 and 156 at a height of 1 m, respectively) than the gas silicate ones (126/120 nSv h^{-1}) or bricks (145/147 nSv h^{-1}). However, the values in houses using coal slag concrete or brick show quite similar results. The gamma dose rates measured in buildings made of concrete (from blocks of flats) and gas silicate without fly ash, were equal to the average indoor level (not indicated in Table 10). In general, the lowest data were estimated in the gas silicate houses, whereas the highest gamma dose rates were measured in houses where coal slag was used.

7.2. ^{226}Ra, ^{232}Th and ^{40}K activity concentration results

Activity concentrations (^{226}Ra, ^{232}Th and ^{40}K), hazard indices and dose valuations are presented with their calculated statistical uncertainties (Tables 11 and 12). To compare the measured hazard indices to their threshold values, two methods were applied:

(i) the index was considered itself ignoring its uncertainty, or

(ii) the index uncertainty was added twice to its value and then this sum was compared to reference values following advice from Stanis1aw Cha1upnik (personal communication, 2012; Rzeczypospolitej Polskiej, 2007). This is a safe, conservative procedure.

Both possibilities were considered, although this has importance only for samples with indices falling slightly below the threshold values. The average and median values provide generally important information in the study and qualify the members of the group. Nevertheless, the deviation of the average from the median refers to the symmetry of the distribution. Standard deviation helps describe whether a sample group is homogeneous or disparate. Therefore, whether the examined properties, such as activity concentrations and hazard indices, are connected to the building material making process, which was used for grouping the samples or something else (e.g. origin, locality of raw materials) may be determined in this way. In certain cases, it is quite difficult to obtain information on the latter. In those particular cases when the given standard deviation is larger than the average for the group of samples a high level of asymmetry in the distribution and/or some outliers is to be expected.

Table 11. Measured ^{226}Ra, ^{232}Th and ^{40}K activity concentrations of the studied building materials together with their uncertainties, averages and standard deviations. All radium results are based on the measurement of the 186 keV peak, including the 5 samples from Ajka city. Sample ID refers to the type of building material and the area of origin. Acronyms of B, CBF, CS, CSC and GS mark the types as brick, concrete (from block of flats), coal slag, coal slag concrete and gas silicate. GS_CHR_1 contains sand instead of fly ash. Acronyms of CHR and AJK indicate Central Hungarian region and Ajka, respectively (Figure 5).

Sample ID	location	$C_{Ra\text{-}226}$ (Bq kg^{-1})	$C_{Th\text{-}232}$ (Bq kg^{-1})	$C_{K\text{-}40}$ (Bq kg^{-1})
B_CHR_1	Budapest	32 ± 4	31 ± 2	484 ± 17
B_CHR_2	Százhalombatta	31 ± 4	31 ± 2	473 ± 18
CBF_CHR_1	Budapest	9 ± 2	7 ± 1	169 ± 6
CBF_CHR_2	Budapest	13 ± 2	5 ± 1	115 ± 6
CS_CHR_1	Budapest	2233 ± 54	43 ± 7	193 ± 22
CS_CHR_2	Budapest	210 ± 8	30 ± 2	282 ± 12
CS_CHR_3	Budapest	142 ± 7	53 ± 3	191 ± 10
CS_CHR_4	Budapest	182 ± 6	45 ± 2	178 ± 9
CS_CHR_5	Budapest	152 ± 6	37 ± 2	149 ± 7
CS_CHR_6	Budapest	345 ± 11	50 ± 3	221 ± 11
CS_CHR_7	Budapest	173 ± 7	22 ± 2	146 ± 9
CS_CHR_8	Budapest	106 ± 4	24 ± 1	147 ± 6
CS_CHR_9	Budapest	205 ± 9	74 ± 4	269 ± 13
CS_CHR_10	Budapest	96 ± 5	28 ± 2	201 ± 10
CSC_CHR_1	Budapest	251 ± 9	25 ± 3	62 ± 8
CSC_CHR_2	Budapest	19 ± 5	7 ± 2	36 ± 8
CSC_CHR_3	Kecskemét	54 ± 7	20 ± 3	110 ± 11
GS_CHR_1	Budapest	16 ± 4	9 ± 2	162 ± 11
GS_CHR_2	Dunaharaszti	42 ± 4	31 ± 2	131 ± 8
GS_CHR_3	Gödöllő	84 ± 7	42 ± 3	279 ± 15
GS_CHR_4	Kecskemét	44 ± 5	23 ± 2	126 ± 9
GS_CHR_5	Kiskunhalas	65 ± 6	37 ± 3	286 ± 15
GS_CHR_6	Kistarcsa	54 ± 7	23 ± 3	166 ± 14
GS_CHR_7	Sülysáp	67 ± 11	25 ± 5	269 ± 23
CS_AJK_1	Ajka	1049 ± 48	20 ± 1	127 ± 6
CS_AJK_2	Ajka	1991 ± 91	34 ± 1	146 ± 7
CS_AJK_3	Ajka	3152 ± 144	40 ± 2	74 ± 6
CS_AJK_4	Ajka	227 ± 11	34 ± 1	284 ± 10
CS_AJK_5	Ajka	1435 ± 66	25 ± 1	143 ± 7
median		*106 ± 7*	*30 ± 2*	*166 ± 10*
average ± st.dev.		*430 ± 783*	*30 ± 15*	*194 ± 104*

The measured ^{226}Ra, ^{232}Th and ^{40}K activity concentrations of the 29 artificial building materials, including 5 test samples used for the methodology development from Ajka (Table 11), show a rather inhomogeneous distribution, with averages and standard deviations of 430 ± 783, 30 ± 15 and 194 ± 104 Bq kg^{-1} and medians of 106, 30 and 166 Bq kg^{-1}, respectively. It is important to note that the distributions are not symmetric in many cases, hence, the medians usually are more informative than the averages. The activity concentration of ^{226}Ra in most of the coal slag samples is much higher (i.e. average: 780 ± 975 Bq kg^{-1}) than that in the other samples (i.e. gas silicates: 59 ± 16 Bq kg^{-1}; coal slag concretes: 108 ± 125 Bq kg^{-1}; bricks: 32 ± 0.8 Bq kg^{-1}, concrete from block of flats: 11 ± 3 Bq kg^{-1}). The samples from Ajka represent a group with extremely high Ra activity concentrations (1571 ± 1092 Bq kg^{-1}). Only the value of CS_CHR_1 sample (2253 ± 54 Bq kg^{-1}) is comparable to these results. Thorium-232 activity concentrations vary between 5-74 Bq kg^{-1}, of which concrete of block of flats, coal slag concretes and a gas silicate sample without fly ash additive show very low (< 25 Bq kg^{-1}) values. Potassium-40 values vary between 36 and 484 Bq kg^{-1}, two brick samples (B_CHR_1 and B_CHR_2), have the highest concentrations with 484 ± 17 and 473 ± 18 Bq kg^{-1}, respectively.

7.2.1. Correlation between the studied radionuclides

No correlation was observed between ^{226}Ra and ^{40}K in the samples, and the correlation coefficient between ^{232}Th and ^{40}K was very weak (r=0.29). However, the correlation between ^{232}Th and ^{226}Ra radionuclides was significant (r=0.57; Figure 15). There is a group, containing 5 coal slag samples, above the majority of the samples showing similar relationship, however having elevated radium content (Figure 15).

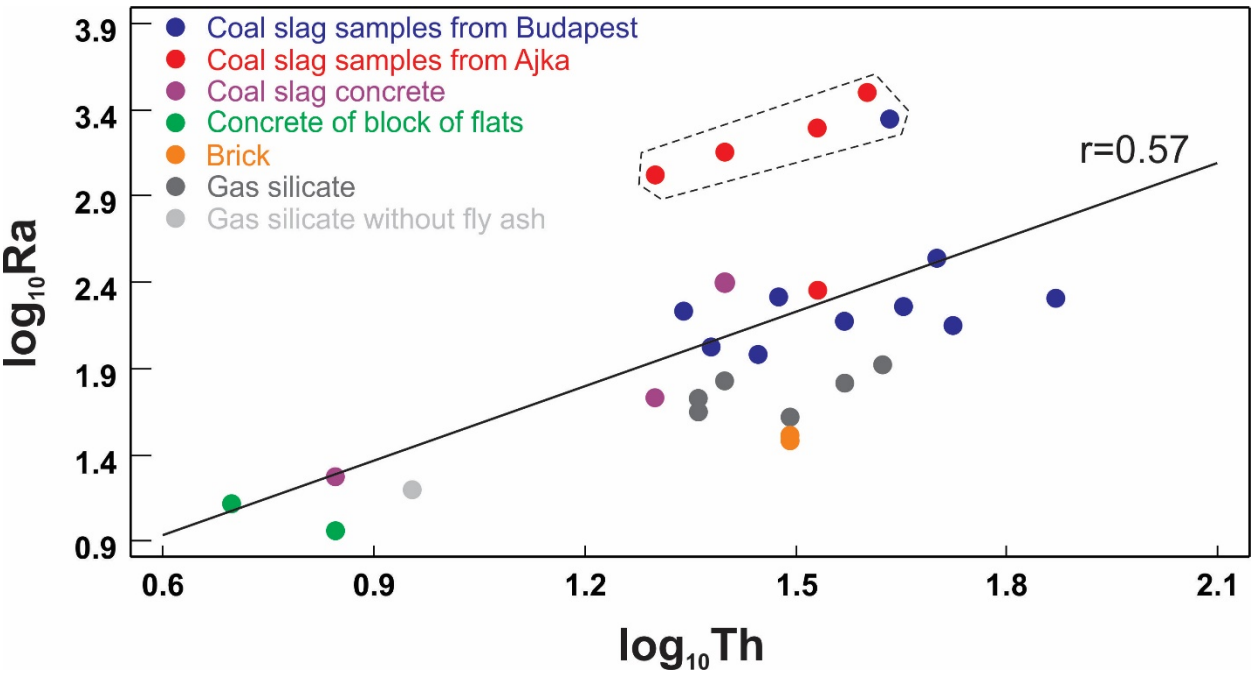

Figure 15. Correlation between ^{226}Ra and ^{232}Th. The different colors of the points indicate different group of the samples explained in the legend. Dashed line indicates a sample group with higher ^{226}Ra activity concentration from samples Ajka (CS_AJK_1-4 and Budapest (CS_CHR_1).

7.3 Building material qualifications

7.3.1. Radium equivalent and activity concentration index

The Ra_{eq} average and standard deviation for the 14 building materials used in bulk amounts is 104 ± 69 Bq kg^{-1} and for the fifteen coal slag samples in restricted usage is 847 ± 971 Bq kg^{-1} with medians of 98 and 297 Bq kg^{-1}, respectively (Table 12). The average activity concentration index (according to Eq. 2) and its standard deviation for the 14 building materials used in bulk amount is 0.37 ± 0.23 and for the fifteen building materials in restricted usage is 2.85 ± 3.23 with medians of 0.34 and 1.02, respectively. The results of artificial building materials are presented in two groups, based on the regulation, which defines different limitations regarding the amount used in the building examined (Chapter 5.1.2.2.; EC, 1999).

Table 12. Calculated indices, their uncertainties and averages, standard deviations for the studied building materials. Absorbed (D_a, Eq. 3) and annual effective (D_e, Eq. 4) dose rates are not given for samples in restricted usage (e.g. used as under-floor filling materials) because the values would not have real meaning. Sample ID refers to the type of building material and the area of origin. Acronyms of B, CBF, CS, CSC and GS mark the types as brick, concrete (from block of flats), coal slag, coal slag concrete and gas silicate. GS_CHR_1 contains sand instead of fly ash. Acronyms of CHR and Ajk indicate Central Hungarian region and Ajka, respectively (Figure 5).

Sample ID		Ra_{eq} (Bq kg^{-1})	I	D_a (nGy h^{-1})	D_e (mSv y^{-1})
Building materials used in bulk amounts					
B_CHR_1	Budapest	114 ± 5	0.42 ± 0.02	103 ± 5	0.50 ± 0.02
B_CHR_2	Százhalombatta	112 ± 6	0.42 ± 0.02	101 ± 5	0.49 ± 0.03
CBF_CHR_1	Budapest	33 ± 2	0.12 ± 0.01	30 ± 2	0.15 ± 0.01
CBF_CHR_2	Budapest	30 ± 3	0.11 ± 0.01	27 ± 3	0.13 ± 0.01
CSC_CHR_1	Budapest	292 ± 10	0.98 ± 0.03	263 ± 9	1.29 ± 0.05
CSC_CHR_2	Budapest	32 ± 6	0.11 ± 0.02	28 ± 5	0.14 ± 0.03
CSC_CHR_3	Kecskemét	92 ± 8	0.32 ± 0.03	81 ± 8	0.40 ± 0.04
GS_CHR_1	Budapest	42 ± 5	0.15 ± 0.02	38 ± 4	0.19 ± 0.02
GS_CHR_2	Dunaharaszti	96 ± 5	0.34 ± 0.02	83 ± 4	0.41 ± 0.02
GS_CHR_3	Gödöllő	166 ± 9	0.59 ± 0.03	146 ± 8	0.72 ± 0.04
GS_CHR_4	Kecskemét	86 ± 6	0.30 ± 0.02	75 ± 5	0.37 ± 0.02
GS_CHR_5	Kiskunhalas	140 ± 8	0.50 ± 0.03	123 ± 7	0.61 ± 0.03
GS_CHR_6	Kistarcsa	100 ± 9	0.35 ± 0.03	88 ± 7	0.43 ± 0.04
GS_CHR_7	Sülysáp	123 ± 13	0.44 ± 0.04	110 ± 11	0.54 ± 0.05
average±st.dev.		*104 ± 69*	*0.37 ± 0.23*	*93 ± 62*	*0.45 ± 0.30*
Building materials used in restricted amounts					
CS_CHR_1	Budapest	2309 ± 55	7.72 ± 0.18		
CS_CHR_2	Budapest	275 ± 9	0.95 ± 0.03		
CS_CHR_3	Budapest	232 ± 8	0.80 ± 0.03		
CS_CHR_4	Budapest	261 ± 7	0.89 ± 0.02		
CS_CHR_5	Budapest	216 ± 7	0.74 ± 0.02		
CS_CHR_6	Budapest	433 ± 12	1.47 ± 0.04		
CS_CHR_7	Budapest	216 ± 8	0.74 ± 0.04		
CS_CHR_8	Budapest	152 ± 4	0.52 ± 0.01		
CS_CHR_9	Budapest	331 ± 11	1.14 ± 0.04		
CS_CHR_10	Budapest	151 ± 6	0.53 ± 0.02		
CS_AJK_1	Ajka	1087 ± 48	3.64 ± 0.16		
CS_AJK_2	Ajka	2051 ± 91	6.86 ± 0.30		
CS_AJK_3	Ajka	3215 ± 144	10.73 ± 0.48		
CS_AJK_4	Ajka	297 ± 11	1.02 ± 0.04		
CS_AJK_5	Ajka	1482 ± 66	4.96 ± 0.22		
average±st.dev.		*847 ± 971*	*2.85 ± 3.23*		

7.3.2. Absorbed and annual effective dose (D_a, D_e)

The evaluated D_a absorbed dose rates (Eq. 3) and D_e annual effective doses (Eq. 4) are shown only for the samples used in bulk amounts but not for the coal slag samples. It would not contain any real information for those buildings in those cases. The average absorbed dose rate and its standard deviation for the samples is 93 ± 62 nGy h^{-1} with median of 86 nGy h^{-1} (Table 12). It is almost twice the assumed background radiation from other sources (cosmic and terrestrial radiation), which was 50 nGy h^{-1} (EC, 1999). Calculated from Eq. 4, the average annual effective dose and its standard deviation for the samples is 0.45 ± 0.3 mSv y^{-1} with a median of 0.42 mSv y^{-1}, respectively (Table 12). The highest value (1.29 ± 0.05 mSv y^{-1}) belongs to the coal slag concrete sample CSC_CHR_1 (Table 12), which is the only sample exceeding the 1 mSv y^{-1} reference value for materials used in bulk amount.

8. Discussion of ^{226}Ra, ^{232}Th and ^{40}K activity concentrations and qualifications of building materials

8.1. In situ gamma dose rates

The values measured indoors contributed to the presence of natural radionuclides (NORM) in the building materials with even higher results where coal slag or coal slag concrete were used (Table 10). The world average gamma-dose in open air at 1m above the ground varies between 18–93 nGy h^{-1} (UNSCEAR, 2000) and the population weighted average is 59 nGy h^{-1}. Indoor exposure, considering the indoor residence time and the shielding of building materials, varies between 20–200 nGy h^{-1}, with a 84 nGy h^{-1} world average (UNSCEAR, 2000). However, the Hungarian average indoor gamma dose rate, based on a survey of 1000 houses, was determined as 95 nGy h^{-1} (11–236 nGy h^{-1}; Nikl, 1996; UNSCEAR, 2000). The results of the in situ gamma dose rate measurements, excluding the coal slag results, are in agreement with the Hungarian average gamma dose rates and the international data. Houses with coal slags have higher results due to the higher ^{226}Ra activity concentration of these materials.

8.2. Discussion of ^{226}Ra, ^{232}Th and ^{40}K activity concentrations

The ^{226}Ra, ^{232}Th and ^{40}K results were compared to the Hungarian and the world average soil and building material activity concentrations, to adobe samples, measured with the same detection system at Eötvös University, and to typical building materials used in the European Commission (Beretka and Mathew, 1985; EC, 1999; Fehér and Deme, 2010; Somlai et al., 2006; Szabó et al., 2013; Tables 13–15).

The activity concentration of ^{226}Ra in most of the studied materials is higher than that in the Hungarian soils (Table 13), Hungarian adobe materials (Szabó, 2014) and some common building materials (e.g. concrete, sand-lime bricks and natural gypsum) used in the European Union (EC, 1999; Table 15). The only exceptions with very low radium activity concentrations (<20 Bq kg^{-1}) were found in four samples. Two concretes from block of flats (CBF_CHR_1, CBF_CHR_2), one coal slag concrete (CSC_CHR_2) and one gas silicate sample (GS_CHR_1, which is mixed only with sand instead of fly ash) indicating the low NORM content of Hungarian concretes (Table 14). If the sample CS_CHR_1, showing an extremely high value (2233 ± 54 Bq kg^{-1}, Table 11), and the samples from CS_AJK_1-5 are not taken into account the average ^{226}Ra activity concentration of the nine remaining coal slag samples will be even thre times as high (179 ± 74 Bq kg^{-1}) as that

of the other types of building materials (56 ± 60 Bq kg^{-1}; Table 11). The high ^{226}Ra-activity concentration of the coal slags is discussed in a separate Chapter.

The average ^{232}Th activity concentration is the same as the one measured in the Hungarian adobe samples (30 ± 5 Bq kg^{-1}; Szabó et al., 2013), and similar to the Hungarian average soil activity concentrations (Table 13). In addition materials, containing coal slag or fly ash, show higher ^{232}Th activity concentrations than the other samples (Table 11). A possible explanation lies in the enrichment of thorium (and uranium) during combustion.

Furthermore, the ^{40}K content of the samples, except the two brick samples, is less than the world and Hungarian soil average (Table 13). In addition, the adobe samples also show much higher ^{40}K activity concentrations (339 ± 36, Szabó et al., 2013). It indicates that ^{40}K is rather concentrated in natural samples (i.e. adobe is also made of soil) as K-bearing minerals, like micas and clay minerals, playing an important role in clayey soils than in coal and other artificial materials (Table 3). Furthermore, the higher concentrations present in the brick samples are also the consequence of K-bearing clay minerals as the main components of brickmaking.

Table 13. The natural radionuclide concentration of soils in the world and in Hungary (Fehér and Deme, 2010).

Where	Amount	Isotope activity concentration (Bq kg^{-1})			
		^{40}K	^{238}U	^{226}Ra	^{232}Th
World	Median	400	35	35	30
	Range	140-850	16-110	17-60	11-64
	Population weighted average	420	33	32	45
Hungary	Average	370	29	33	28
	Range	79-570	12-66	14-76	12-45

Table 14. The average natural radionuclide concentrations of concrete and brick produced in Hungary (Fehér and Deme, 2010) and the studied concrete from block of flats (CBF) and brick (B) building materials

Isotope/radionuclide	Activity concentration (Bq kg^{-1})			
	Concrete	Studied Concretes (CBF) (n=2)	Brick	Studied Bricks (B) (n=2)
^{40}K	200	142	555	479
^{226}Ra	13	11	56	32
^{232}Th	10	6	48	31

Table 15. Typical and maximal ^{226}Ra- ^{232}Th- and ^{40}K activity concentrations of building materials and industrial by – products used for building materials in the European Union (EC, 1999).

Material	**Typical activity concentrations (Bq kg^{-1})**			**Maximum activity concentrations (Bq kg^{-1})**		
Most common building materials	^{226}Ra	^{232}Th	^{40}K	^{226}Ra	^{232}Th	^{40}K
Concrete	40	30	400	240	190	1600
Aerated and light-weight concrete	60	40	430	2600	190	1600
Clay (red) bricks	50	50	670	200	200	2000
Sand-lime bricks	10	10	330	25	30	700
Natural building stones	60	60	640	500	310	4000
Natural gypsum	10	10	80	70	100	200
Most common industrial by-products used in building materials						
Phosphogypsum	390	20	60	1100	160	300
Blast furnace slag	270	70	240	2100	340	1000
Coal fly ash	180	100	650	1100	300	1500

8.2.1. Discussion of the elevated ^{226}Ra content in coal slag samples

Coal slag radium activity concentration results vary over a wide range, the values from Budapest are observed between 96 ± 5 and 2233 ± 54 Bq kg^{-1}, in contrast to the significantly higher values of the samples from Ajka (227 ± 11 to 3152 ± 144 Bq kg^{-1}; Table 16). It should be noted that the results between the two areas would be more significant without the high value of the CS_CHR_1 sample. All measured data show higher activity concentrations than the reference value (50 Bq kg^{-1}) provided by UNSCEAR (1993) for ^{226}Ra activity concentration in building materials. Additionally, some samples exceed the maximum ^{226}Ra activity concentrations (2100 Bq kg^{-1}) measured in most common industrial by-products of the European Union (EC, 1999; Table 15).

In another Hungarian study, Somlai et al. (2006) measured coal slag samples at three locations from the Transdanubian Central Range. In that paper the ^{226}Ra activity concentration of the coal slag from cities of Ajka (mean: 1962 Bq kg^{-1}), Tatabánya (mean: 1912 Bq kg^{-1}) and Várpalota (mean: 298 Bq kg^{-1}; Table 16) significantly exceeded the reference value (UNSCEAR, 1993) for building materials. These elevated values indicate an overall high ^{226}Ra activity concentration in coal slags in this region (Chapter 2.4), which is comparable to the measured results (Table 11).

On an international scale the ^{226}Ra activity concentrations of the Transdanubian Central Range (Ajka, Tatabánya) stand out as the highest ones (Table 16). The results, not taking into account the result of CS_CHR_1, from Budapest and Australia are comparable and somewhat higher than the data for one power plant from Greece published in the references (Beretka and Mathew, 1985; Coles et al., 1978; Karangelos et al., 2004; Kumar et al., 1999; Somlai et al., 2006; Table 16).

Among the materials a high level of standard deviations was observed in all results (Table 11). Even after dividing these samples into subgroups (brick, concrete, coal slag, coal slag concrete and gas silicate), significant differences, mostly in ^{226}Ra activity concentration, were found (Table 11). In the case of coal slags and coal slag concrete samples the ^{226}Ra content is not determined only by the building material making process, which is the base of the sample groups. However it is also strongly influenced probably by the origin of the coal (Bódizs et al., 1993; Szabó et al 2013; Völgyesi et al., 2014a). Whenever coal slag or coal slag additive building materials are studied a high level of standard deviation has to be considered, unless filtering information is

available about its origin. Much less significant heterogeneity was found for ^{232}Th and ^{40}K activity concentrations (Table 11).

In Ajka the source of the high value is the use of the local waste products from the power plant and other burners (Somlai et al., 2006). The lower levels of the samples from Budapest indicate that the coal burned in Budapest probably does not originate from the Transdanubian region, as coal from other locations in the country have lower radioactive isotope content. The different Ra activity concentration levels of coal slags reveal the wide range of Hungarian coals transported to the capital. The preceding notwithstanding, the coal slag sample from Budapest (CS_CHR_1) is comparable to the results from the Ajka region, indicating that the precise traceability of the transport routes, identification of coal sources within the country and study of houses, where this material was used is necessary.

Table 16. The average ^{226}Ra activity concentration results compared to coal slag samples reported in the literature.

Location	Origin	Reference	Ave. ^{226}Ra ac. (Bq kg^{-1})
Hungary	Ajka	This work	1571±72
	Budapest		384±653[a] (179 ±74)
Greece	Megalopolis-B Power Plant	[Karangelos et al. 2004]	583±5
	Ptolemais Power Plant		127±6
USA	Plant-A western part of USA	[Coles et al. 1978]	70[b]
	Plant-B western part of USA		93[b]
India	Kasimpur and Parichha of the state of Uttar Pradesh, India	[Kumar et al., 1999]	67 ± no data
Australia	New South Wales and South Australia	[Beretka and Mathew, 1985]	181 ± no data
Hungary (Transdanubian Central Range)	Ajka	[Somlai et al., 2006]	1962 (578-2893)[c]
	Tatabánya		1912 (843-2407)[c]
	Várpalota		298 (160-523)[c]

[a]samples from Budapest include the CS_Budapest_1 sample with very high Ra content, the results without this sample are in brackets
[b]data were converted from piC g^{-1} to Bq kg^{-1}. The error was indicated as 10% in Coles et al., 1978
[c]min-max. data (Bq kg^{-1}) in Somlai et al., 2006
ac.: activity concentration

8.2.2. Correlation between the studied radionuclides

The correlation between ^{226}Ra and ^{232}Th activity concetrations indicates the common source and common geochemical behaviour of these materials (Figure 15). Concrete from block of flats and the gas silicate without fly ash represent a sample group with low radium and thorium content revealing a natural radionuclide level. The gas silicates and most coal slag samples from Budapest showed a broader range of thorium content with higher radium in the coal slags, whereas still indicating common features. The most varying results were found in coal slag concrete samples, which is probably the result of the randomly used raw materials and the mixed coal or coal slag components with unknown sources. A group composed of the 4 coal slag samples from Ajka (CS_AJK_1-4) and one coal slag from Budapest (CS_CHR_1), with very high radium activity concentrations, was observed as a separate group on Figure 15. It corroborates the previous finding in Chapter 8.2.1. that this sample may originate from Ajka, hence, coals were transported from different regions of Hungary to the capital.

El Afifi et al. (2006) studied heavy mineral sands and also found the strongest relationship between ^{226}Ra and ^{232}Th activity concentrations with a high correlation coefficient (r=0.87). It was explained that the analyzed sample population was dominated by ^{232}Th- and ^{238}U-bearing monazite. In Szabó et al. (2013), the strongest linear relationship was observed between ^{226}Ra and ^{232}Th in adobe building material samples, too. Referring to the work of Manolopoulou and Papastefanou (1992), who found an inverse correlation between ^{226}Ra (and ^{238}U and ^{210}Pb, too) and ^{40}K, and a strong positive correlation between ^{232}Th (and ^{228}Ra, too) and ^{40}K analyzing radionuclides in lignite samples. They explained that uranium and its decay products are associated with the organic materials in the coal, whereas the thorium and its daughter products, as well as K are associated with the inorganic materials, such as minerals.

The relationship between these radionuclides suggests that radium before combustion was not associated with the organic compounds, but with the inorganic fraction, and it remained unchanged after combustion, which probably explains the presence of secular equilibrium between uranium and radium in the coal slag samples (Chapter 6.4.).

8.3. Discussion of qualifications and dose estimations of building materials

8.3.1. Radium equivalent and activity concentration index

Six coal slag samples exceeded the 370 Bq kg^{-1} limit value (OECD, 1979; Table 12). Based on the further limitations (Chapter 5.1.2.2.), the coal slag sample CS_CHR_6 could have been used only as an industrial building material not as a building material for residences, the CS_AJK_1, CS_AJK_2, and CS_AJK_5 could have been used only for roads and railways and the coal slag sample CS_CHR_1 and CS_AJK_3 could have been used only as a landfill material (Somlai et al., 1996).

Since the Ra_{eq} is the most widely used index in the radiation hazard qualification of building materials, the calculated results were compared to similar studies (Beretka and Mathew, 1985 and references therein; Kovler et al., 2002; Kumar et al., 1999; Somlai et al., 1996) performed in different countries (Table 17). To make a relevant comparison, the results were averaged. The average of brick samples was compared to clay brick (unfired and fired) building materials in the cited references (Table 17). In the case of concrete (from block of flats) and coal slag concrete, where coal slag is an additive, the comparison was made to concrete block/tile samples reported in the paper of Beretka and Mathew (1985) and references therein. Coal slag samples were

compared to samples named in the same way, however gas silicate building materials were considered being ‘normal-weight concrete with fly ash as part of the sand’ studied by Kovler et al. (2002). Despite the fact that the brick has a high K content, their Ra_{eq} is lower than those in the literature. In the case of concrete (from block of flats) and coal slag concrete building materials it was found that the averages are in the range of the values measured in other countries. Coal slag samples show elevated levels in Hungary compared to those in Australia, Finland, Germany and India and, as previously described, the results were comparable to the values measured by Somlai et al. (1996). Values of Ra_{eq} in gas silicate samples show a value twice as high as the reference values (Kovler et al., 2002).

Table 17. Radium equivalent index (Ra_{eq}) averages of differently grouped types of building materials in this study and comparison to international references. In those cases if the number of samples was reported, it is given in brackets after the Ra_{eq} average.

Building material type	Ra_{eq} average (Bq kg^{-1})										
	This study		Beretka and Mathew (1985) and references therein						Kovler et al. (2002)	Kumar et al. (1999)	Somlai et al. (1996)
	Hungary		Australia	Finland	Germany	Norway	Sweden	United Kingdom	Israel	India	Hungary: Ajka (Figure 1)
Brick	113 (2)		218 (25)	241	204	274	352	170		134 (3)	
concrete (from block of flats)	31 (2)	41 (5)	85 (5)	-	155	133	-	-	-	-	-
coal slag concrete	138 (3)										
coal slag	847 (15)	-	340 (3)	215	422	-	-	-	-	190 (3)	1779 (11)
gas silicate	107 (7)	-	-	-	-	-	-	-	47	-	-

The results of activity concentration index corroborated those ascertained from the Ra equivalent index. The CSC_CHR_1 is the only sample exceeding the reference value (I=1) for materials used in bulk amounts, which means >1 mSv annual dose from external sources. Although, this limitation is only valid for materials used in bulk amounts, ten coal slag samples reached this refrence value, which attracts attention to the potential risk of these materials. In some cases twice of their statistical uncertainty were added to the value to provide a safer qualification. In addition, the samples CS_CHR_1, CS_AJK_2 and CS_AJK_3 exceed even the limit value of 6 for building materials used in restricted amount.

8.3.2. Absorbed and annual effective dose rates (D_a, D_e) and risk assessment of the building materials

The annual doses calculated for potentially hazardous samples, like coal slag and fly ash, are not widely available in the literature. Somlai and his coworkers (2000) measured dose rates and the time children spend in kindergartens, schools, dwellings and playgrounds where coal slag and fly ash were used. They found the external gamma dose to be 33 mSv up to age 18, whereas the world average was calculated as 9.6 mSv. These results were measured in a city located in the Transdanubian Central Range, with very high Ra content (850–2400 Bq kg^{-1}) in the building materials used in playgrounds and as additives in concrete blocks, where the total amount and exposure of this material is much higher than when it is only employed as insulation material. Considering the activity concentration index (I), one coal slag concrete sample (reference value: I>1; CSC_Budapest_1) and three coal slag samples (reference value: I>6; CS_CHR_1, CS_AJK_2 and CS_AJK_3) exceed the 1 mSv annual effective dose, revealing the potential risk of these materials.

Cement, concrete and brick samples are more frequently analyzed in many countries. According to Mavi and Akkurt (2010), who reported values ranging from 0.13 to 0.42 mSv y^{-1} for different Turkish building materials, with samples of brick and gypsum showing the highest values. Moharram et al. (2012) also measured annual effective doses of concrete, red clay brick and cement mix materials (a mixture of sand, cement and water). They estimate 0.052 mSv y^{-1}, 0.06 mSv y^{-1} and 0.026 mSv y^{-1}, respectively. These are one magnitude lower than the analyzed materials from Hungary (Table 12). Results for bricks and concretes (0.03 mSv y^{-1} and 0.04 mSv y^{-1}, respectively) measured by Sharaf et al. (2013) were in the same range as those reported by

Moharram et al. (2012). However, even the less hazardous Hungarian materials used in bulk amounts show higher annual effective dose (Table 12) than the Turkish building materials.

Table 18 summarizes the hazardous (i.e. not dangerous, but risky) building materials studied based on the Ra_{eq}, and I indices and dose calculations. A joint evaluation using these indices and dose limitations provides useful information on the hazardous samples. Considering all materials, seven hazardous samples (CS_CHR_1, CS_CHR_6, CS_AJK_1, CS_AJK_2, CS_AJK3, CS_AJK_5, CSC_CHR_1), with elevated radium activity concentrations, indices, and doses were found (Table 18). These results point to the importance of building material qualification practices and that the impact of industry in the past still influences our indoor environment.

Table 18. Summary of hazardous building materials in the present study based on dose estimations (D_e: effective dose) and different calculated indices and their threshold values: radium equivalent index (Ra_{eq}), activity concentration index (I).

Index	Hazardous sample
Ra_{eq}	CS_CHR_1, CS_AJK_3: landfill material, CS_CHR_6: for industrial use, CS_AJK_1, CS_AJK_2, CS_AJK_5: for roads and railways
I	I>6 (restricted amounts): CS_CHR_Budapest1, CS_AJK_2, CS_AJK_3, I>1 (bulk amount): CSC_Budapest_1
D_e	CSC_Budapest_1

9. Results and discussion of the urban geochemical research in Ajka using attic dust samples

9.1 Results of univariate summary statistics of toxic elements

All As, Pb and Zn attic dust concentrations, including the measured minimum values, exceed the Hungarian regional geochemical background (HRGB) level, whereas Ni (4 samples below background), Cd (2 samples), Hg (2samples) and Cu (1 sample) concentrations remained below the HRGB values (for more details, see Table 19 and Appendix 11). Enrichment factors follow the order of Pb>>Zn>Hg>>Cu>=Cd>As>Ni (Table 19). It should be noted that the HRGB levels are the same as the European mean topsoil levels (Salminen et al., 2005), with tiny differences with respect to Cd and Hg (Table 19).

At least 50% of the samples are contaminated with As (*Md*=15 mg/kg), Cd (*Md*=1.33 mg/kg) and Zn (*Md*=276 mg/kg) as compared to the Hungarian national pollution limit (hereinafter referred to as pollution limit) value for geological materials (Table 19). The medians of As, Cd, Hg, Pb and Zn are around the pollution limit value. Extreme values, represented by the maximum concentrations, exceed the pollution limit values for Cd (11x), Pb (8x), followed by Hg and Zn (4x), and As (2x; Table 19), suggesting that attic dust in Ajka is clearly contaminated at individual locations with Cd, Pb, Hg, Zn and As. The Range/Md statistics of variability, sensitive to extreme values, corroborate these results. Lead and Cd have the highest values (9.6 and 8.5, respectively) suggesting anthropogenic point-source pollution (Table 19). The relative variability of Zn, Pb and Hg, expressed as the IQR/Md statistics, standing out with the highest values (0.9–1.39), indicates that they have source(s), which produce(s) a highly diverse distribution of airborne particulate concentrations (Table 19).

Table 19. Main statistical parameters (Min = minimum, LQ = lower quartile, Md = median, UQ = upper quartile, Max = maximum, IQR = inter quartile range) of the studied 27 attic dust samples and environmental legislation values and background values for the measured toxic elements.

Element	unit	Statistical parameters											HRGB[1]	FOREGS[2]	Hungarian Govt. Decree No. 6/2009.[3]
		Min	LQ	Md	UQ	Max	IQR	Average	Standard deviation	EF	IQR/ Md	Range/ Md	Background value	Topsoil mean value	Pollution limit
		mg/kg	mg/kg	mg/kg	mg/kg	mg/kg	mg/kg	mg/kg	mg/kg				mg/kg	mg/kg	mg/kg
As		*7.0*	*10.7*	***15.0***	***18.4***	***34.5***	7.7	15.5	5.9	2.4	0.51	1.8	6.3	6	15
Cd		0.383	*0.846*	***1.33***	***1.67***	***11.7***	0.824	1.77	2.15	2.7	0.62	8.5	0.5	0.15	1
Cu		14.1	*31.5*	*41.6*	*49.7*	***128***	18.2	46.1	23.1	2.8	0.44	2.7	15	12	75
Hg		0.058	*0.184*	*0.335*	***0.648***	***1.97***	0.464	0.469	0.391	4.2	1.39	5.7	0.08	0.037	0.5
Ni		12.1	*17.8*	*23.9*	*28.2*	***43.1***	10.4	24.6	8.1	1.5	0.44	1.3	16	14	40
Pb		*38.8*	*57.4*	*88.1*	***149***	***881***	91.6	139	169	6.8	1.04	9.6	13	15	100
Zn		*90.2*	*174*	***276***	***422***	***919***	248	345	238	6.0	0.90	3.0	46	48	200

EF: Enrichment Factor computed by dividing the median element concentration in the dust sample by the Hungarian regional geochemical background level (HRGB); IQR/Md refers to the relative variability and Range/Md characterizes the extreme environmental geochemical processes. Those values, which exceed the Hungarian regional geochemical background value are in italics, those reaching or exceeding the Hungarian pollution limit are in bold.

[1] The Hungarian regional geochemical background (HRGB) value is determined by the Geological Institute of Hungary for this geochemical region by using stream sediment samples (Ódor et al., 1996).

[2] The European mean topsoil (sampling depth 0–25 cm) value published in FOREGS – Geochemical Atlas of Europe (Salminen et al., 2005).

[3] The Hungarian national pollution limit value for geological materials (soil and sediment) declared by Hungarian environmental legislation (Joint Government Decree No 6/2009).

9.2. Discussion of univariate summary statistics of toxic elements

The analyses of univariate summary statistics (Table 19) imply that Pb, Cd, Hg and Zn, characterized by high concentrations and enrichment factors, high overall variability and high extreme variability, are most likely dominated by anthropogenic, mainly point-source, contamination (Cizdziel and Hodge, 2000; Davis and Gulson, 2005; Gosar et al., 2006; Hlawiczka et al., 2003; Sajn, 2005). Arsenic and Cu, and particularly Ni, (Table 19) have low concentrations at the natural background level, low enrichment and low overall variability with few outliers. Therefore, these elements are probably associated with wind-blown soil particles, and their spatial distribution is not driven by prominent point sources (Sajn, 2005). However, anthropogenic emissions of the analyzed elements, due to industrial activity such as the operation of coal and lignite-fired power plants and mining (Glodek and Pacyna, 2009; Gosar and Miler, 2011; Sajn, 2002), and fuel combustion from heavy traffic (Davis and Gulson, 2005), may explain the observed high values and high variability.

Considering that, in the absence of regional airborne dust survey results and environmental standards for attic dust, it was reasonable to compare the measured attic dust composition to available geochemical soil and sediment background data and the Hungarian national pollution limit values for geological materials (soil and sediments; Joint Government Decree 6/2009). This draws attention to the fact that special attention needs to be given to data interpretation, when comparing geochemical composition of different geological materials.

9.3. Results of spatial distribution analyses of toxic elements

The assumptions mentioned in Chapter 9.1. are further analyzed using the concentration results and their population distributions demonstrated on histograms (Table 19 and Figures 16-25). The results are presented with spatial distribution maps and, where remarkable patterns were found, also with TIN (see Chapter 5.4.2) interpolated contour maps.

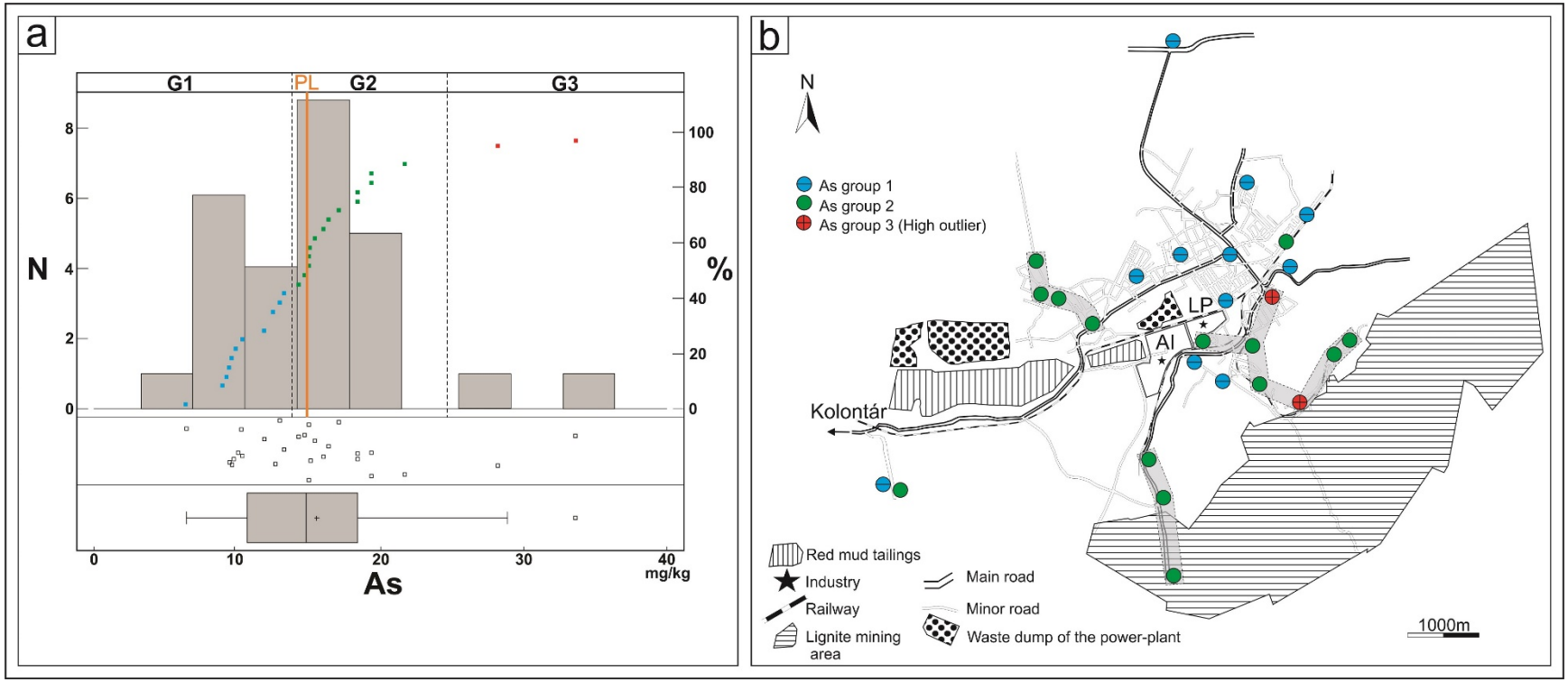

Figure 16. Univariate exploratory data analysis and As distribution map in Ajka attic dust. Figure 16a-upper part: frequency histogram of As concentration and its cumulative distribution function. Vertical dashed lines: separation of sub-populations, based on histogram analysis and homogeneity test. G1 to G3 correspond to groups of samples. Figure 16a-lower part: scatter plot and box-and-whiskers plot of original As data. Figure 16b: spatial distribution of the As sub-groups in the attic samples. Different colors, circles and circles with minus and with plus signs: sample populations (group 1, group 2 and group 3). Light gray: samples belonging to a homogeneous group displaying a spatial pattern. See Figure 7 for additional legend information (page: 39). The orange line indicates the pollution limit (PL).

It is apparent that the three sub-groups of arsenic, two associated with the bimodal distribution and one with the two outliers, can be identified in the attic dust samples, which display a systematic spatial pattern (Figures 16 and 17). The two high outlier samples (with concentrations of 28.9 mg kg^{-1} and 34.5 mg kg^{-1}) and the higher sub-population members of the two major As populations are located at the lignite mines and next to the waste dump of the power plant (Table 19, Figure 16). Eighty-five % of the samples, falling in the higher group, already exceed the pollution limit value (Figure 16).

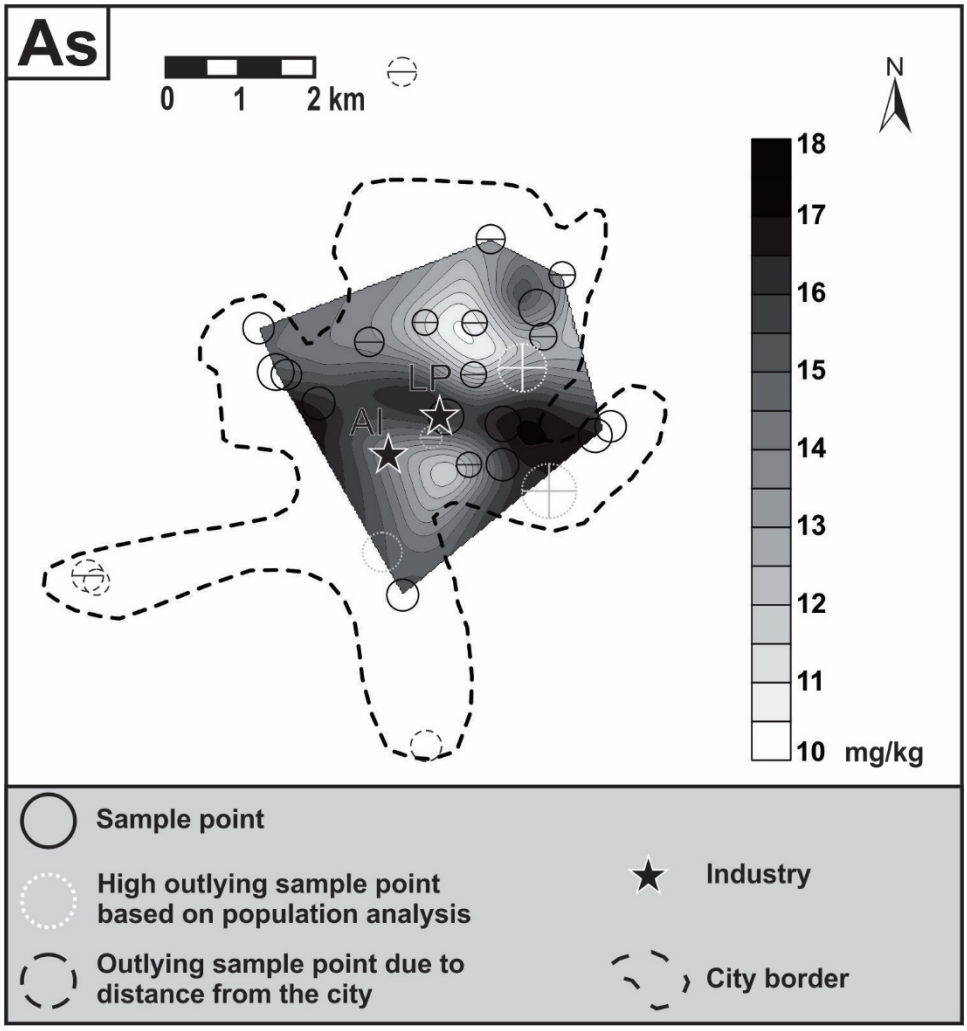

Figure 17. Arsenic contour map at Ajka. Circles and circles with minus and plus signs show sample populations (group 1, group 2 and group 3) based on the statistical analysis (Figure 16). The circle diameter is proportional to element concentrations. Circles in dashed lines: samples, which were not used to create the contour map due to their distance from other points. Circles in dotted lines were also removed from the contour map due to low or high concentrations disturbing the spatial trend of element concentrations in the attic samples following the method of Reimann et al. (2008).

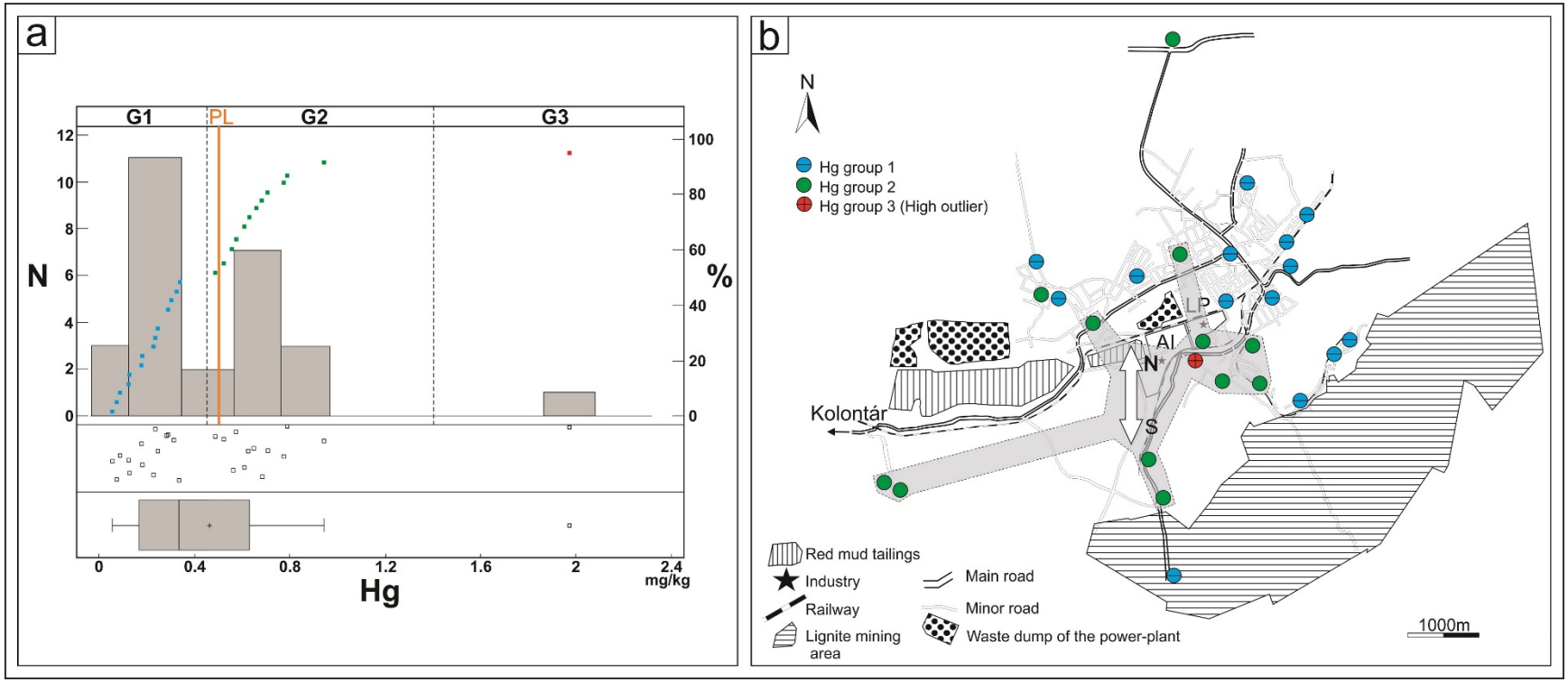

Figure 18. Univariate exploratory data analysis and Hg distribution map in Ajka attic dust. Figure 18a-upper part: frequency histogram of Hg concentration and its cumulative distribution function. Vertical dashed lines: separation of sub-populations, based on the histogram analysis and homogeneity test. G1 to G3 correspond to groups of samples. Figure 18a-lower part: scatter plot and box-and-whiskers plot of original Hg data. Figure 18b: spatial distribution of the mercury sub-groups in the attic samples. Different colors, circles and circles with minus and with plus signs: sample populations (group 1, group 2 and group 3). Light gray area: samples belonging to a homogeneous group displayin a spatial pattern. White arrow: N–S trend of the Hg concentration sub-parallel to the prevailing wind direction in Ajka. See Figure 7 for additional legend information (page: 39). The orange line indicates the pollution limit (PL).

The higher sub-group of Hg, where eleven concentration values lie above the pollution limit (Table 19, Appendix 11), and the outlier sample (1.97 mg kg^{-1}) depict a well-defined area around the power plant (Figures 18 and 19). The lower group of samples (Hg ≤0.335 mg kg^{-1} with 14 samples) shows a higher relative overall variability than the extreme values (Figure 18a). Based on the maps, a N–S oriented trend can be seen in the centre of the study area (Figure 18b and Figure 19).

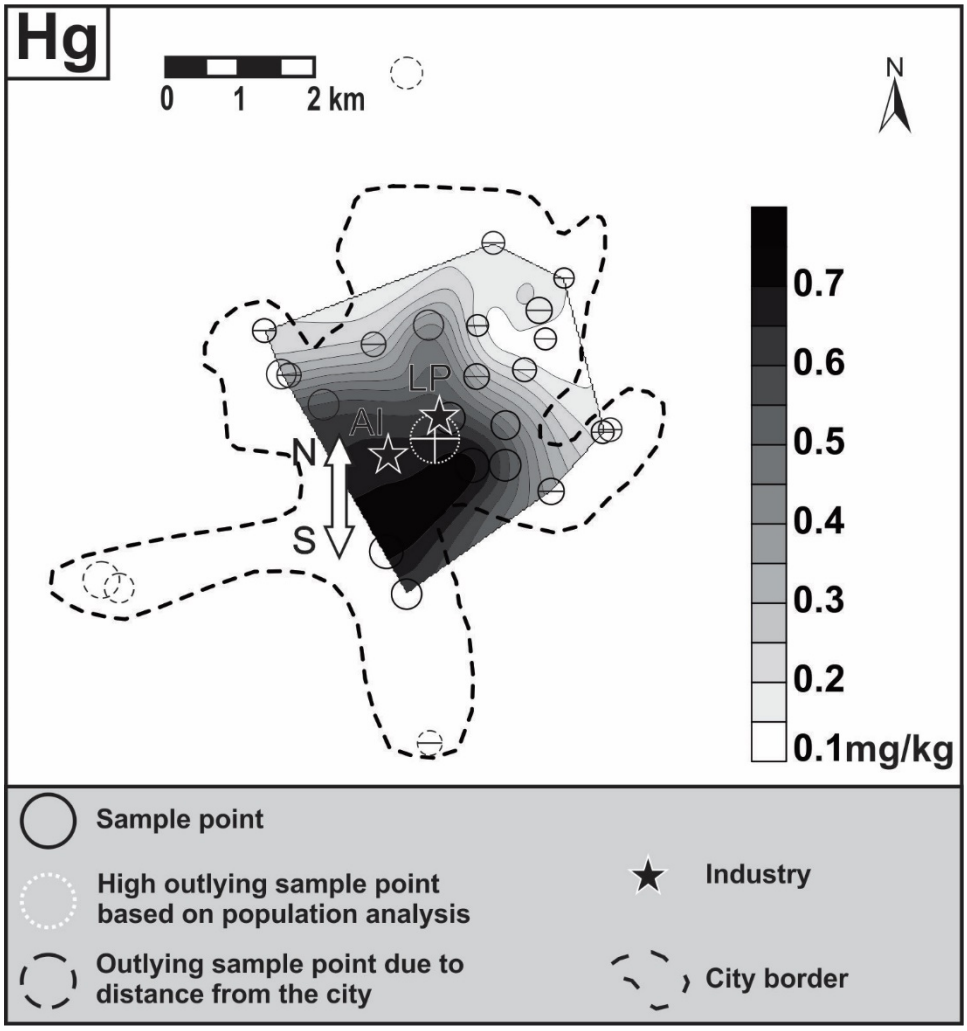

Figure 19. Mercury contour map at Ajka. Circles and circles with minus and plus signs show sample population (group 1, group 2 and group 3) based on the statistical analysis (Figure 18). The circle diameter is proportional to element concentrations. Circles in dashed lines: samples, which were not used to create the contour map due to their distance from other points. Circles in dotted lines were also removed from the contour map due to low or high concentrations disturbing the spatial trend of element concentrations in the attic dust samples following the method of Reimann et al. (2008). White arrows indicate the N–S trend of the Hg concentration sub-parallel to the prevailing wind direction in Ajka.

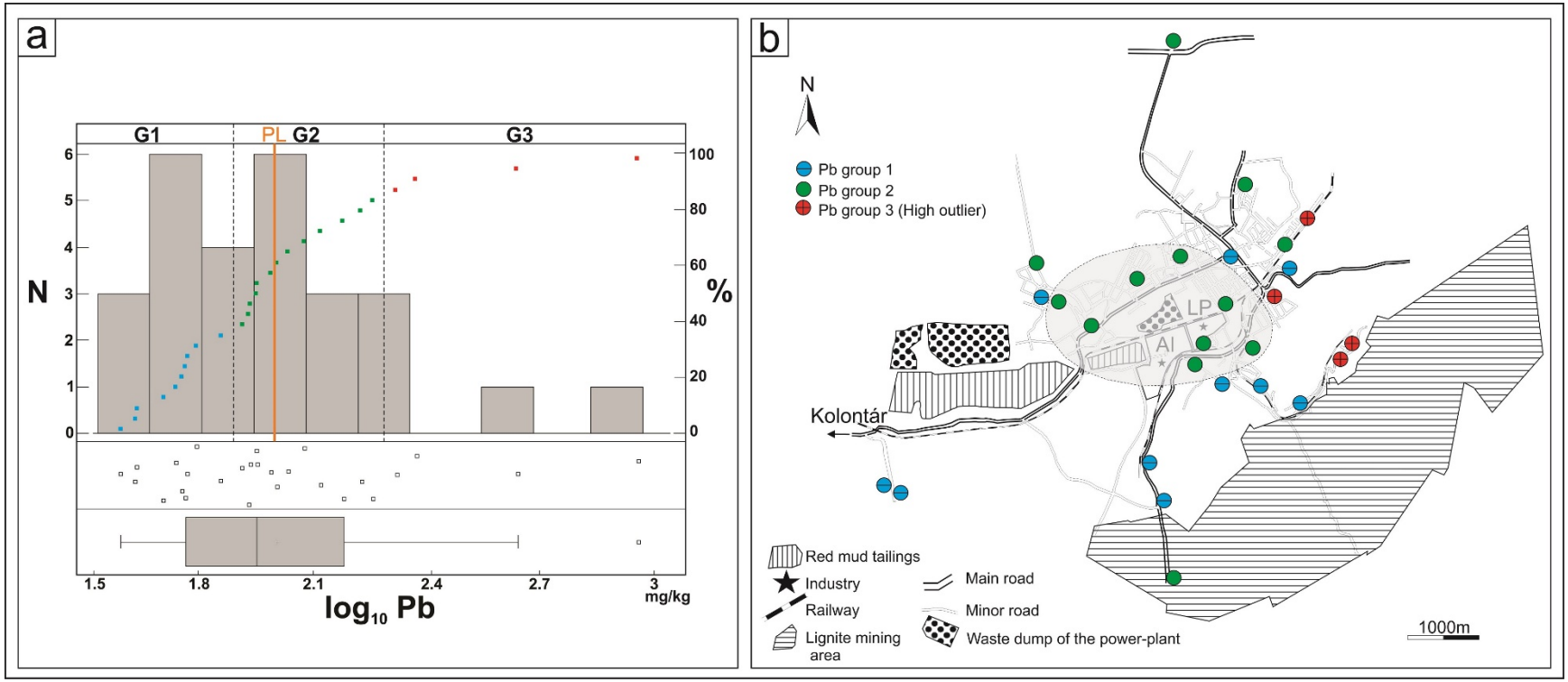

Figure 20. Univariate exploratory data analysis and Pb distribution map in Ajka attic dust. Figure 20a-upper part: frequency histogram of Pb concentration and its cumulative distribution function. Vertical dashed lines: separation of sub-populations, based on the histogram analysis and homogeneity test. G1 to G3 correspond to groups of samples. Figure 20a-lower part: scatter plot and box-and-whiskers plot of original Pb data. Figure 20b: spatial distribution of the Pb sub-groups in the studied attic dust samples. Different colors, circles and circles with minus and with plus signs: sample populations (group 2, group 1 and group 3). Light gray area: samples belonging to a homogeneous group displaying a spatial pattern. See Figure 7 for additional legend information (page: 39). The orange line indicates the pollution limit (PL).

The statistical distribution of Pb concentrations resembles those of As and Hg, with a few, yet very high outliers (4 outliers for Pb; Figure 20a). The outliers stem from the mining area and along traffic lines, most prominently along major roads and train tracks leading to the mining and industrial areas (Figure 20b). The samples of the extreme group are mainly from the city, taken along major roads and train tracks, whereas the location of the lower Pb group (from 39 to 71 mg kg^{-1}) is found mainly in the southern area (Appendix 11; Figure 20). The Pb concentration trend map (Figure 21) is consistent with the findings of the statistical histogram analysis (Figure 20).

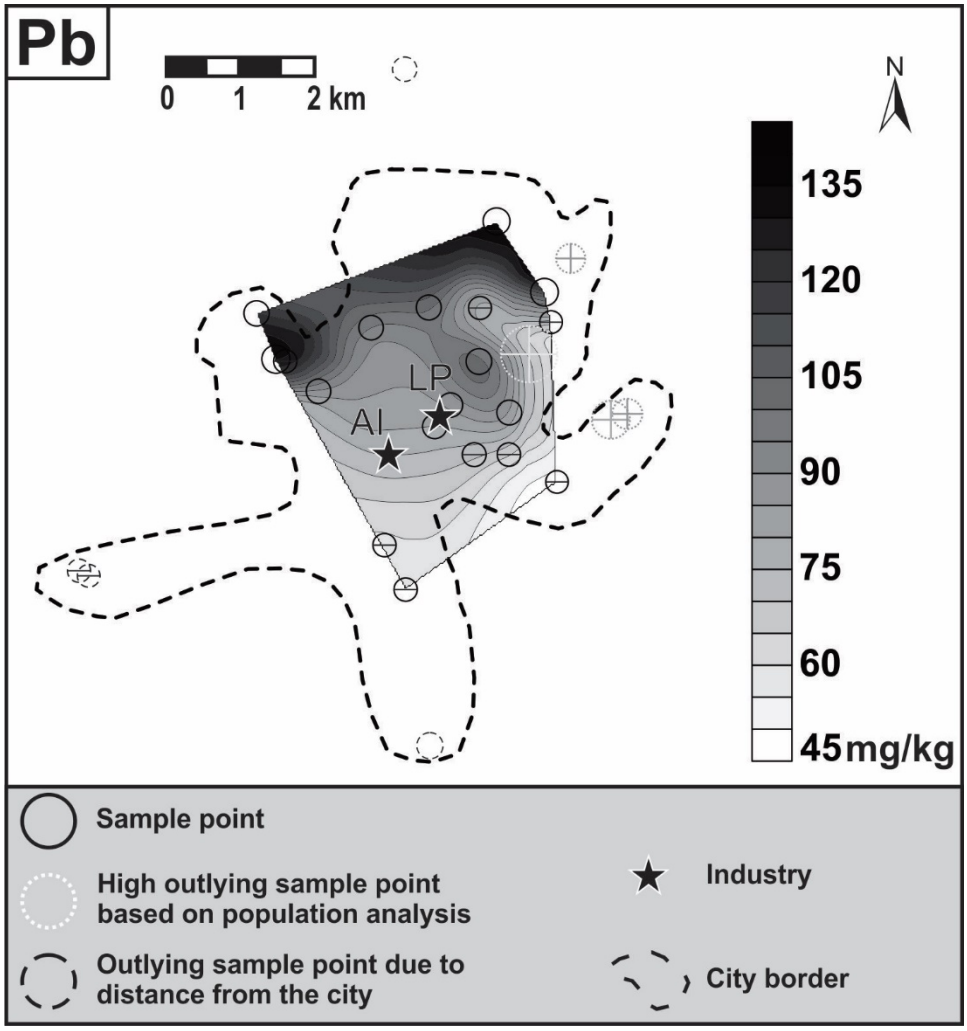

Figure 21. Lead contour map at Ajka. Circles and circles with minus and plus signs show sample population (group 1, group 2 and group 3) based on the statistical analysis (Figure 20). The circle diameter is proportional to element concentrations. Circles in dashed lines: samples, which were not used to create the contour map due to their distance from other points. Circles in dotted lines were also removed from the contour map due to low or high concentrations disturbing the spatial trend of element concentration in the attic dust samples following the method of Reimann et al. (2008).

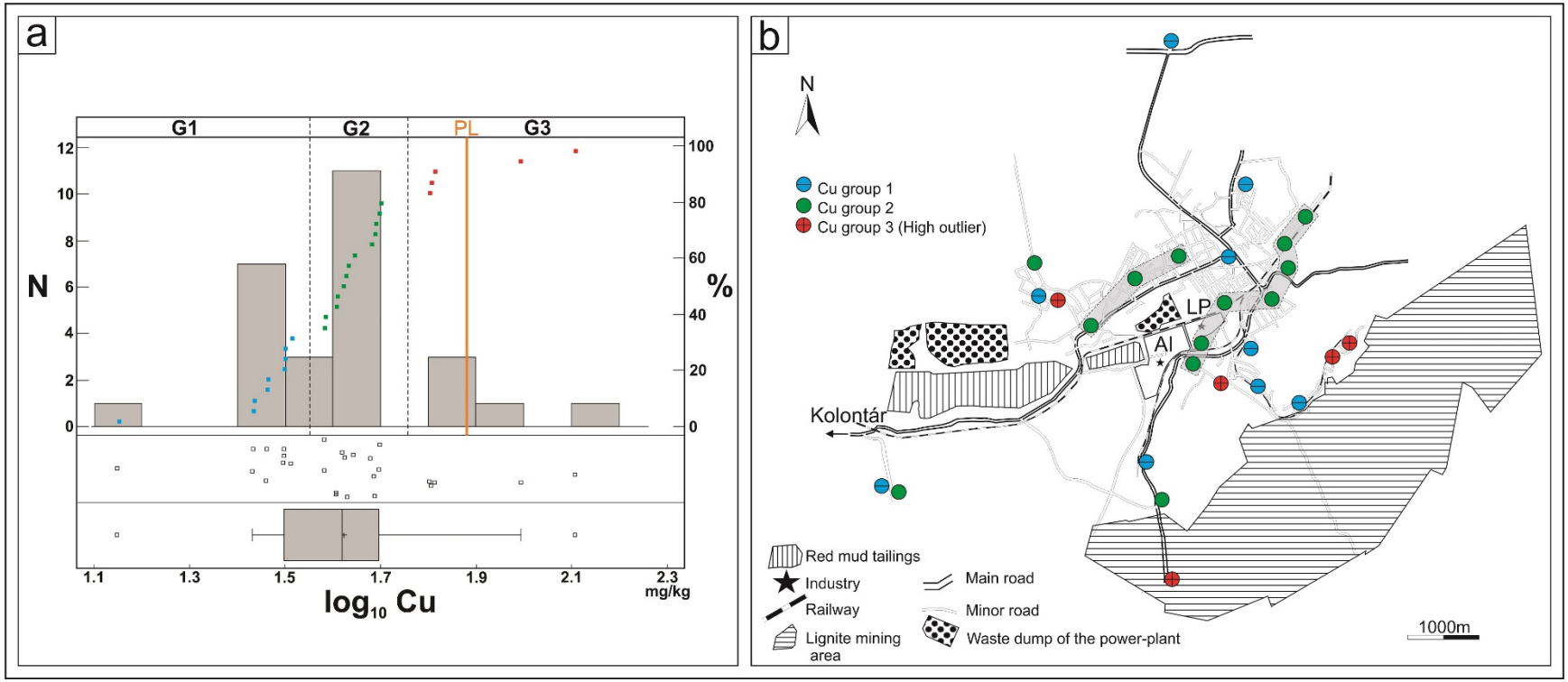

Figure 22. Univariate exploratory data analysis and Cu distribution map in Ajka attic dust. Figure 22a-upper part: frequency histogram of Cu concentration and its cumulative distribution function. Vertical dashed lines: separation of sub-populations based on histogram analysis and homogeneity test. G1 to G3 correspond to groups of samples. Figure 22a-lower part: scatter plot and box-and-whiskers plot of original Cu data. Figure 22b: spatial distribution of the copper sub-groups in the attic dust samples. Different colors, circles and circles with minus and with plus signs: sample populations (group 1, group 2 and group 3). Light gray area: samples belonging to a homogeneous group displaying a spatial pattern. See Figure 7 for additional legend information (page: 39). The orange line indicates the pollution limit (PL).

Copper, similar to As, Hg and Pb, is also characterized by heterogeneity, and 3 sub-groups can be distinguished in the histogram of the attic dust samples (Figure 22a). Four of the five Cu-outlier samples are situated in the southeastern region at the lignite mines and the industrial area (Figure 22b). Only two of these exceed the value of the pollution limit (75 mg kg^{-1}, Figure 22a). The higher sub-population shows a larger relative variability than the lower sub-group of 9 samples (Appendix 11). The higher sub-group containing 13 samples of the two major groups (Figure 22a) range from 38.1 mg kg^{-1} to 50 mg kg^{-1} (Table 19) and it has larger relative variability than the lower sub-group of 9 samples.

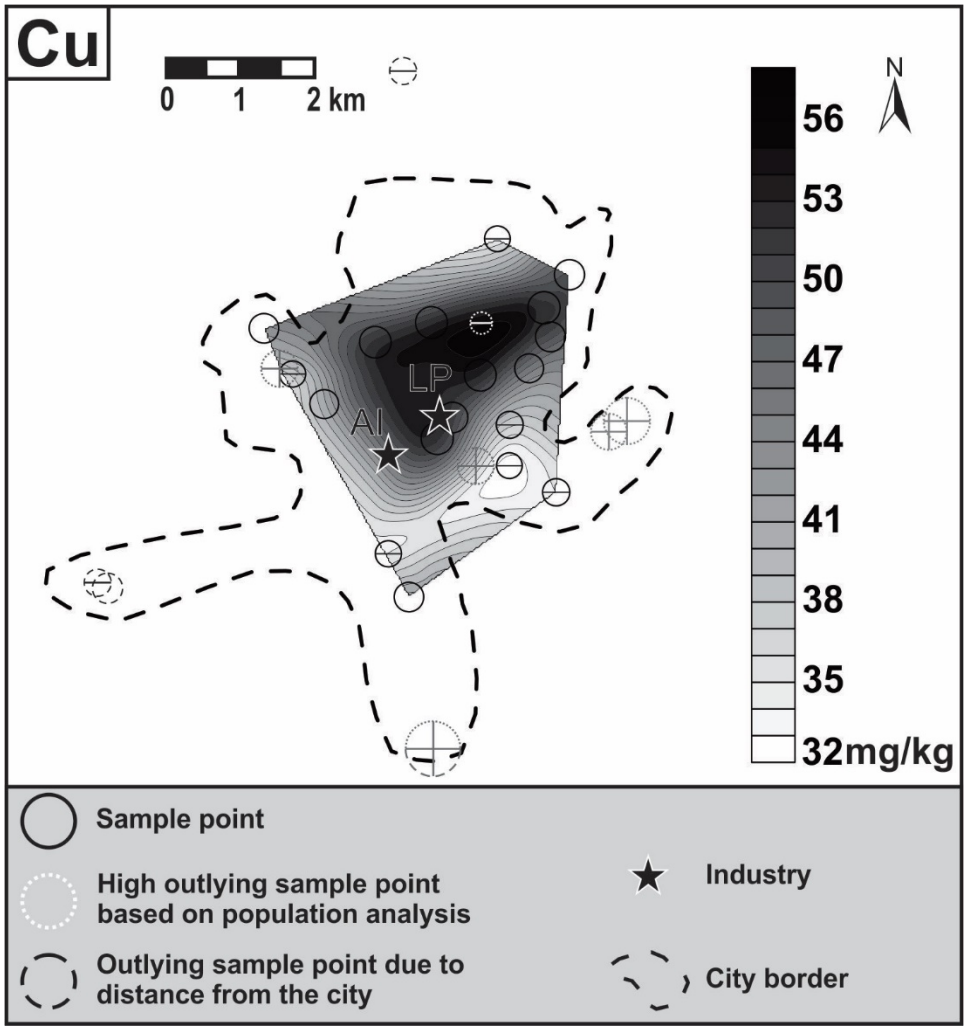

Figure 23. Copper contour map at Ajka. Circles and circles with minus and plus signs show sample population (group 1, group 2 and group 3) based on the statistical analysis (Figure 22). The circle diameter is proportional to element concentrations. Circles in dashed lines: samples, which were not used to create the contour map due to their distance from other points. Circles in dotted lines were also removed from the contour map due to low or high concentrations disturbing the spatial trend of element concentration in the attic dust samples following the method of Reimann et al. (2008).

Cadmium, zinc and nickel are presented separately (Figures 24, 25 and 26), without trend surface maps, because they belong to a homogeneous uni-modal group with several outlier values. Cadmium and Zn have high value outliers found mainly in the south-eastern part of the city around the industrial and lignite mining area and next to the waste dump of the power-plant (Figures 24 and 25). Cadmium and zinc have 19 and 17 samples above the pollution limit value, respectively (Appendix 11). The uni-modal homogeneous Ni distribution is quite similar to Zn and Cd, but Ni has no outlier samples (Figures 24-26).

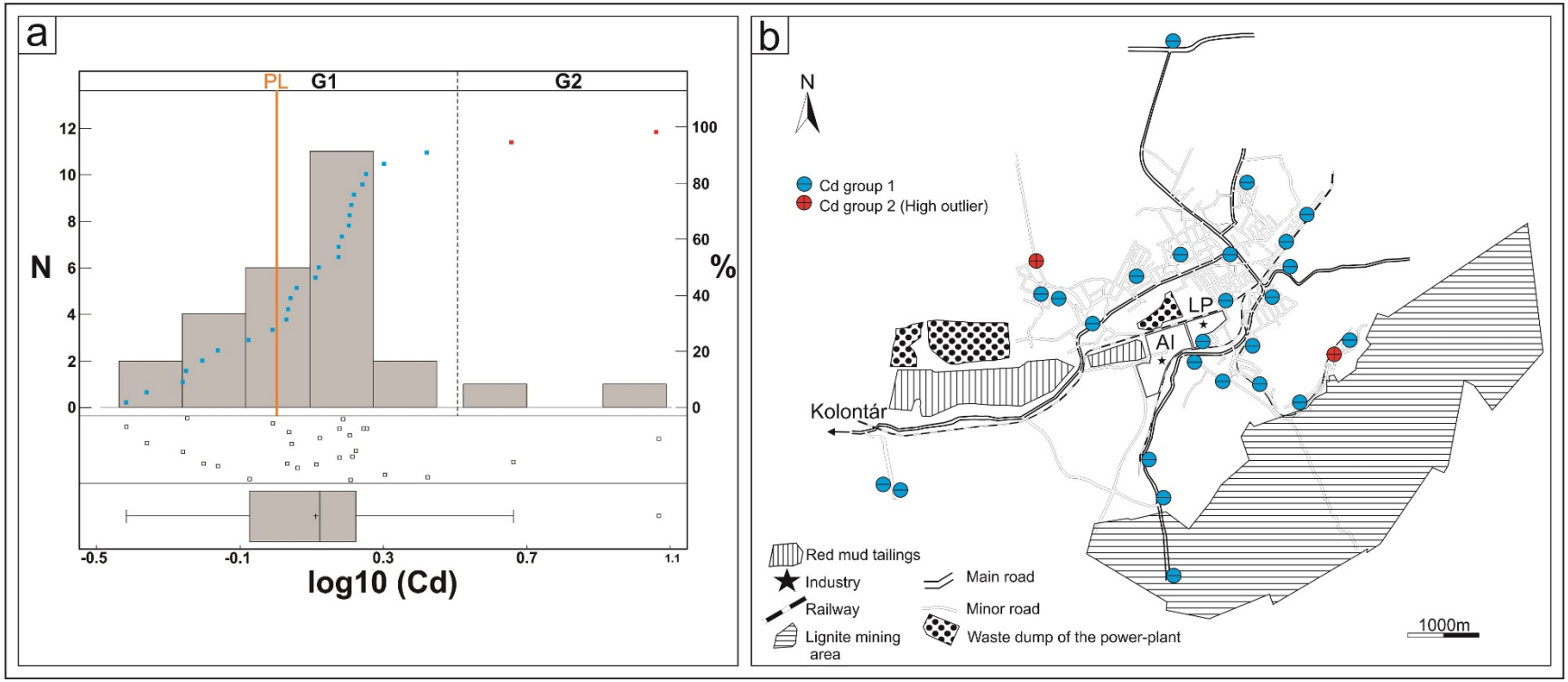

Figure 24. Univariate exploratory data analysis and Cd distribution map in Ajka attic dust. Figure 24a-upper part: frequency histogram of Cd concentration and its cumulative distribution function. Vertical dashed lines: separation of sub-populations based on histogram analysis and homogeneity test. G1–G2 correspond to groups of samples. Figure 24a-lower part: scatter plot and box-and-whiskers plot of original Cd data. Figure 24b: spatial distribution of the Cd sub-groups in the studied attic dust samples. Different colors, circles with minus and circles with plus signs: sample populations (group 1 and group 2-high outliers). See Figure 7 for additional legend information (page: 39). The orange line indicates the pollution limit (PL).

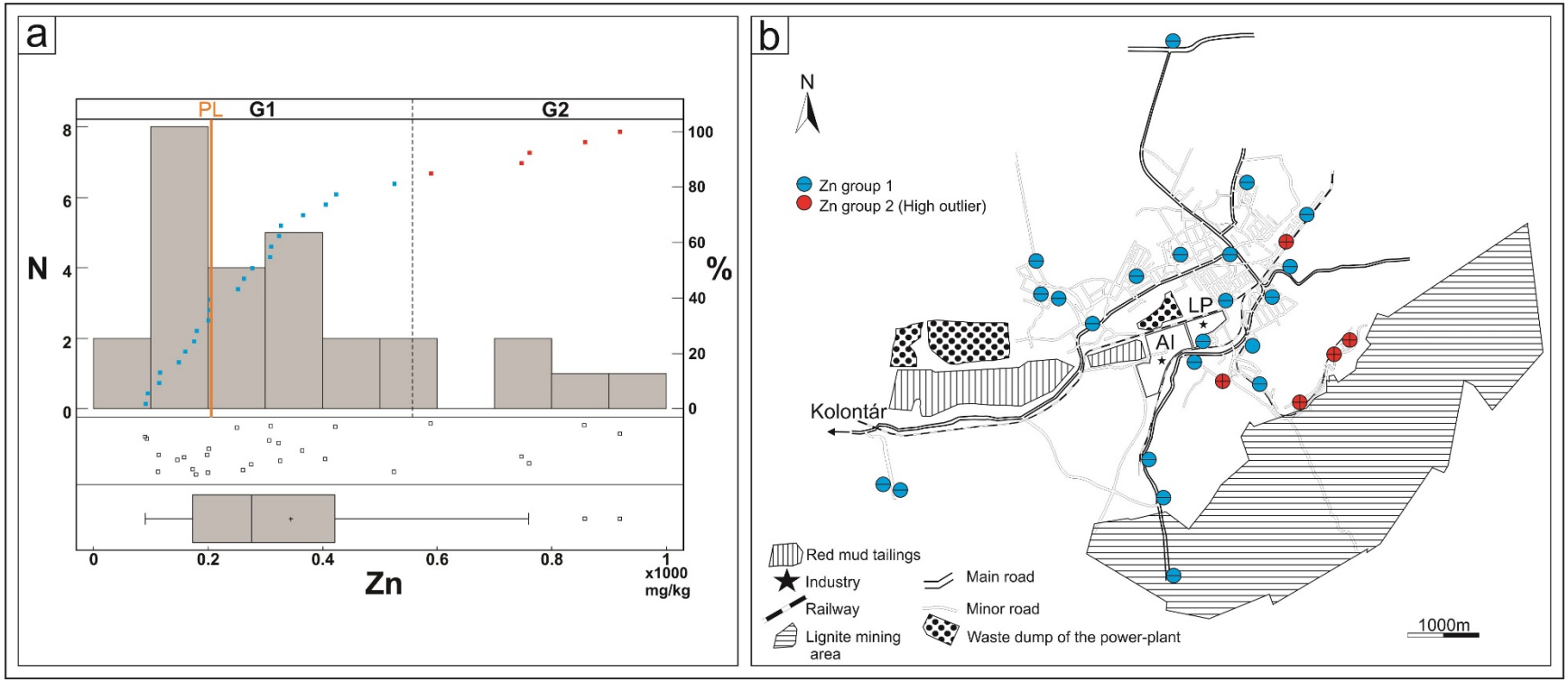

Figure 25. Univariate exploratory data analysis and Zn distribution map in Ajka attic dust. Figure 25a-upper part: frequency histogram of Zn concentration and its cumulative distribution function. Vertical dashed lines: separation of sub-populations based on histogram analysis and homogeneity test. G1 ⁻G2 correspond to groups of samples. Figure 25a-lower part: scatter plot and box-and-whiskers plot of original Zn data. Figure 25b: spatial distribution of the zinc sub-groups in the studied attic dust samples. Different colors, circles with minus and circles with plus signs: sample populations (group 1 and group 2-high outliers). See Figure 7 for additional legend information (page: 39). The orange line indicates the pollution limit (PL).

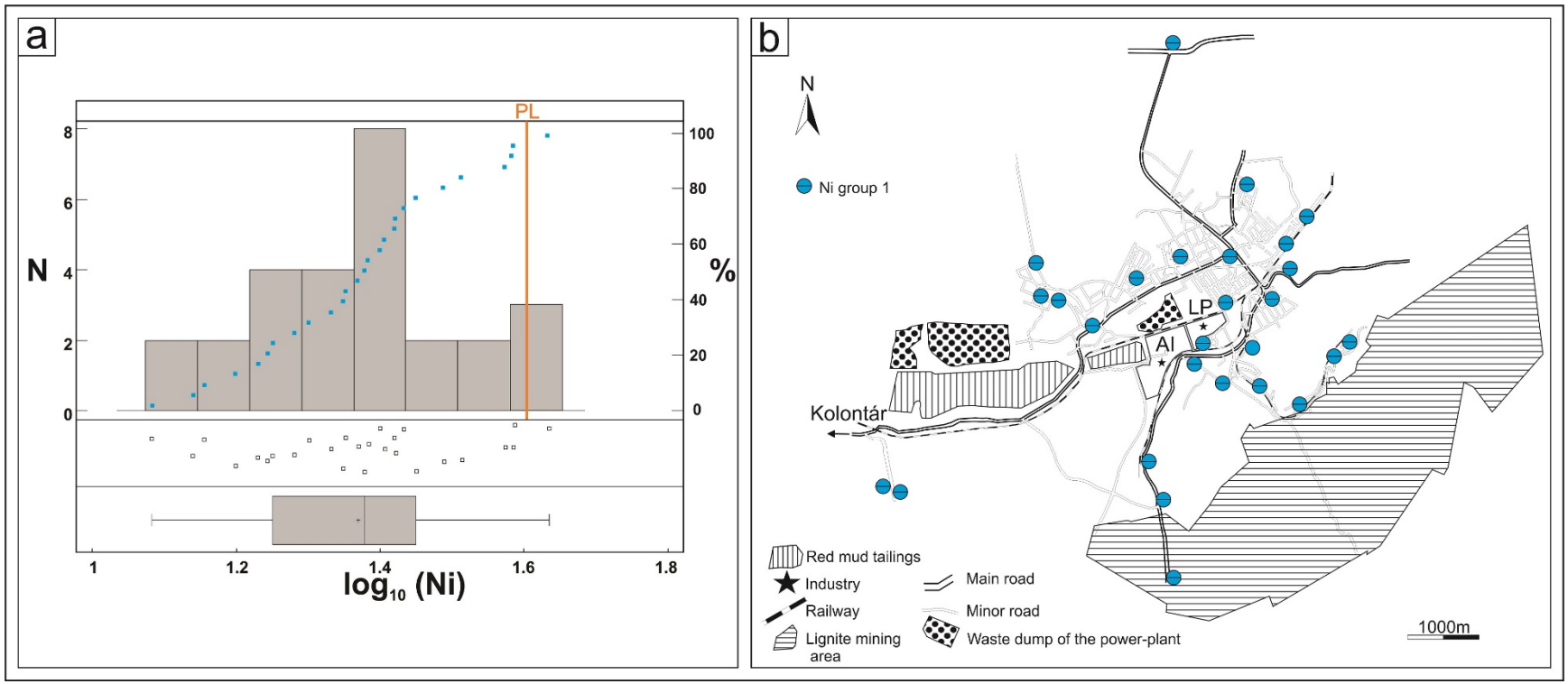

Figure 26. Univariate exploratory data analysis and Ni distribution map in Ajka attic dust. Figure 26a-upper part: frequency histogram of Ni concentration and its cumulative distribution function. Figure 26a-lower part: scatter plot and box-and-whiskers plot of original Ni data. Figure 26b: spatial distribution of the nickel groups in the studied attic dust samples. Blue circles with minus sign: sample population (group 1). See Figure 7 for additional legend information (page: 39). The orange line indicates the pollution limit (PL).

9.4. Discussion of spatial distribution analyses of toxic elements

Spatial distribution analysis was used to ascertain the statements of the univariate analysis. The results were compared to other attic dust studies available in the literature, soil samples from Ajka studied by Zacháry et al. (submitted) and other relevant urban geochemical studies.

Table 20. Comparison table with other attic dust studies available in the literature and a soil campaign also performed in Ajka.

Reference, location, number of attic dust samples	Specification	Statistics	As	Cd	Cu	Hg	Ni	Pb	Zn
Cizdziel and Hodge, 2000, southern Nevada and Utah (USA) (n=8)	Urban area (old attics, *n*=5)	mean	12	2.4	81	-	-	860	860
		EF	6.7	12	1.5	-	-	66.2	12.3
	Urban area (new attics, *n*=3)	mean	14	1.3	51	-	-	140	320
		EF	7.8	6.5	0.9	-	-	10.8	2.4
Davis and Gulson, 2005, Sydney (Australia) (*n*=37)	Industrial (*n*=10)	mean	31.2	17.8	272	-	49	1830	23.673
		median	26.3	15.7	274		44	1960	23.700
		EF	5.1	-	11.9	-	-	104	596
	Semi- industrial (*n*=17)	mean	50.4	4.1	227	-	52	1462	2825
		median	16.3	2.5	224	-	49	1022	1070
		EF	1.7	-	9.7	-	-	73	47
	Non-industrial (*n*=10)	mean	12.8	2.2	140	-	28	604	603
		median	11.7	2	116	-	27	621	562
		EF	2.3	-	5.4	-	-	30	20
Hensley et al., 2007, southern Alabama (USA), (*n*=11)	Study around a wood treatment facility	average	29.8		33.9				
		median	7		26.5				
Tye et al., 2006, Humberside (UK), (*n*=7)	Study around a non-ferrous smelter	average	146	20	563		76	1935	799
		mean	171	23	352		80	1180	501
Gosar et al., 2006, Idrija (Slovenia) (*n*=100)	Most polluted area (n=32)	median				129			
	Intermediately polluted area (*n*=31)	median				17			
	Wider area (*n*=37)	median				6.1			
Balabanova et al., 2011, Radoviš (Macedonia) (*n*=29)	Copper mining area	(aritm) mean	11.3	2.02	52.1		23.1	28.8	50.9
		median	9.58	1.98	26.8		17.2	20.4	49.5
Sajn, 2005, Celje (Slovenia) (*n*=99)	Surrounding of Celje (*n*=64)	med	28	15	129	0.52	53	466	3001
	Celje-Store urban area (*n*=35)	med	63	53	218	0.68	67	1154	8178
Ajka (this study) (*n*=27)	Ajka city	average	15.5	1.77	46.1	0.469	24.6	139	345
		median	15.0	1.33	41.6	0.335	23.9	88.1	276
Zacháry et al., submitted, (*n*=44)	Ajka, Soil samples	average	6.03	0.33	11.7	0.137	19.1	13.1	43.4
		median	6.16	0.34	11.3	0.05	19.6	12.6	44.6

Spatial distribution of arsenic is a good example for the demonstration of effects related to lignite mining. Since coal can contain appreciable amounts of As (Fordyce et al., 2005; Goodarzi, 2009; Salminen et al., 2005), the effect of the lignite mining area and the waste dump of the power plant is obvious, as shown by the statistical analysis and population spatial pattern of As concentrations (Figures 16 and 17). Eighty-five percent of the members of the higher As group exceed the pollution limit value, indicating that areas are uniformly As contaminated (Figure 16; Table 19). A value of 14.3 mg As kg^{-1} can be used as a tentative threshold to delineate areas impacted by lignite mining. The As contamination nature of the higher sub-group is supported by its extreme variability, which is higher than that of the lower significant sub-group (Figure 16a). Thus, the samples from the lower group are affected by one source, most probably the natural background. The maps show the transport of As bearing lignites from mines to the central industrial area and the waste dump of the lignite-fired power plant (Figures 7, 16 and 17), corroborating the lignite-bound As content of the attic dust samples (Yudovich and Ketris, 2005). It is interesting to note that the basic statistical evaluation and data comparison (Chapters 9.1 and 9.2) have not refered to any particular anthropogenic impact; however, the spatial analysis was even suitable for pointing out different processes influencing As distribution.

The average As concentration values are comparable with the results of attic dust studies from southern Nevada and Utah (Cizdziel and Hodge, 2000) and the copper mining area of Radoviš (Balabanova et al., 2011), but the average As values of industrial and semi-industrial areas in Sydney (Davis and Gulson, 2005), southern Alabama (Hensley et al., 2007), Humberside (Tye et al., 2006) and Celje (Sajn, 2005) show higher As concentrations (Table 20). These areas are mostly affected by heavy industrial (point) sources, such as Zn-galvanized products, cement works, ferrous and non-ferrous metal industries, petrochemical industries, scrap metal recovery, ceramic industries, former wood treatment facilities, tin smelters, and the production of Zn and sulphuric acid, respectively (Table 20). The As concentrations were also compared to urban soil samples from the same area analyzed by Zacháry et al. (submitted). The soil median value is 2.5 times lower than the median of attic dust samples (Table 20). However, the lignite mining area is also a well-determined area by most of the potentially toxic elements in the urban soil study, except Hg and Cu (Table 22). In addition, peat land, wet reedy places and playground equipment were also emphasized as local sources of higher As concentrations in the studied urban soils.

A mixture of non-contaminating geochemical processes, such as natural background and the potential contribution of an additional anthropogenic source, defines Hg concentrations in the lower group (Figure 18). Whereas the lower variability of the group with higher Hg results agrees with the observation that the extreme Hg values derive from a single source (Figure 18), the trend surface contour map (Figure 19) indicates that the Hg concentrations steadily decrease away from the lignite-fired power plant in a well-defined concentric manner, showing the fast and short-distance deposition of larger particles (Gosar et al., 2006; Shah et al., 2008; Huggins and Goodarzi, 2009; Figures 18b and 19). Mercury is most probably bound to finer particles in the background (wider) attic dust (Balabanova et al., 2011; Gosar et al., 2006; Huggins and Goodarzi, 2009). In addition, Hg speciation also influences atmospheric transport and residence time (Gosar et al., 2006; Shah et al., 2008). The N-S oriented trend is sub-parallel to the prevailing NW-SE wind direction, suggesting that the atmospheric pathway is the main Hg-transport route. Recent spatial pattern analysis of soil samples showed similar results, indicating a strong association between soil and attic dust in Ajka (Zacháry et al., submitted); however, the average concentrations of Hg in soil are much lower than in attic dust (Table 20).

Attic dust Hg results are available in Slovenia from the Idrija mercury mine area with a long history of Hg mining (Gosar et al., 2006) and Celje city and its surroundings with almost two centuries of high industrial activity (Sajn, 2005). The Hg values from Ajka are in the same range as the values from the Celje area, whereas attic dust Hg content in Idrija is extremely high not even on a local, but also on a global scale (Figure 18; Table 20). Gosar et al. (2006) divided the study area into three sub-regions based on the measured concentrations, where also the least contaminated wider area (area 3) shows results 20 times higher results than the Hg median value from Ajka (Tables 19 and 20).

Beside the Hg enrichment around the power plant in Ajka, other publications also confirm that coal-fired power plants have significant environmental effects due to Hg emission (e.g. Glodek and Pacyna, 2009; Hlawicka et al., 2003; Huang et al., 2004) as coal combustion is usually the prime source of anthropogenic mercury emissions in countries with high levels of coal consumption (e.g. South Africa, Poland, China; Link 11; Glodek and Pacyna 2009).

Based on Figure 20, it is stated that the spatial distribution of lead is dominated by two sources, of which a simple, probably natural, source is observed beside an overall anthropogenic source as a result of the anthropogenic activity. Coal mining and power plants, with the specific

additional source of leaded gasoline combustion and emission by cars, are considered as potential industrial sources (Cizdziel and Hodge, 2000; Ilacqua et al., 2003).

After removing the four high outlier samples, a clear spatial trend was observed in the northern part of the map, starting from the city center and showing the effects of traffic within the city and the presence of the east-west major road crossing the northern part of the studied area (Figures 7, 20 and 21). Here, the spatial and statistical analyses were shown to be an applicable tool for the examination of lead sources in the studied area.

Detailed lead analysis was used in attic dust studies in Sydney, Australia (Davis and Gulson, 2005) and in Nevada and Utah, (USA, Czidziel and Hodge, 2000; Table 20). Czidziel and Hodge (2000) identified 'urban elements', because their sources were related to the city, such as traffic, building/construction, metal corrosion, and solid waste incineration, of which Pb stood out with the highest values. Old houses (n=5) in Nevada and Utah showed significantly higher average concentrations than new houses (n=3; Table 20), and a high correlation coefficient between lead concentrations and the age of the houses (R^2=0.87) was found. However, the number of the samples analyzed was very limited (n=8), they explained three factors causing different results:

(i) 'the preferential accumulation of fine particles in attics;
(ii) 'the fact that older attics generally have larger vents and/or more holes for dust to infiltrate; and
(iii) 'the decreased input of Pb to these environs over the past few decades, primarily a result of the decreased use of leaded gasoline and municipal waste incineration.'

A Kruskal-Wallis test, conducted by Davis and Gulson (2005), also showed significantly higher values not just for Pb, but also for As, Cd, Cu, Sb,W and Zn in older houses than in more recent ones in Sydney (Davis and Gulson, 2005). Ilacqua et al. (2003) demonstrated lead concentrations in the attics as being a function of the age of the houses and the results showed low lead amounts in the houses built in the 1990s and the late 1980s. However, a moderate increase in the 1970s and a sharp increase in the 1960s and 1950s were found. They observed differences between a model calculation and real data based on the fact that the mass of settled dust is not conserved over time. As the lead virtually disappeared in the 1990s, using the model calculation, air concentration of lead did not drop as sharply, due to the effect of re-suspension of soil and dust and also a consequence of other possible local contamination sources. The Pb-concentrations of

the attics from Ajka did not show any trend with the age of the analyzed houses, which is probably caused by the different anthropogenic and natural sources in Ajka and possible disturbances causing local effects in the attics. The correlations were tested also between the other six toxic elements and the age of the studied houses, where only As showed such a relationship, with a correlation coefficient of r=0.57.

The average Pb concentrations in Table 20 are all higher than in Ajka, even in areas described as 'non-industrial' regions, except the urban area of Nevada and Utah, where equal concentrations were found (Cizdziel and Hodge, 2000) and the Radoviš mining area (Balabanova et al, 2011), where the average is 6 times lower than in Ajka (Table 20).

Although Pb in attic dust showed high extreme values (Table 19), its concentrations in the soil samples were only moderately high (average and median: 13.1 mg kg^{-1} and 12.6 mg kg^{-1}, respectively, Table 20), which reveals the lower sensitivity of the attic dust samples to environmental impacts and the higher sensitivity of distinct, probably local or point sources. A spatial trend was also identified in the northern area by using soil samples, which is probably related to the traffic on the east-west major road crossing through the study area.

An obvious spatial correspondence is observed between the locations of samples belonging to the higher concentration group and routes of the main roads and railways (Figures 22a and 22b). In contrast, this linear spatial Cu pattern is not invisible on the contour map (Figure 23), hence the grid-based trend surface map (Figure 23) is not sufficient for the identification of the linear pattern and the effects of transport in Ajka. This underlines the relevance of the detailed statistical and data analysis prior to the generation of the geochemical map (Reimann et al., 2008). The simple and detailed statistical analyses of data revealed an important transportation related contamination Cu source in Ajka, similar to observations in Birmingham, Coventry (UK; Charlesworth et al., 2003) and in Ulsan (South-Korea; Duong and Lee, 2011).

The average Cu-values from Ajka are comparable to the Cu-results measured in the attics of new houses built in southern Nevada and Utah (Cizdziel and Hodge, 2000; Table 20), from southern Alabama (Hensley et al., 2007) and from Macedonia (Balabanova et al., 2011). It is interesting that the values around a Cu mining area were not significantly higher than in Ajka (Balabanova et al., 2011; Table 20). In contrast, the Cu-values from old attics in southern Nevada and Utah, the whole Sydney area, the smelter from Humberside and the Celje area are consistently higher (Table 20). However, the mean and median values of the attic dust samples from Ajka were

four times higher than in the soil samples, while Cu concentrations in soil delineate enrichments around the power plant and in the northern area of the city, which may shed light on the traffic related Cu enrichment (Table 20, Zacháry et al., submitted).

The majority of the Cd and Zn samples belongs to a homogeneous uni-modal group (Figures 23 and 24), dominated by a single process, most likely traffic, fossil fuel combustion and mining (e.g. Balabanova et al., 2011; Lu et al., 2009a, b; Sammut et al., 2008; Salminen et al., 2005) as was also indicated in the univariate statistical description (Chapters 9.1 and 9.2). The spatial distribution of the outliers of Cd and Zn corroborates these findings. At Ajka the uni-modal homogeneous Ni distribution is quite similar to that of Zn and Cd, but Ni has no outlier samples, and only one sample exceeds the pollution limit value, indicating a simple natural source (Figures 23–25; Table 12).

Average Cd concentrations of other attic dust studies are higher in all regions compared to Ajka, except the urban area of southern Nevada and Utah (Cizdziel and Hodge, 2000). Besides, the average Cd concentrations of the Ajka soils are five times lower than the average Cd in attic dusts (Table 20). Average Zn concentrations are higher than those of zinc in houses around the copper mining area in Macedonia (Balabanova et al., 2011) and comparable with the Zn values measured in the urban regions of southern Nevada and Utah (Czidziel and Hodge, 2000). All other average and median Zn values in the literature are significantly higher than the ones in the attic dusts from Ajka. Moreover, only the measured Zn extremes (Figure 24, Table 19) are comparable with the data published by Tye et al. (2006), Davis and Gulson, (2005) and Cizdziel and Hodge, 2000 (Table 20). However, the Zn contcentration measured in the industrial areas of Celje and Sydney are still much larger. Similar estimations can be made with respect to Ni. Its average concentrations are similar to the non-industrial Sydney area (Davis and Gulson, 2005; Table 20) and to the copper mining area (Balabanova et al., 2011; Table 20). The other Ni results are 2–3 times higher in the published references (Table 20). Attic dust and soil Ni values in Ajka are in the same range (Table 20). In addition, an interesting phenomenon was observed in the urban soils of Ajka, where Ni had the highest probability (>50%) of having anomalous high concentration in the Ajka urban topsoils, and Ni was found to be the only element (out of the same 7 toxic elements) having an enrichment factor >1 (Zacháry et al., submitted).

9.5. The results of attic dust analyses compared to the results of soil analyses

Table 21. Comparing the attic dust results with soil results.

Parameter	Attic dust	Urban soil
Median > HRGB[1]	As, Cd, Cu, Hg, Ni, Pb, Zn	Ni
Maximum > HRGB[1]	As, Cd, Cu, Hg, Ni, Pb, Zn	Hg, Cd, Cu
EF (med/HRGB)[1]	Pb(6.8), Zn(6.0), Hg(4.2), Cu(2.8), Cd(2.7), As(2.4), Ni(1.5)	Ni(1.2), As(1.0), Pb(1.0), Zn(0.1), Cu(0.8), Cd(0.7), Hg(0.6)
EF sequence	Pb>>Zn>Hg>>Cu>=Cd>As>Ni	Ni>As=Pb=Zn>Cu>Cd>Hg
Hungarian National Pollution Limit[2]	Median values of As, Cd, Hg, Pb and Zn are around the pollution limit value and at least 50% of the samples are contaminated by As, Cd, Zn	Hg: two samples show higher concentrations than the pollution limit
Maximum exceeds the pollution limit values	Cd(11x), Pb(8x), Hg and Zn(4x), As(2x)	Hg(35.5x)
Unimodal histogram	Cd, Zn, Ni	Cd
Bimodal distribution	As, Hg, Pb, Cu	As, Ni, Zn
Multimodal distributions		Cu, Pb, Hg

EF: Enrichment Factor computed by dividing the median element concentration in the dust/soil sample by the Hungarian regional geochemical background level (HRGB)

[1] Hungarian regional geochemical background (HRGB) value is determined by the Geological Institute of Hungary for this geochemical region by using stream sediment samples (Ódor et al., 1996).

[2] The Hungarian national pollution limit value for geological materials (soil and sediment) declared by Hungarian environmental legislation (Joint Government Decree No 6/2009).

Table 22. Attic dust and soil toxic elements' spatial distribution patterns based on the grouping after univariate statistical analysis and the outlying values in Ajka. An 'X' means the given toxic element displays a spatial pattern with the following - PP: power plants, LM: lignite mining area, WDPP: waste dump of the power plant, N-S trend: north-south trend.

	Attic dust					Urban soil					
Source/ trend	PP	LM	WDPP	Roads, train tracks	N-S trend	PP	LM	WDPP	N-S trend	Northern area	Connection between the PP and LM
As		X	X			X	X			X	
Hg	X				X	X			X		
Pb		X		X		X	X			X	X
Cu		X		X		X				X	
Cd		X	X			X	X			X	X
Zn		X				X	X			X	
Ni						X	X			X	X

As it was observed in the course of the spatial analysis of attic dust samples, the median and average values of the toxic elements in attic dust were higher than in the soil (Table 19 and Table 20). In addition, all the medians of attic dust samples were higher than the HRGB values; on the other hand, only the median of nickel, calculated from the soil results, exceeded the background value (Table 21). Furthermore, taking into consideration the maximum values, only three elements of soil samples (i.e. Hg, Cd and Cu) exceeded the HRGB values (Table 21). This was further verified by the enrichment factors of soil samples (EF), where only Ni showed higher value (EF=1.2) than the background, which was even lesser than the Ni enrichment factor of attic dust (EF=1.5). It should be noted that Ni was the least enriched among other toxic elements measured in attic dust samples compared to the HRGB values (Table 19). Soil sample analysis revealed only two samples, where, due to the extreme Hg-content, the pollution limit was exceeded (Table 21). In contrast, in the attic dusts, where at least 50% of the samples were contaminated by As, Cd and Zn, furthermore, the medians of Hg and Pb were found to be around the pollution limit value.

If the histograms are considered, Cd in soil samples was the only element having unimodal distribution, beside the bimodal distribution of As, Ni, and Zn, and the multimodal distributions of Cu, Pb and Hg. When the common spatial trends are taking into consideration, As concentrations in soils and attic dusts revealed the effect of lignite mining and Hg distribution showed similar enrichment around the power plant together with the N-S trend due to the prevailing wind direction (Table 22). Lead distribution, using the attic dust samples, indicated the

traffic related source, which was not clearly found in the soil lead distribution. However, a traffic related connection was found between the power plant and the mining area.

Higher attic dust toxic element concentrations compared to soil results were also found in Slovenian urban geochemical studies (Alijagic and Sajn, 2006; Gosar et al., 2006; Sajn, 2005). Gosar et al. (2006) found good agreement between the Hg content in soils and attic dust, and highlighted that it depends very much on the morphology of the terrain. Considering the relatively small differences of altitudes in the morphology of Ajka and its vicinity, this should not influence the Hg spatial differences between attic dust and soil. Gosar et al. (2006) identified enrichment in soils, beside atmospheric emissions, where soil parent material (e.g. unsmelted ore waste, ore smelting residues, ore residue dumps outcropping of mineralized rocks) was the main source of Hg emission. The high industrial activity and, as a result, the produced and deposited waste dumps and by-products may cause some spatial differences regarding the soil toxic element concentrations in Ajka. In the course of the soil survey (Zacháry et al., submitted), a remarkable pattern was found in the densely populated northern part of the city for all of the toxic elements, except for Hg (Table 22), which was not delineated by using the attic dust samples. It has been emphasized that the potential utilization of coal combustion by-products as relief equalization material may cause anomalies beside local industrial sources (Dezső et al., 1997; Zacháry et al., submitted).

On the whole, the more bimodal and multimodal histograms of the soil samples (Table 21) suggest that soil is a highly complex environmental medium with a lot of natural and anthropogenic impacts which are difficult to identify separately. However, attic dust is a more sensitive medium, therefore more suitable to demonstrate anthropogenic impacts in the study area than soil. A good example for the application of attic dust to shed light on anthropogenic spatial pattern instead of soil is found in Celje (Slovenia; Sajn, 2005). In this study, only attic dust revealed the halo of Ti-dioxide production instead of soil samples, which showed a naturally controlled Ti pattern. This means the geogenic and anthropogenic distribution patterns were traceable with soil analysis, while anomalous anthropogenic patterns were demonstrated with a remarkable degree of contrast in attic dusts (Sajn, 2005).

9.6. Results of correlation analysis of toxic elements

Bivariate analysis includes a correlation analysis to estimate metal adsorption to Fe-oxy-hydroxide phases in the Ajka attic dust, an important environmental parameter to study the

geochemical behaviour of elements in urban environments (e.g. Contin et al., 2007; Reimann et al., 2008; Table 23, Appendix 11). If the measured Fe represents the adsorbing fraction then the partial correlation with Fe removes its effect and the previously strong virtual correlation between the two metals may drop, indicating that their relationship is due to the effect of Fe as a background variable (Jordan et al., 1997; Table 23). Besides providing a first insight into the controlling geochemical processes, this analysis may reveal the sources of the contaminants since Fe-oxy-hydroxides are major components of the alumina industry red mud (e.g. Brunori et al., 2005; Li, 2001).

Significant and mutual correlations (r=0.53–0.88) exist within the Pb-Zn-Cd-Ni-Cu group. This is particularly strong (r>0.75) among Pb-Cd-Zn (Table 23 and Figure 27). Most of the correlations remain unchanged, when the possible effect of Fe-oxy-hydroxide sorption is taken into account by applying partial correlation with Fe to these relationships (Table 23). Nevertheless, the correlation between Cu-Pb, Cu-Ni and Zn-Ni is decreasing significantly (>50%) after the partial correlation with Fe. Mercury and As do not show any correlation with each other, nor with the other elements, except for the correlation (r=0.76) between As and Ni. The discussed correlation and regression relationships are statistically significant at the 95% confidence level.

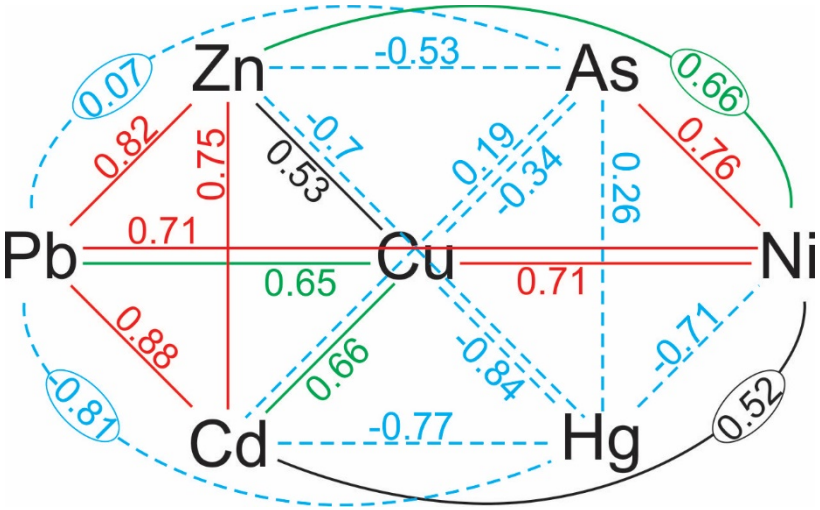

Figure 27. Correlations between the toxic elements in the studied attic dust samples. Correlations between the elements are shown with dashed blue lines if the Pearson's linear correlation coefficient (r) < 0.50, with black lines if r=0.50-0.60, with green lines if r=0.60-0.70, and with red lines if r > 0.70.

Table 23. Correlation matrices of the studied elements, correlation with Fe and partial correlation with Fe. Results are statistically significant at the 95% confidence level.

	Correlation coefficient						
Attic dust samples *bivariate regression*	**As**	**Cd**	**Cu**	**Ni**	**Pb**	**Zn**	**Hg**
As							
Cd	0.19						
Cu	-0.34	0.66					
Ni	0.76	0.52	0.71				
Pb	0.07	0.88	0.65	0.71			
Zn	-0.53	0.75	0.53	0.66	0.82		
Hg	-0.26	-0.77	-0.84	-0.71	-0.81	-0.70	
Attic dust samples *Correlation with Fe*	**As**	**Cd**	**Cu**	**Ni**	**Pb**	**Zn**	**Hg**
Fe	0.71	0.52	0.19	0.94	0.45	0.37	-0.53
Attic dust samples *partial correlation with Fe*	**As**	**Cd**	**Cu**	**Ni**	**Pb**	**Zn**	**Hg**
As							
Cd	-0.36						
Cu	-0.36	0.51					
Ni	0.15	0.50	-0.06				
Pb	-0.09	0.64	0.26	0.50			
Zn	-0.42	0.77	0.49	0.17	0.49		
Hg	0.25	-0.40	-0.13	-0.20	-0.29	-0.27	

A significant correlation (r=0.71) was found between Fe and As (Figure 28a), and Fe explains ~50% of the As variability. It is interesting that all three samples from the waste heaps of the lignite mining area fit to the regression line (Figure 28a), displaying similar linear behavior. There are a few samples with high As concentrations, falling above the Fe-As regression line, corresponding to samples with excessive As that are not controlled by Fe-compound sorption (Figure 28a). In addition, two samples from the waste dump of the power plant were below the regression line, showing that these samples are depleted with respect to the volatile As content as compared to the total Fe content in the ash.

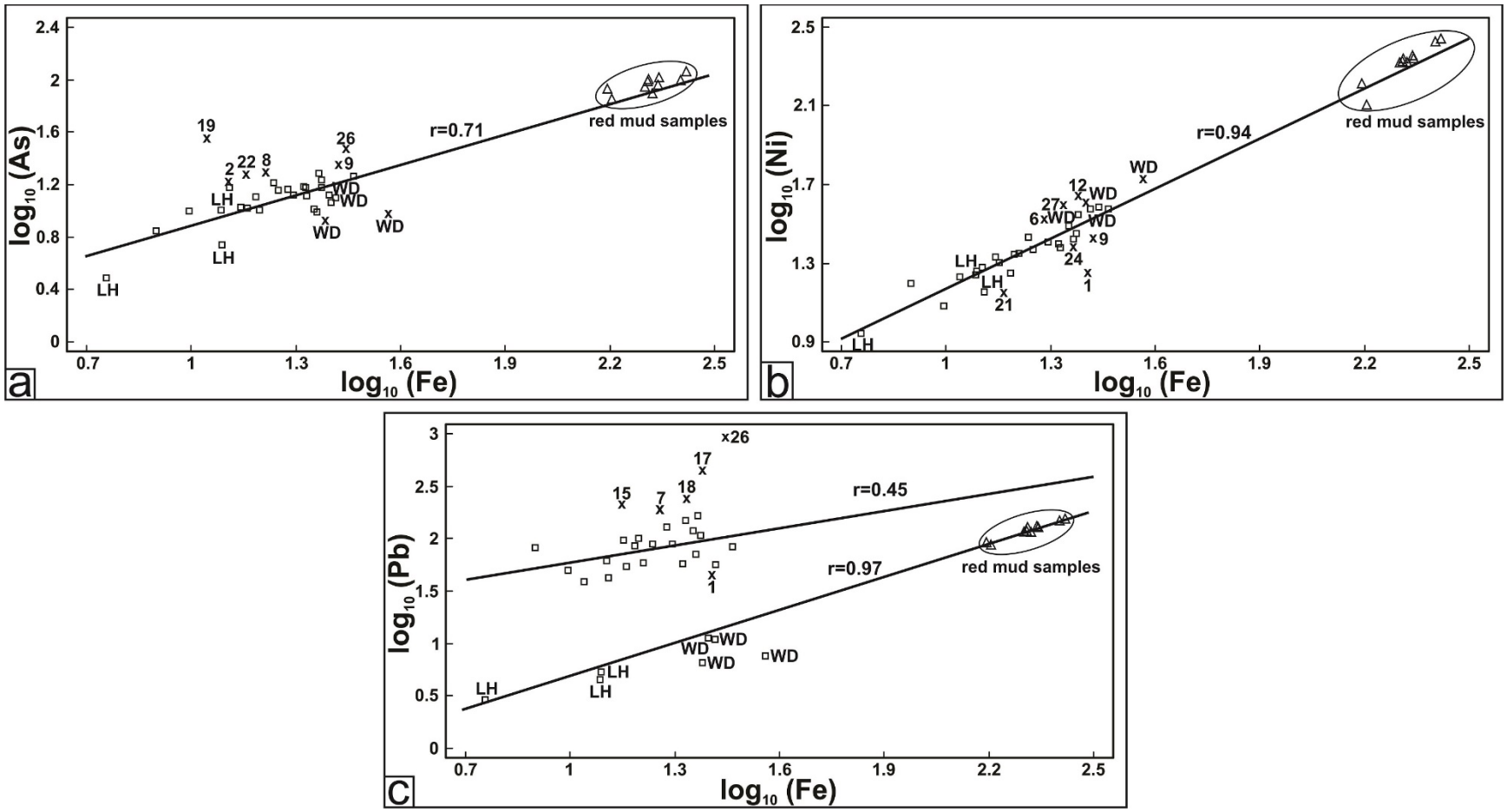

Figure 28. Pearson's correlation coefficients (Pearson, 1896) of As, Ni and Pb with Fe. The sampling points fitting on the regression line are indicated as '□' and bivariate outliers are indicated with an x. 'CH' corresponds to samples from coal waste heap, and 'WD' corresponds to samples from the waste dump of the lignite-fired power plant. Triangles indicate red mud samples. Concentrations of Fe, are given in g kg^{-1}, whereas the other elements are given in mg kg^{-1}.

In the strong correlation between Fe and Ni (r=94), iron explains more than 92% of the Ni variability (Figure 28). The samples which do not fit on the line are found as randomly situated samples with elevated or depleted Ni-concentration.

There is a moderate correlation (r=0.45) between Fe and Pb, explaining only 20% of the Pb variability in the majority of the dust samples (Figure 28c). Bivariate outliers, falling above the Fe-Pb regression line (samples 7, 15, 17, 18, 26), are randomly situated samples in the studied area. All attic dust samples lie far above the seven samples from the waste heaps in the mining area and the waste dump of the power plant.

9.7. Discussion of correlation analysis of toxic element

The partial correlation of Cu and Ni with Fe showed that the correlations of these elements were mainly influenced by Fe-oxy-hydroxide compounds as a background parameter (Table 23). It means they do not have common sources, but it is Fe that keeps these element pairs together (Table 23).

In some published papers (Czidziel and Hodge, 2000; Davis and Gulson, 2005) dealing with attic dust, Pb, Zn and Cd were members of a group called 'urban elements' and their concentrations were higher in industrial settings, because their sources are related to city life (e.g. traffic, building construction, metal corrosion, and solid waste incineration). Similarly strong correlation coefficients (0.81–0.98) between Cd-Zn-Pb were found in attic dusts in settlements around a non-ferrous Sn smelter (Tye et al., 2007). This study confirmed that the strong association of these typical metal industry related elements is connected to their common source(s) (Davis and Gulson, 2005; Sajn, 2005). It is not driven by their common sorption to Fe-compounds in airborne soil particles. It is highly interesting that neither Hg nor As display any notable correlation with the other elements (Table 23), clearly indicating that their origin and geochemistry is different from the other potential contaminants.

The As-Fe regression line has the same slope as the regression line for the Ajka urban soil samples (Zacháry et al., submitted; Figure 28a). This indicates that the studied attic dust is characterized by wind-blown soil and As is adsorbed to Fe compounds in the dust, which is a common geochemical As behaviour in soils (e.g. Alijagić and Sajn, 2006; Sadiq, 1997; Yudovich and Ketris, 2005). The outlier samples above the regression line are found mostly in the lignite mining area and close to the lignite-fired power plant (Figures 7 and 28a), suggesting that As is present in other chemical forms as well, most likely associated with sulphur forming

As-sulphides in the original Ajka lignite. Goodarzi (2009) and Shah et al. (2008), studying coal-fired power plants in Canada and in Australia, reported similar findings.

The strong correlation (r=0.94) between Fe and Ni for most of the samples illustrates the similar geochemical behaviour of Fe and Ni in natural geological materials (e.g. Kabata-Pendias and Pendias, 2000; Figure 28b). The overall low Ni concentration in the studied attic dust samples, together with the results of the statistical data analyses described above, is in agreement with the primary natural soil particle Ni source. This is confirmed by the very strong Fe-Ni correlation (r=0.93) in the soil samples of the urban area (Zacháry et al., submitted). The Ni values of bivariate outliers are most probably affected by local sources within the studied houses. In these attic dust samples, Ni most probably derives from industry related activities using metal equipment and machinery. Alijagić and Sajn (2006) and Sajn (2005) found Ni from anthropogenic sources in Slovenian industrial sites and Sajn (2005) found a strong correlation between Fe and Ni in attic dust from Celje, explained by the fact that they were produced by iron metallurgy. Tye et al. (2006) established a correlation (r=0.71), comparing to other correlations in the study, in attic dust from Humbreside, UK.

The Pb-Fe correlation indicates the general sorption mechanism between Fe-oxides and Pb (Banerjee, 2003). Outlying samples which not fit on the line probably show local Pb-sources within the attic. This slight correlation reveals that processes other than sorption by Fe-compounds primarily control the Pb-distribution in the airborne attic dust. The Pb most likely originates from traffic, as was observed in attic dust samples from Las Vegas, Toquerville, Washington City, Dover and New Jersey (US) by Ilacqua et al. (2003) and Cizdziel and Hodge (2000), respectively. All additional samples from the waste heaps in the mining area and from the waste dump of the power plant prove that excessive Pb content of the dust samples originates from another source, most probably from the traffic in the study urban area.

Summary

The main objective of this research was to study the effect of industrial activities on the human environment, based on qualification of coal slag and fly ash bearing building materials from certain localities within Hungary. Another goal was to introduce a methodology improvement of gamma-ray spectrometry and to investigate multi-source industrial effects via the study of attic dust samples from an industrial area in Ajka, western Hungary. To reach these goals, 29 building material samples and 27 attic dust samples were examined (Figure 5).

Radium-226, ^{232}Th and ^{40}K measurements were performed on the samples at the Eötvös University (Department of Atomic Physics) to qualify building materials. For radium determination, the natural uranium isotopic ratio and the presence of secular equilibrium between ^{226}Ra and ^{238}U were assumed. These verification of these assumptions motivated the development of a measurement system leading to the revitalization of a low background counting chamber at the Center for Energy Research (Hungarian Academy of Sciences). The steps of this process resulted in the development of a relatively cheap and simple radon-leakage-free HDPE sample container and the corresponding measurement equipment. The results obtained by the analysis of coal slag samples verified the natural isotopic ratio between uranium isotopes and the secular equilibrium between radium and uranium, hence approved the measurement of the samples' radium content from the own peak of ^{226}Ra at 186 keV. Secular equilibrium was found between radium and uranium in 8 coal slag samples out of the 9 samples studied. Most probably these radionuclides were in the same phase in the coal and were not influenced during combustion. Out of the 29 building materials, seven (six coal slags and one coal slag concrete) were considered hazardous, i.e. risky to use, based on the results of building material qualifications and dose calculations. This is because of higher radium activity concentrations, mostly in coal slag samples. Coal slag, being a by-product of coal combustion, is enriched in radionuclides after the coal is burned in a power plant. The wide range in radium activity concentrations of coal slags underline the fact that coal is transported to the capital from various different locations. Still, the measured coal slag sample from Budapest is comparable to the results from the Ajka region, indicating that the precise tracing of transport flows, identification of coal sources within the country, and the study of houses where these materials were used, are necessary.

The attic dust method was used for the first time in Hungary to investigate toxic elements in an urban area impacted by multi-source industry. Basic statistics of the results indicated that Zn,

Pb, Hg and Cd distributions in Ajka were likely to be dominated by anthropogenic, mainly point sources, whereas the As, Cu and Ni were not dominated by prominent point sources. Pollution and enrichment estimations were carried out by comparing the results to regional background and pollution limit values. After bimodal distributions of As, Hg, Pb and Cu, with several outliers, and unimodal distributions of Cd, Zn and Ni were identified, a spatial analysis was performed, in which delineated areas with houses where lignite mining (As and Zn distributions, Figures 16 and 25), the lignite-fired power plant (Hg distribution, Figure 18), the waste dumps (As distribution, Figure 16) and traffic (Pb and Cu distributions, Figures 20 and 22) might have impacted deposited airborne dust. The findings of the spatial analysis were expanded with correlation analysis, which corroborated common geochemical behavior, anthropogenic impacts and similarities between attic dust and soil samples. The overall average toxic element concentrations were lower in attic dust from Ajka than in other attic dust studies found in the literature, except for a few cases. There were no significant correlations between toxic elements and the age of the houses, revealing the applicability of attic dust rather for spatial analysis instead of temporal studies in Ajka. Comparing the spatial modelling results of attic dust and soil, it was established that attic dust is a more reliable method for demonstrating the effects of industrial activities in Ajka, Hungary.

It has to be pointed out that all the attic dust sample sites were selected in close collaboration with the local community and many building material investigations were made at the owners' request. This demonstrates the willingness of the Hungarian population to learn more about their indoor environment and about the potential pollution sources.

In Hungary, coal mining and combustion, the aluminum industry, traffic-related sources, smelting and metallurgy are considered as the most important sources of by-products and potential industrial pollutants. Although many coal-fired power plants have been closed or converted to gas or biomass fired ones (e.g. Inota, Tiszapalkonya, Berente, Kelenföld, Győr, Dorog, Tatabánya, Komló, Oroszlány, Pécs and Ajka; Figure 1) in the last decade, in 1980 the Hungarian solid contaminant emission from power plants was about 220 kt. The main hazardous material of the aluminum industry is red mud, the highly alkaline by-product of alumina. Aluminum smelters were found nation-wide (in Csepel, Tatabánya, Ajka and Inota; Figure 1). As a result of the alumina production approximately 75 Mt red mud has been produced in Hungary. The environmental impact of metallurgy is mostly the emission of fine and coarse particles from mechanical and high temperature processes. The Hungarian steel and metallurgical industry is

located in Dunaújváros, Ózd, Salgótarján and Diósgyőr (Figure 1). Additionally, the glass (e.g. Ajka, Salgótarján; Figure 1) and cement industries (e.g. Beremend, Lábatlan; Figure 1) were also significant industrial sites in the country. In conclusion, the results of the thesis and the legacy of the aforementioned industrial sites all over the country suggest that present and former industry still impacts our environment. On a local scale, taking into consideration the number of industrial areas around the country, the analysis and qualification of building materials, in particular coal combustion by-products, and the investigation of the indoor environment (e.g. with attic dust analysis) around urban areas are necessary, not only from scientific, but also from a social point of view. On a global scale, the demographical prognosis undeniably suggests that the urban environment will soon become the predominant human habitat for the first time in history, hence the adequate urban geochemical knowledge of these areas is indispensable.

Theses

1. I have made a contribution to the development of a gamma-ray spectrometry measurement system for the accurate and fast determination of ^{226}Ra. The applied HDPE sample holder tests showed with >95% probability that radon leakage was negligible, i.e. less than 2% of the decay constant. The difference between the result of the efficiency transfer method and the control measurement was less than 5% (Kis et al., 2013). With the system I confirmed the existence of natural uranium activity ratio (weighted average: 0.0466 ± 0.0030) and secular equilibrium between uranium and radium (determined from the comparison of the peak of the ^{234m}Pa and that of radon decay products, ^{214}Pb and ^{214}Bi) in coal slag samples. I concluded that the 186 keV gamma-peak can be used for efficient radium measurement without a radon-tight sample holder and without a ~30 days waiting period (Völgyesi et al., 2014a).

2. I have qualified 29 artificial building material samples from the central Hungarian Region and the city of Ajka, among which I identified seven hazardous samples (six coal slags and one coal slag concrete) with an elevated Ra_{eq}, I index, and annual effective dose values. The ^{226}Ra activity concentration in most of the coal slag samples was much higher (780 ± 975 Bq kg^{-1}) than that in the other samples, and the world references. Samples from Ajka represent a group with extremely high activity concentrations (1571 ± 1092 Bq kg^{-1}). Th-232 and ^{40}K activity concentration results were comparable to the international values with few outlying values (e.g. high ^{40}K content of bricks) (Szabó et al., 2013; Völgyesi et al., 2014a). These statements were confirmed by in situ gamma dose rate measurements. All of these shed light on necessity of the examination of houses in the Central Hungarian Region where coal slag was used.

3. I have applied attic dust as a new sample medium to study the relation between potential industrial contamination sources and spatial distribution and behaviour of the toxic elements in a Hungarian industrial area. The enrichment calculations (Pb>>Zn>Hg>>Cu>=Cd>As>Ni) showed that the studied dust is mostly contaminated with Hg, Pb and Zn compared to the regional geochemical background values. Considering the pollution limit, the highest contamination exists for As, Cd, Hg and Pb, in addition to Zn, with occasional extremely high concentrations. There was no remarkable contamination with Ni and Cu, their concentrations lie very close to the limit values (Völgyesi et al., 2014b).

4. I have demonstrated that the spatial distribution analysis of the toxic elements revealed the impact of lignite mining (As and Zn distributions), the lignite-fired power plant (Hg distribution), the power plant waste dumps (As distribution) and traffic (Pb and Cu distributions) in attic dust samples from Ajka. Arsenic, Hg, Pb and Cu dust showed multi-modal distributions and delineated areas impacted by airborne dust from the anthropogenic sources. Cadmium and Zn showed uni-modal distributions with extreme outliers, suggesting that the anthropogenic (point) source(s) determine(s) their geochemical distribution. Nickel has low overall variability with one outlier and its spatial distribution is not driven by prominent point sources. By means of As, Pb and Cu distributions the advantage of using statistical and spatial analysis was verified (Völgyesi et al., 2014b).

5. I have studied the relationship between soil and attic dust samples and established that attic dust is a sensitive sample medium, and is therefore highly suitable for the demonstration of anthropogenic industrial impacts. However, there were no significant correlations between concentrations of toxic elements and the age of the houses, indicating the applicability of attic dust in Ajka rather for spatial than temporal analysis. Even though average toxic element concentration range was smaller in soils than in attic dust, As, Hg and Pb showed similar spatial patterns. Our study on soils supports that soil is a highly complex environmental medium with a lot of natural and anthropogenic impacts difficult to identify separately (Zacháry, et al., submitted; Völgyesi et al., 2014b).

6. I have concluded that the mutual correlations (r=0.53–0.88) between the toxic elements of the Pb-Zn-Cd-Ni-Cu group in attic dust samples confirm their common industry related source which was even stronger among Pb-Cd-Zn elements (r>0.75). The partial correlations of Ni and Cu with Fe pointed out that the correlation of these two elements (Ni-Cu) is mainly due to their connection to iron-oxy-hydroxide compounds, hence Fe keeps these elements appearing together. Neither Hg nor As displayed any notable correlation with the other elements indicating clearly that their origin and geochemistry is different from the other potential contaminants. The correspondence between the correlation of As and Fe in soil and attic dust indicated the wind-blown origin of As in attic dust and corroborated the common As distributions in both sample medium. The weak correlation between Pb and Fe in attic dust confirmed the traffic related Pb source (Zacháry, et al., submitted; Völgyesi et al., 2014b).

Tézisek

1. Hozzájárultam egy gamma-spektrometriai mérőrendszer kifejlesztéséhez, amely alkalmas a ^{226}Ra pontos és gyors meghatározására. Az alkalmazott HDPE mintatartó tesztje alapján több, mint 95%-os valószínűséggel állítható, hogy a radon-szökés mértéke kisebb, mint a radon bomlási állandójának 2%-a, vagyis elhanyagolható. A számított hatásfok és a kontrol mérés hatásfoka közti különbség kisebb, mint 5%-nak adódott (Kis et al., 2013). A mérőrendszerrel sikerült igazolnom az uránizotópok természetes aktivitás arányát (súlyozott átlag: 0.0466 ± 0.0030) és az ^{238}U és ^{226}Ra közötti szekuláris egyensúly meglétét (a ^{234m}Pa 1001 keV-os csúcsának és a radon leányelemek ^{214}Pb and ^{214}Bi csúcsainak összehasonlítása alapján) salakmintákban. Így azt a következtetést vontam le, hogy a 186 keV-os csúcs alkalmas a rádium aktivitás koncentrációjának pontos mérésére, amely során nincs szükség radont záró mintatartóra és a ~30 napos várakozási időre (Völgyesi et al., 2014a).

2. Elvégeztem 29 építőanyag minta minősítését, amelyek a Közép-magyarországi régióból és Ajkáról származnak. Ezek közül 7 kockázatos mintát (6 salak és 1 salakbeton minta) azonosítottam megnövekedett rádium ekvivalens és aktivitás koncentráció index, valamint dózis értékek alapján. A salakok rádium aktivitás koncentrációja (780 ± 975 Bq kg^{-1}) a legtöbb mintában lényegesen nagyobb, mint a többi építőanyag mintában mért értékek és a világátlag, amelyek közül kiemelkedik az Ajkáról származó salakok csoportja (1571 ± 1092 Bq kg^{-1}). A minták ^{232}Th és ^{40}K tartalma a nemzetközi átlagos értékekkel egyezik meg, néhány kiugró eredménytől eltekintve (pl. a téglák nagy ^{40}K aktivitás-koncentrációja) (Szabó et al., 2013; Völgyesi et al., 2014a). Az in situ gamma dózisteljesítmény mérések igazolták ezeket a megállapításokat. Eredményeim felhívják a figyelmet olyan Közép-magyarországi régióban található épületek vizsgálatának szükségességére, amelyekhez salak-tartalmú építőanyagot használtak.

3. A padlásport mint új mintavételi közeget elsőként alkalmaztam annak tanulmányozására, hogy a potenciális ipari szennyező források hogyan kapcsolódnak a toxikus elemek térbeli eloszlásához és viselkedéséhez egy magyarországi ipari területen. A természetes geokémiai háttérhez viszonyított dúsítási tényezők (Pb>>Zn>Hg>>Cu>=Cd>As>Ni) alapján megállapítottam, hogy a vizsgált porok leginkább higannyal, ólommal és cinkkel szennyezettek. A szennyezettségi határértékeket figyelembe véve a legjelentősebb kontaminációt az As, Cd, Hg és Pb, valamint

néhány mintában a Zn esetében tapasztaltam. A Ni és a Cu kapcsán nem mutatható ki jelentős szennyezés, az értékek kisebbek, mint a szennyezettségi határérték (Völgyesi et al., 2014b).

4. Kimutattam a toxikus elemek térbeli eloszlásának vizsgálatával a szénbányászat (As és Zn eloszlás), a szénerőmű (Hg eloszlás), az erőművi meddőhányó (As eloszlás) és a közlekedés (Pb és Cu eloszlás) ajkai padlás porokra gyakorolt hatását. Demonstráltam, hogy a padlásporokban található As, Hg, Pb és Cu multi-modális eloszlást mutatnak, és olyan területeket jelölnek ki potenciális forrásul, amelyeket az antropogén hatások egyértelműen befolyásoltak. A kadmium és cink esetében extrém kiugró értékekkel rendelkező uni-modális eloszlást kaptam, amely arra utal, hogy antropogén (pont)források határozzák meg ezen elemek geokémiai eloszlását. A nikkel kis változékonysággal és egy kiugró értékkel jellemzhető, továbbá térbeli eloszlását semmilyen prominens forrás nem befolyásolja. Emellett rámutattam az As, Pb és Cu eloszlás vizsgálatával a statisztikai és térbeli vizsgálatok együttes használatának fontosságára (Völgyesi et al., 2014b).

5. Megvizsgáltam a padláspor és talaj közötti kapcsolatot a toxikus elemek vonatkozásában és megállapítottam, hogy a padláspor egy érzékeny mintavételi közeg, amely alkalmasabb az ipari szennyező források hatásának kimutatására, mint a talaj. A toxikus elemek koncentrációja és a házak életkora közötti korreláció hiánya alapján a padláspor inkább térbeli, mint időbeli folyamatok vizsgálatára használható Ajkán. Továbbá megfigyeltem, hogy az As, Hg és Pb eloszlások esetében hasonló térbeli mintázat alakult ki, annak ellenére, hogy a talajok átlagos koncentráció tartománya kisebb, mint a padlásporoké. A talajok esetében megfigyelt több bi- és multi-modális hisztogram arra utal, hogy a talaj komplexebb környezeti közeg, amelyet számos, nehezen elkülöníthető természetes és mesterséges folyamat befolyásol (Zacháry, et al., benyújtott; Völgyesi et al., 2014b).

6. Megállapítottam az Pb-Zn-Cd-Ni-Cu toxikus elemek csoportjának közös korrelációs tényezői (r=0.53–0.88) alapján, hogy ezek az elemek közös ipari tevékenységhez kötődő forrás jelenlétére utalnak. A korreláció a Pb-Cd-Zn elemek között még erősebbnek adódott (r>0.75). A nikkel és a réz vassal való parciális korrelációja azt sejteti, hogy ezeknek az elemeknek (Ni-Cu) az összetartozásában a vas-oxihidroxidok játszanak döntő szerepet, vagyis korrelációjuk a vashoz való kötődésük következménye. A higany és az arzén nem mutatott figyelemre méltó korrelációt a többi vizsgált szennyező elemmel, amely nyilvánvalóvá teszi, hogy ezen elemek eredete és geokémiája különbözik a többi elemétől. A vas és arzén korrelációi közti összefüggés a talajban

és a padlásporban a por arzén-tartalmának talaj eredetére utal, amit megerősít az arzén azonos térbeli eloszlása mindkét közegben. A padláspor mintákban megfigyelt gyenge korreláció az ólom és a vas között jelzi az ólom közlekedéshez köthető eredetét (Zacháry, et al., benyújtott; Völgyesi et al., 2014b).

Abstract

Environment geochemical research was carried out by gamma-ray spectrometric analysis of Hungarian building material samples, supplemented by a measurement improvement method and by the analysis of attic dust samples from Ajka, Hungary. The major goals were to qualify Hungarian building materials containing coal combustion by-products, using qualification indices (i.e. Ra_{eq} and I), and to develop an appropriate measuring system, with which the accurate determination of ^{226}Ra can be proven. The attic dust study aims to determine the geochemical behavior of As, Cd, Cu, Hg, Ni, Pb and Zn in the multi-source industrial area of Ajka, using chemical and statistical analysis. The test of the developed HDPE sample holder showed with >95% probability that radon leakage was less than 2% of the decay constant. The difference between the result of the efficiency transfer method and the control measurement was less than 5%. With the system the existence of natural uranium activity ratio (weighted average: 0.0466 ± 0.0030) and secular equilibrium between uranium and radium, determined from the comparison of the peak of the ^{234m}Pa and that of radon decay products (i. e. ^{214}Pb and ^{214}Bi), was confirmed in coal slag samples. Hence, the 186 keV gamma peak can be used for efficient radium measurement without a radon-tight sample holder and without a ~30 days waiting period. Twenty-nine artificial building material samples from the central Hungarian Region and the city of Ajka were qualified, among which I identified seven hazardous samples (i.e. six coal slags and one coal slag concrete) with an elevated Ra_{eq}, I index, and annual effective dose values. The ^{226}Ra activity concentration in most of the coal slag samples was much higher (780 ± 975 Bq kg^{-1}) than that in the other samples and the world references. The enrichment calculations showed that the studied 27 attic dust samples are mostly contaminated by Hg, Pb and Zn. Spatial distribution analysis revealed impacts of the lignite mining (As and Zn), the lignite-fired power plant (Hg), the power plant waste dumps (As) and the traffic (Pb and Cu). Correlation analysis was used to supplement the spatial analysis and specialize geochemical behaviors of the toxic elements in Ajka. It was established that attic dust is a more sensitive sampling media than soil, therefore, analyzing attic dust is a more suitable method to demonstrate anthropogenic industrial impacts. It can be concluded, that mistakes committed in the past still influence our environment and there are many industrial sites in Hungary which needs to be studied in view of environmental geochemistry.

Magyar nyelvű összefoglaló

Egy környezetgeokémiai kutatás részeként a magyarországi építőanyagok gamma-spektrometriai elemzésére, egy mérőrendszer kifejlesztésére és ajkai padlás por minták vizsgálatára került sor. A gamma-spektrometriai vizsgálatok során célja a főként erőművi melléktermékeket tartalmazó építőanyagok különböző indexekkel történő minősítése volt és egy olyan mérőrendszer kifejlesztése, amivel igazolni lehet a rádium gyors és pontos meghatározását. A padláspor vizsgálat célja az As, Cd, Cu, Hg, Ni, Pb és Zn geokémiai viselkedésének tanulmányozása volt egy, több potenciális szennyező forrással rendelkező területen, amelyet kémiai és statisztikai módszerek segítségével végeztem el. Az alkalmazott HDPE mintatartó tesztje alapján több mint 95%-os valószínűséggel állítható, hogy a radon-szökés mértéke kisebb, mint a radon bomlási állandójának 2%-a. A számított hatásfok és a kontrol mérés hatásfoka közti különbség kisebb, mint 5%-nak adódott. Az eredmények az uránizotópok természetes aktivitás arányát (súlyozott átlag: 0.0466 ± 0.0030) és az ^{238}U és ^{226}Ra közötti szekuláris egyensúly meglétét (a ^{234m}Pa 1001 keV-os csúcsának és a radon leányelemek ^{214}Pb and ^{214}Bi csúcsainak összehasonlítása alapján) mutatták a salakmintákban. Tehát a 186 keV-os csúcs alkalmas a rádium aktivitás koncentrációjának pontos mérésére, amely során nincs szükség radont záró mintatartóra és a ~30 napos várakozási időre. Összesen 29 építőanyag minta minősítésére került sor, amelyek közül a 7 kockázatos mintát (6 salak és 1 salakbeton minta) azonosítottam megnövekedett rádium ekvivalens és aktivitás koncentráció index, valamint dózis értékek alapján. A salakok rádium aktivitás koncentrációja (780 ± 975 Bq kg^{-1}) a legtöbb mintában lényegesen nagyobb a többi építőanyag mintában mért értékeknél és a világátlagnál. A vizsgált 27 padláspor minta dúsulási faktorainak számítása alapján (Pb>>Zn>Hg>>Cu>=Cd>As>Ni) a Hg, Pb és Zn értékek mutattak a geokémiai háttérhez képest jelentős koncentrációkat. A toxikus elemek térbeli eloszlásának analízise a kőszén bánya (As és Zn), a szénerőmű (Hg), az erőművi meddőhányó (As) és a közlekedés (Cu és Pb) hatásait mutatta ki. A korrelációs vizsgálatok kiegészítették a térbeli analízis során kapott eredményeket és specifikálták az elemek geokémiai viselkedését. A padláspor és talaj összehasonlítása alapján a padláspor alkalmasabb az ipari szennyező források hatásának kimutatására. A kutatás rávilágított a környezetgeokémiai vizsgálatok fontosságára és arra, hogy a múltban elkövetett hibák jelenleg is hatással vannak környezetünkre.

References

Abejón, R. Garea, A. "A bibliometric analysis of research on arsenic in drinking water during the 1992–2012 period: An outlook to treatment alternatives for arsenic removal." *Journal of Water Process Engineering* 6 (2015): 105-119.

Abo-Elmagd, M. Soliman, H. A. Salman, Kh. A. El-Masry, N. M. "Radiological Hazards of TENORM in the Wasted Petroleum Pipes." *Journal of Environmental Radioactivity* 101 (2010): 51–54.

Ajmone-Marsan, F. Biasioli, M. Kralj, T. Grčman, H. Davidson, C. M. Hursthouse, A. S. Madrid, L. Rodrigues, S. "Metals in Particle-Size Fractions of the Soils of Five European Cities." *Environmental Pollution* 152 (2008): 73–81.

Alijagić, J. Šajn, R. "Influence of Ironworks on Distribution of Chemical Elements in Bosnia and Herzegovina and Slovenia." *Geologija* 49 (2006): 123–132.

Al-Khasman, O.A. "Heavy metal distribution in dust, street dust and soil from the workplace in Karak industrial estate, Jordan." *Atmospheric Environment* 38 (2004): 6803‑6812.

Al-Sulaiti, H. Alkhomashi, N. Al-Dahan, N. Al-Dosari, M. Bradley, D.A. Bukhari, S. Matthews, M. Regan, P.H. Santawamaitre, T. "Determination of the natural radioactivity in Qatarian building materials using high-resolution gamma-ray spectrometry." *Nuclear Instruments and Methods in Physics Research* 652 (2011): 915-919.

Arafa, W. "Permeability of Radon-222 through Some Materials." *Radiation Measurements* 35 (2002): 207–211.

Ashry, A. H. Abou-Leila, M. Abdalla, A. M. "Measurement of Radon Permeability through Polyethylene Membrane Using Scintillation Detector." *Radiation Measurements* 46 (2011): 149–152.

ATSDR, 2011. The priority list of hazardous substances. Agency for Toxic Substances and Disease Registry, Atlanta, USA.

Balabanova, B. Stafilov, T. Šajn, R. Bačeva, K. "Distribution of Chemical Elements in Attic Dust as Reflection of Their Geogenic and Anthropogenic Sources in the Vicinity of the Copper Mine and Flotation Plant." *Archives of Environmental Contamination and Toxicology* 61 (2011): 173–184.

Banerjee, A. D. K. "Heavy Metal Levels and Solid Phase Speciation in Street Dusts of Delhi, India." *Environmental Pollution* 123 (2003): 95–105.

Benke, R. R. Kearfott, K. J. "Accounting for 222 Rn Loss during Oven Drying for the Immediate Laboratory Gamma-Ray Spectroscopy of Collected Soil Samples." *Applied Radiationa and Isotopes* 52 (2000): 271–287.

Beretka, J. Mathew, P.J. "Natural radioactivity of Australian building materials, industrial wastes and by-products." *Health Phyics 48* (1985): 87-95.

Bertalan, É. Bartha, A. Ballók, I. Varga-Barna, Zs. "The influence of experimental leaching conditions for the determinations of the soluble element content of soil and stream sediment samples." *International Journal of Environmental Analytical Chemistry* 82 (2003): 771-784.

Bé, M-M. Chisté, V. Dulieu, C. Mougeot, X. Chechev, V. P. Kondev, F. G. Nichols, A. L. Huang, X. Wang, B. "Monographie BIPM-5—Table of radionuclides." *Bureau International des Poids et Mesures (BIPM)* (2013): Sevres.

Bhanarkar, A. D. Gavane, A.G. Tajne, D.S. Tamhane, S.M. Nema, P. "Composition and Size Distribution of Particules Emissions from a Coal-Fired Power Plant in India." *Fuel* 87 (2008): 2095–2101.

Bijen, J. "Benefits of Slag and Fly Ash." *Construction and Building Materials* 10.5 Special Issue (1996): 309–314.

Bódizs, D. Gáspár, L., Keömlei, G. "Radioactive emission from coal fired power plants." *Periodica Polytechnica Ser. Physics* 1 (1993): 87–99.

Bódizs, D. „Atommag-sugárzások méréstechnikái" (IN Hungarian) Typotex Budapest, 2nd. Ed. (2006): 272.

Breitner, D. "Geochemical and mineralogical study of overburden profiles in glaciated terrain, Finland – implication for the assessment of radon emission –." PhD Thesis, Eötvös University, Lithospere Fluid Research Laboratory (2011): 159.

Brunori, C. Cremisini, C. Massanisso, P. Pinto, V. Torricelli, L. "Reuse of a treated red mud bauxite waste: studies on environmental compatibility." *Journal of Hazardous Materials* 117 (2005): 55–63.

Campa, M. Castanas, E. "Human health effects of air pollution." *Environmental Pollution* 151 (2008): 362–367.

Charlesworth, S. M. Lees, J. "The Distribution of Heavy Metals in Deposited Urban Dusts and Sediments, Coventry, England." *Environmental Geochemistry and Health* 21 (1999): 97–115.

Charlesworth, S. Everett, M. McCarthy, R. Ordonez, A. De Miguel, E. "A comparative study of heavy metal concentration and distribution in deposited street dusts in a large and a small urban area: Birmingham and Coventry, West Midlands, UK." *Environmetn International* 29 (2003): 563–573.

Cizdziel, J. V. Hodge, V. F. "Attics as Archives for House Infiltrating Pollutants: Trace Elements and Pesticides in Attic Dust and Soil from Southern Nevada and Utah." *Microchemical Journal* 64 (2000): 85–92.

Cizdziel, J. V. Hodge, V. F. Faller, S. H. "Plutonium Anomalies in Attic Dust and Soils at Locations Surrounding the Nevada Test Site." *Chemosphere* 37 (1998): 1157–1168.

Coles, D. G. Ragaini, R. C. Ondov, J. M. "Behavior of Natural Radionuclides in Western Coal-Fired Power Plants." *Environmental Science & Technology* 12 (1978): 442–446.

Coles, D. G. Ragaini, R. C. Ondov, J. M."Chemical Studies of Stack Fly Ash from a Coal-Fired Power Plant"*American Chemical Society* 13 (1979): 455-459.

Condomines, M. Loubeau, O. Patrier, P. "Recent mobilization of U-series radionuclides in the Bernardan U deposit (French Massif Central)" *Chemical Geology* 244 (2007): 304-315.

Contin, M. Mondini, C. Leita, L. De Nobili, M. "Enhanced soil toxic metal fixation in iron (hydr)oxides by redox cycles." *Geoderma* 140 (2007): 164–175.

Császár, G. “Magyarország és környezetének regionális földtana. I. Paleozoikum paleogén (in Hungarian).” ELTE Eötvös Kiadó, Budapest, (2005): 328.

Davis, J. J. Gulson, B. L. “Ceiling (attic) Dust: A ‘Museum’ of Contamination and Potential Hazard.” *Environmental Research* 99 (2005): 177–194.

Daza, M. J. Quintana, B. Garcia-Talavera, M. Fernandez, F. “Efficiency Calibration of a HPGe Detector in the [46.54-2000] keV Energy Range for the Measurement of Environmental Samples.” *Nuclear Instruments and Methods in Physics Research, Section A: Accelerators, Spectrometers, Detectors and Associated Equipment* 470 (2001): 520–532.

Damla, N. Cevik, U. Kobya, A.I. Celik, A. Yildirim, I. “Assessment of natural radioactivity and mass attenuation coefficients of brick and roofing tile used in Turkey.” *Radiation Measurements* 46 (2011): 701-708.

Darnley, A.G. Bjorklund, A. Bolviken, B. Gustavsson, N. Koval, P.V. Plant, J.A. “A global geochemical database for environmental and resource management.” In: Recommendations for International Geochemical Mapping — Final Report of IGCP Project 259. Earth Science Report (1995): 19. UNESCO Publishing Paris, 122 <http://www.globalgeochemicalbaselines.eu/wp-content/uploads/2012/07/Blue_Book_GGD_IGCP259.pdf>. (Last accessed 01 June 2015)

De Corte, F. Vandenberghe, H. U. D. De Wispelaere, A. Van den Haute, P. “Direct Gamma-Spectrometric Measurement of the 226Ra 186.2 keV Line for Detecting 238U/226Ra Disequilibrium in Determining the Environmental Dose Rate for the Luminescence Dating of Sediments.” *Applied Radiation and Isotopes Special Issue* 63 (2005): 589–598.

De Miguel, E. Llamas, J.F. Chacón, E. Mazadiego, L.F. “Sources and pathways of trace elements in urban environments: a multi-elemental qualitative approach.” *Science of the Total Environment* 235 (1999): 355–357.

Dezső, Z. Papp, Z. Daróczy, S. “Radioactive pollution and radiation load of the population caused by a combustion power station at Ajka.” *Fizikai Szemle* 8 (1997): 244.

Duong, T. T. T. Lee. B. K. “Partitioning and Mobility Behavior of Metals in Road Dusts from National-Scale Industrial Areas in Korea.” *Atmospheric Environment* 43 (2009): 3502–3509.

Duong, T. T. T. Lee, B. K. “Determining contamination level of heavy metals in road dust from busy traffic areas with different characteristics.” *Journal of Environmental Management* 92 (2011): 554–562.

DuPont (2012) http://www.dupontelastomers.com/Products/Viton/ techInfo.asp. (Last accessed 1 June 2015)

Ebaid, YY. El-Mongy, S. A. Allam, K.A “^{235}U γ-emission contribution to the 186 keV energy transition of ^{226}Ra in environmental samples activity calculations.” *International Congress Series* 1276 (2005): 409–411

El Afifi, E. M. Hilal, M. A. Khalifa, S. M. Aly, H. F. “Evaluation of U, Th, K and emanated radon in some NORM and TENORM samples.” *Radiatiation Measurements* 41 (2006): 627-633.

ERIKS (2012) http://oring.info/en/products/bycompound/vitonfkm/. (Last accessed 1 June 2015)

Eskenazy, G. M. Velichkov, D. “Radium in Bulgarian coals” *International Journal of Coal Geology* 94 (2012): 296–301.

European Commission. “Radiological Protection Principles Concerning the Natural Radioactivity of Building Materials.” Radiation Protection Report No. 112, Luxemburg (1999): 16.

Fabbrizio, A. Schmidt, M. W. Günther, D. Eikenberg, J. “Experimental Determination of Radium Partitioning between Leucite and Phonolite Melt and ^{226}Ra-Disequilibrium Crystallization Ages of Leucite.” *Chemical Geology* 255 (2008): 377–387.

Fehér, I. Deme, S. “Sugárvédelem” (in Hungarian) ELTE Eötvös Kiadó (2010): 576.

Ferreira da Silva, E. Zhang, C. Pinto, L.S. Patinha, C. Reis, P. “Hazard Assessment on Arsenic and Lead in Soils of Castromil Gold Mining Area, Portugal.” *Applied Geochemistry* 19 (2004): 887–898.

Ferreira-Baptista, L. De Miguel, E. “Geochemistry and Risk Assessment of Street Dust in Luanda, Angola: A Tropical Urban Environment.” *Atmospheric Environment* 39 (2005): 4501–4512.

Fordyce, F.M. Brown, S.E. Ander, E.L. Rawlins, B.G. O’Donnell, K.E. Lister, T.R. Breward, N. Johnson, C.C. “GSUE: urban geochemical mapping in Great Britain.” *Geochemistry: Exploration Environment Analysis* 4 (2005): 325‑336.

Gajzágó, A. „A salgótarjáni iparvidék.” (In Hungarian) *Nógrád Megyei Munkásmozgalmi Múzeum*, Salgótarján. (1962): 286.

Gáspár, L. “Másodlagos nyersanyagok az útépítésben.” (In Hungarian) *IHU Kht* (2005): 255.

García-Talavera, M. . Laedermann, J. P. Décombaz, M. Daza, M.J. Quintana, B. “Coincidence summing corrections for the natural decay series in γ-ray spectrometry” “Applied Radiation and Isotopes” (2001): 769-776.

Gelencsér, A. Kováts, N. Turóczi, B. Rostási, A. Hoffer, A. Imre, K. Nyiró-Kósa, I. Csákberényi-Malasics, D. Tóth, A. Czitrovszky, A. Nagy, A. Nagy, S. Ács, A. Kovács, A. Ferincz, A. Hartyáni, Z. Pósfai, M. “The red mud accident in Ajka (Hungary): Characterization and potential health effects of fugitive dust.” *Environmental Science and Technology* 45 (2011): 1609-1615.

Glodek, A. Pacyna, J.M. “Mercury emission from coal-fired power plants in Poland” *Atmospheric Environment* 43 (2009): 5668‑5673.

Gilmore, G. R. “Radioactive Decay and the Origin of Gamma and X-Radiation, in Practical Gamma-Ray Spectrometry.” 2nd Edition. John Wiley & Sons, Ltd, Chichester, UK. (2008)

Goodarzi, F. “Morphology and Chemistry of Fine Particles Emitted from a Canadian Coal-Fired Power Plant.” *Fuel* 85 (2006): 273–280.

Goodarzi, F. “Environmental assessment of bottom ash from Canadian coal-fired power plants.” *The Open Environmental & Biological Monitoring Journal* 2 (2009): 1–10.

Gosar, M. Sajn, R. “Mercury in soil and attic dust as a reflection of Idrija mining and mineralization (Slovenia).” *Geologija* 44 (2001): 137‑159. http://www.geologija-revija.si/dokument.aspx?id=688 (Last accessed 01 June 2015)

Gosar, M. Šajn, R. Biester, H. “Binding of Mercury in Soils and Attic Dust in the Idrija Mercury Mine Area (Slovenia).” *Science of the Total Environment* 369 (2006): 150–162.

Gosar, M. Miler, M. “Anthropogenic Metal Loads and Their Sources in Stream Sediments of the Meža River Catchment Area (NE Slovenia).” *Applied Geochemistry* 26 (2011): 1855–1866.

Joint (KvVM-EüM-FVM) Government Decree No 6/2009. Joint Government Decree on the environmental standards for geological materials, B pollution threshold. http://www.complex.hu/jr/gen/hjegy_doc.cgi?docid=A0900006.KVV&kif (Last accessed: 01 June 2015)

Guibas, L. Stolfi, J. “Primitives for the manipulation of general subdivisions and the computation of Voronoi diagrams.” *ACM Trans. Graph.* 4 (1985): 74–123.

Gulson, B. L. Davis, J. J. Mizon, K. J. Korsch, M.J. Bawden-Smith, J. “Sources of lead in soil and dust and the use of dust fallout as a sampling medium.” *Science of the Total Environment* 166 (1995): 245‑262.

Hamilton, E. I. “The relative radioactivity of building materials.” *American Industrial Hygiene Association Journal* 32 (1971): 398-403.

Hedwall, R. Erlandsson, B. “Radioactivity concentrations in non-nuclear industries” *Journal of Environmental Radioactivity* 32 (1996): 19-31

Hensley, A.R. Scott, A. Rosenfeld, P.E. Clark, J.J.J. “Attic Dust and Human Blood Samples Collected near a Former Wood Treatment Facility.” *Environmental Research* 105 (2007): 194–199.

Hiroshi, H. Horie, K. Gauthier-Lafaye, F. “Transport and Selective Uptake of Radium into Natural Clay Minerals.” *Earth and Planetary Science Letters* 264 (2007): 167–176.

Hlawiczka, S. Kubica, K. Zielonka, U. “Partitioning factor of mercury during coal combustion in low capacity domestic heating units.” *Science of the Total Environment* 312 (2003): 261–265.

Hogervorst, J. Plusquin, M. Vangronsveld, J. Nawrot, T. Cuypers, A. Van Hecke, E. Roels, H.A. Carleer, R. Staessen, J. A. “House Dust as Possible Route of Environmental Exposure to Cadmium and Lead in the Adult General Population.” *Environmental Research* 103 (2007): 30–37.

Huang, Y. Jin, B. Zhong, Z. Xiao, R. Tang, Z. Ren, H. “Trace elements (Mn, Cr, Pb, Se, Zn, Cd and Hg) in emissions from a pulverized coal boiler” *Fuel Processing Technology* 86 (2004): 23-32.

Huggins, F. Goodarzi, F. “Environmental assessment of elements and polyaromatic hydrocarbons emitted from a Canadian coal-fired power plant.” *Coal Geology* 77 (2009): 282–288.

Hull, C. D. Burnett, W. C. “Radiochemistry of Florida phosphogypsum” *Journal of Environmental Radioactivity* 32 (1996): 213-238.

Hunt, A. Johnson, D. L. Griffith, D.A. Zitoon, S. “Citywide Distribution of Lead and Other Element in Soils and Indoor Dusts in Syracuse, NY.” *Applied Geochemistry* 27 (2012): 985–994.

Huy, N. Q. Luyen, T. V. “A Method to Determine ^{238}U Activity in Environmental Soil Samples by Using 63.3-keV-Photopeak-Gamma HPGe Spectrometer.” *Applied Radiation and Isotopes* 61 (2004): 1419–1424.

ICRP No. 50. “Lung cancer risk from indoor exposures to radon progeny.” (1987): Pergamon Press, Oxford, New York

ICRP (International Commission on Radiological Protection) “Recommendations of the ICRP.” *ICRP Publication* 60. (1990): Ann. ICRP 21(1-3).

ICRP (International Commission on Radiological Protection) “Low-dose extrapolation of radiation-related cancer risk.” *ICRP Publication* 99. (2005): Ann. ICRP 35(4).

ICRP (International Commission on Radiological Protection) “The 2007 recommendations of the ICRP.” *ICRP Publication* 103. (2007): Ann. ICRP 37(2-4).

ICRP (International Commission on Radiological Protection) “Review, New ICRP recommendations.” *Journal of Radiological Protection* 28, (2008): 161–168.

ICRU (International Commission on Radiation Units and Measurements) (1985) Determination of dose equivalents resulting from external radiation sources. ICRU Report 39. Bethesda.

Ilacqua, V. Freeman, N. C. J. Fagliano, J. Lioy, P. J. “The Historical Record of Air Pollution as Defined by Attic Dust.” *Atmospheric Environment* 37 (2003): 2379–2389.

Jobbágy, V. “NORM Anyagok Radionuklid Koncentrációját És Emanációját Befolyásoló Paraméterek Vizsgálata Építőipari Felhasználhatóság Szempontjából.” (In Hungarian) Pannon Egyetem (2007): 130.

James, A. C. “Lung Dosimetry” (1988): In: Nazaroff, W.W. and Nero, A.V. Jr. (1988): “Radon and its decay products in indoor air” John Wiley & Sons, New York, 518.

Janis v4.0, OECD Nuclear Energy Agency (2013) http://www.oecd-nea.org/janis/. (Last accessed 01 June 2015)

Jia, G. Jia, J. “Determination of Radium Isotopes in Environmental Samples by Gamma Spectrometry, Liquid Scintillation Counting and Alpha Spectrometry: A Review of Analytical Methodology.” *Journal of Environmental Radioactivity* 106 (2012): 98–119.

Johnston, A. Martin, P. “Rapid Analysis of ^{226}Ra in Waters by Gamma-Ray Spectrometry.” *Applied radiation and isotopes : including data, instrumentation and methods for use in agriculture, industry and medicine* 48 (1997): 631–638.

Jordan, G. Szucs, A. Qvarfort, U. Szekely, B. “Evaluation of metal retention in a wetland receiving acid mine drainage.” In: Xie, Xuejin (Ed.), Proceedings, IGC 30, *Geochemistry* 19 (1997): 189–206.

Jostes, R. F. „Genetic, cytogenetic, and carcinogenic effects of radon: a review.” *Mutation research* 340 (1996): 125-139.

Kabata-Pendias, A. “Trace Elements in Soils and Plants” CRC Press (2000): 432.

Karangelos, D. J. Petropoulos N. P. Anagnostakis, M. J. Hinis, E. P. Simopoulos, S. E. “Radiological Characteristics and Investigation of the Radioactive Equilibrium in the Ashes Produced in Lignite-Fired Power Plants.” *Journal of Environmental Radioactivity* 77 (2004): 233–246.

Keith, L.S. Faroon, O. M. Fowler, A. “Uranium” *Handbook on the Toxicology of Metals 3E* (2007): 881-903.

Kis, Z. Völgyesi, P. Szabó, Zs. “DÖME - revitalizing a low-background counting chamber and developing a radon-tight sample holder for gamma-ray spectroscopy measurements.”*Journal of Radioanalytical and Nuclear Chemistry* 298 (2013): 2029-2035.

Kovler, K. Haquin, G. Manasherov, V. Ne’eman, E. Lavi, N. “Natural Radionuclides in Building Materials Available in Israel.” *Building and Environment* 37 (2002): 531–537.

Kozma, K. “Az Ajkai Erőmű Története” (In Hungarian) *Bakonyi Erőmű Rt* (1996): 399.

Köhler, M. Niese, S. Gleisberg, B. Jenk, U. Nindel, K. “Simultaneous Determination of Ra and Th Nuclides, ^{238}U and ^{227}Ac in Uranium Mining Waters by γ-Ray Spectrometry.” *Applied Radiation and Isotopes* 52 (2000): 717–723.

Köteles, Gy. „Radon a környezetünkben” (In Hungarian) *Fizikai szemle* (1994): 6

Kristo, M. J. Tumey, S. J. “The state of nuclear forensic.” *Nuclear Instrumental Methods in Physic ResearchB* 294 (2013): 656-661.

Kumar, V. Ramachandran, T. V. Prasad, R. “Natural radioactivity of Indian building materials and by-products.” *Applied Radiation and Isotopes* 51 (1999): 93-96.

Li, L. Y. “A Study of Iron Mineral Transformation to Reduce Red Mud Tailings.” *Waste Management* 21 (2001): 525–534.

Ljung, K. Selinus, O. Otabbong, E. “Metals in Soils of Children’s Urban Environments in the Small Northern European City of Uppsala.” *Science of the Total Environment* 366 (2006): 749–759.

Lu, X. Li, L. Y. Wang, L. Lei, K. Huang, J. Zhai, Y. “Contamination Assessment of Mercury and Arsenic in Roadway Dust from Baoji, China.” *Atmospheric Environment* 43 (2009a): 2489–2496.

Lu, X. Wang, L., Lei, K., Huang, J., Zhai, Y. “Contamination assessment of copper, lead, zinc, manganese and nickel in street dust of Baoji, NW China.” *Journal of Hazardous Materials* 161 (2009b) 1058–1062.

Lyons, W. B. Harmon, R. S. “Why Urban Geochemistry?” *Elements* 8 (2012): 417–422.

Manolopoulou, M. Stoulos, St, Mironaki, D. Papastefanou, C. “A New Technique for the Accurate Measurement of 226Ra by Gamma Spectroscopy in Voluminous Samples.” *Nuclear Instruments and Methods in Physics Research, Section A: Accelerators, Spectrometers, Detectors and Associated Equipment* 508 (2003): 362–366.

Manolopoulou, M. Papastefanou, C. “Behavior of Natural Radionuclides in Lignites and Fly Ashes.” *Journal of Environmental Radioactivity* 16 (1992): 261–271.

Mann, H. B. Whitney, D. R. “On a test of whether one of two random variables is stochastically larger than the other.” *Ann. Math. Stat.* 18 (1947): 50–60.

Mauring, A. Gäfvert, T. “Radon Tightness of Different Sample Sealing Methods for Gamma Spectrometric Measurements of ^{226}Ra.” *Applied Radiation and Isotopes* 81 (2013): 92–95.

Mavi, B. Akkurt, I. “Natural radioactivity and radiation hazards in some building materials used in Isparta, Turkey.” *Radiat. Physics and Chemistry* 79 (2010): 933-937.

Morawska, L. and Phillips, C.R. "Dependence of the radon emanation coefficient on radium distribution and internal structure of the material." *Geochimica et Cosmochimica Acta* 57 (1993): 1783-1797.

Meyer, I. Heinrich, J. Lippold, U. "Factors Affecting Lead and Cadmium Levels in House Dust in Industrial Areas of Eastern Germany." *The Science of the total environment* 234 (1999): 25–36.

Mielke, H. W. Gonzales, C. R. Smith, M. K. Mielke, P. W. "The urban environment and children's health: Soils as an integrator of lead, zinc, and cadmium in New Orleans, Louisiana, U.S.A." *Environmental Research Section A* 81 (1999): 117‑129.

Moens, L. De Donder, J. Xi-lei, L. De Corte, F. De Wispelaere, A. Simonits, A. Hoste, J. "Calculation of the absolute peak efficiency of gamma-ray detectors for different counting geometries" *Nuclear Instrumental Methods in Physic Research* 187 (1981): 451–472.

Moens, L. De Corte, F. Simonits, A. Xilei, L. De Wispelaere, A. De Donder, J. Hoste, J. "Calculation of the absolut peak efficiency for different counting geometries of Ge and Ge (Li) detectors." *Journal of Radioanalytical and Nuclear Chemistry* 70 (1982): 539–550.

Moharram, B. M. Suliman, M. N. Zahran, N. F. Shennawy, S. E. El Sayed, A. R. "External Exposure Doses due to Gamma Emitting Natural Radionuclides in Some Egyptian Building Materials." *Applied Radiation and Isotopes* 70 (2012): 241–248.

Mølhave, L. Schneider, T. Kjargaard, S. K. Larsen, L. Norn, S. Jorgensen, O. "House Dust in Seven Danish Offices." *Atmospheric Environment* 34 (2000): 4767–4779.

Moura, C. L. Artur, A. C. Bonotto, D. M. Guedes, S. Martinelli, C. D. "Natural radioactivity and radon exhalation rate in Brazilian igneous rocks." *Applied Radiation and Isotopes* 69 (2011): 1094-1099.

Nagy, H É. Breitner, D. Horváth, Á. Szabó, Cs. "Mitteilungen der Österreichischen Mineralogischen Gesellschaft." *Österreichische Mineralogische Gesellschaft* (2009): 109.

Németh, Cs. Somlai, J. Kanyár, B. "Estimation of External Irradiation of Children due to the Use of Coal-Slag as Building Material in Tatabánya, Hungary." *Journal of Environmental Radioactivity* 51 (2000): 371–378.

Nikl, I. "The radon concentration and absorbed dose rate in Hungarian dwellings." *Radiation Protection Dosimetry* 67 (1996): 225–228.

Nuccetelli, C. Pontikes, Y. Leonardi, F. Trevisi, R. "New perspectives and issues arising from the introduction of (NORM) residues in building materials: A critical assessment on the radiological behaviour" *Construction and Building Materials* 82 (2015): 323-331.

Odor, L. Horvath, I. Fugedi, U. "Low-density geochemical survey of Hungary." *Volume of abstracts, Environmental Geochemical Baseline Mapping in Europe Conference, Spisska Nova Ves, Slovakia* (1996): 53‑57.

OECD (Organization for Economic Cooperation and Development), 1979. Exposure to radiation from the natural radioactivity in building materials, Report by a Group of Experts of the OECD Nuclear Energy Agency, Paris

Olszewski, G. Boryło, A. Skwarzec, B. “Uranium (234U, 235U and 238U) contamination of the environment surrounding phosphogypsum waste heap in Wiślinka (northern Poland)”*Journal of Environmental Radioactivity* 146 (2015): 56-66.

Ottesen, R. T.Alexander, J. Langedal, M. Haugland, T. Høygaard, E. “Soil Pollution in Day-Care Centers and Playgrounds in Norway: National Action Plan for Mapping and Remediation.” *Environmental Geochemistry and Health* 30 (2008): 623–637.

Papachristodoulou, C. Assimakopoulos, P. A. Patronis, N.E. Ioannides, K. G. “Use of HPGe γ-Ray Spectrometry to Assess the Isotopic Compositiion of Uranium in Soils.” *Journal of Environmental Radioactivity* 64 (2003): 195–203.

Papastefanou, C. “Escaping radioactivity from coal-fired power plants (CPPs) due to coal burning and the associated hazards: A Review.” *Journal of Environmental Radioactivity* 101 (2010): 191–200.

Papp, Z. Dezső, Z. Daróczy, S. “Measurement of the Radioactivity of ^{238}U, ^{232}Th, ^{226}Ra, ^{137}Cs and ^{40}K in Soil Using Direct Ge(Li) γ-Ray Spectrometry.” *Journal of Radioanalytical and Nuclear Chemistry* 222 (1997): 171–176.

Papp, Z. Dezső, Z. Daroczy, S. “Significant radioactive contamination of soil around a coal-fired thermal power plant.” *Journal of Environmental Radioactivity* 59 (2002): 191‑205.

Pearson, K. “Mathematical contributions to the theory of evolution, III: Regression, heredity and pan- mixia.” *Philosophical Transactionsof the Royoyal Society London* (A) 187 (1896): 253–318.

Porstendörfer, J. “Properties and behaviour of radon and thoron and their decay products in the air.” *Journal of Aerosol Science* 25 (1994): 219–263.

Quispe, D. Pérez-López, R. Silva, L. F. O. Nieto, J. M. “Changes in Mobility of Hazardous Elements during Coal Combustion in Santa Catarina Power Plant (Brazil).” *Fuel* 94 (2012): 495–503.

Reimann, C. Filzmoser, P. Garrett, R.G. Dutter, R. “Statistical Data Analysis Explained: Applied Environmental Statistics with R.” *John Wiley & Sons* (2008): 343.

Révay, Z. Belgya, T. Molnár, G. L. “Application of Hypermet-Pc in Pgaa, Journal of Radioanalytical and Nuclear Chemistry” *Journal of Radioanalytical and Nuclear Chemistry* 265 (2005): 261–265.

Rosholt, J.N. “Open System model for uranium-series dating of Pleistocene samples.” *Analytical Chemistry* 29 (1957): 1398.

Rzeczypospolitej Polskiej (Republic of Poland), 29. Rozporzadzenie Rady Ministrów (29th Ministerial Regulation, in Polish), Dziennik Ustaw, 4 (2007): 137-139.

Sadiq, M. “Arsenic chemistry in soils: an overview of thermodynamic predictions and field observations.” *Water Air Soil Pollution* 93 (1997): 117‑136.

Saeedi, M. Li, L. Y. Salmanzadeh, M. “Heavy Metals and Polycyclic Aromatic Hydrocarbons: Pollution and Ecological Risk Assessment in Street Dust of Tehran.” *Journal of Hazardous Materials* 227-228 (2012): 9–17.

Sajn, R. Gosar, M. Bidovec, M. “Geochemical properties of soil, overbank sediment, household and attic dust in Mezica area (Slovenia).” *Geologija* 43 (2000): 235‑245. http://www.geologija-revija.si/dokument.aspx?id=729 (Last accessed 1 June 2015)

Sajn, R. “Geochemical research of soil and attic dust in Celje area (Slovenia).” *Geologija* 44 (2001): 351‑362. http://www.geologija-revija.si/dokument.aspx?id=706 (Last accessed 1 June 2015)

Sajn, R. “Influence of mining and metallurgy on chemical composition of soil and attic dust in Meža valley. Slovenia.” *Geologija* 45 (2002): 547–552.

Sajn, R. “Using Attic Dust and Soil for the Separation of Anthropogenicand Geogenic Elemental Distributions in an Old Metallurgic Area (Celje, Slovenia).” *Geochemistry: Exploration, Environment, Analysis* 5 (2005): 59–67.

Sajn, R. “Factor Analysis of Soil and Attic-Dust to Separate Mining and Metallurgy Influence, Meza Valley, Slovenia.” *Mathematical Geology* 38 (2006): 735–747.

Sakoda, A. Hanamoto, K. Ishimori, Y. Nagamatsu, T. Yamaoka, K. “Radioactivity and radon emanation fraction of the granites sampled at Misasa and Badgastein.” *Applied Radiation and Isotopes* 66 (2008): 648–652.

Sakoda, A. Nishiyama, Y. Hanamoto, K. Ishimori, Y. Yamamoto, Y. Kataoka, T. Kawabe, A. Yamaoka, K. “Differences of natural radioactivity and radon emanation fraction among constituent minerals of rock or soil.” *Applied Radiation and Isotopes* 68 (2010): 1180-1184.

Salminen, R., (Chief-editor), Batista, M.J., Bidovec, M., Demetriades, A., De Vivo, B., De Vos, W., Duris, M., Gilucis, A., Gregorauskiene, V., Halamic, J., Heitzmann, P., Lima, A., Jordan, G., Klaver, G., Klein, P., Lis, J., Locutura, J., Marsina, K., Mazreku, A., OConnor, P.J., Olsson, S.A., Ottesen, R.T., Petersell, V., Plant, J.A., Reeder, S., Salpeteur, I., Sandstrom, H., Siewers, U., Steenfelt, A., Tarvainen, T., 2005. FOREGS Global Geochemical Baselines Programme. Geochemical Atlas of Europe. <http://weppi.gtk.fi/publ/foregsatlas>.

Sammut, M.L. Rose, J. Masion, A. Fiani, E. Depoux, M. Ziebel, A. Hazemann, J.L. Proux, O. Borschneck, D. Noack, Y. “Determination of zinc speciation in basic oxygen furnace flying dust by chemical extractions and X-ray spectroscopy.” *Chemosphere* 70 (2008): 1945‑1951.

Sammut, M. L. Noack, Y. Rose, J. Hazemann, J. L. Proux, O. Depoux, M. Ziebel, A. Fiani, E. “Speciation of Cd and Pb in Dust Emitted from Sinter Plant.” *Chemosphere* 78 (2010): 445–450.

Sharaf, J. M. Hamideen, M. S. “Measurement of Natural Radioactivity in Jordanian Building Materials and Their Contribution to the Public Indoor Gamma Dose Rate.” *Applied Radiation and Isotopes* 80 (2013): 61–66.

Sas, Z. Somlai, J. Szeiler, G. Kovács, T. “Radon emanation and exhalation characteristic of heat-treated clay samples.” *Radiation Protection Dosimetry* 152 (2012): 51–54.

Schmidt, S. Cochran, J. K. “Radium and radium-daughter nuclides in carbonates: a brief overviewof strategies for determining chronologies.” *Journal of Environmental Radioactivity* 101 (2010): 530-537.

Shah, P. Streezov, V. Prince, K. Nelson, P.F. “Speciation of As, Cr, Se, and Hg under coal fired power station conditions.” *Fuel* 87 (2008): 1859–1869.

Siddique, R. “Utilization of Coal Combustion by-Products in Sustainable Construction Materials.” *Resources, Conservation and Recycling* 54 (2010): 1060–1066

Siegel, F.R. “Environmental Geochemistry of Potentially Toxic Metals.” Springer-Verlag, Berlin, Heidelberg. (2002) 218.

Somlai, J. Kanyár, B. Bodnár, R. Németh, Cs. Lendvai, Z. “Radiation Dose Contribution from Coal-Slags Used as Structural Building Material.” *Journal of Radioanalytical and Nuclear Chemistry* 207 (1996): 437–443.

Somlai, J. Németh, Cs, Lendvai, Z. Bodnár, R. “Dose Contribution from School Buildings Containing Coal Slag Insulation with Elevated Concentrations of Natural Radionuclides.” *Journal of Radioanalytical and Nuclear Chemistry* 218 (1997): 61–63.

Somlai, J. Horváth, M. Kanyár, B. Lendvai, Z. Németh, Cs. “Radiation hazard of coal-slags as building material in Tatabánya town (Hungary).” *Health Physics* 75 (1998): 648–651.

Somlai, J. Jobbágy, V. Németh, Cs. Gorjánácz, Z. Kávási, N. Kovács, T. “Radiation Dose from Coal Slag Used as Building Material in the Transdanubian Region of Hungary.” *Radiation Protection Dosimetry* 118 (2006): 82–87.

Sysalova, J. Szakova, J. “Mobility Assessment and Validation of Toxic Elements in Tunnel Dust Samples-Subway and Road Using Sequential Chemical Extraction and ICP-OES/GF AAS Measurements.” *Environmental Research* 101 (2006): 287–293.

Szabó, Zs. Völgyesi, P. Nagy, H. É. Szabó, Cs. Kis, Z. Csorba, O. “Radioactivity of natural and artificial building materials – a comparative study.” *Journal of Environmental Radioactivity* 118 (2013): 64-74.

Szabó, Zs. “Terrestrial radioactivity in Hungarian adobe building material and dwellings with a focus on thoron (^{220}Rn).” PhD Thesis. EötvösUniversity, Lithosphere Fluid Research Laboratory (2014): 128.

Szerbin, P. “Radon a Rudas-fürdő légterében.” *Fizikai Szemle* 6 (1994): 241.

Tadmor, J. “Radioactivity From Coal-Fired Power Plants: A Review” *Journal of Environmental Radioactivity* 4 (1986): 177–204.

Takeno, N. “Atlas of Eh-pH Diagrams. Intercomparison of thermodynamic databases.” *Open File Report No. 419. Geological Survey of Japan* (2005): 285.

Tanner, A. B “Radon migration in the ground: a review.” (1964): 161–190. In: Adams, J.A.S., Lowder, W.M. “The natural radiation environment” University of Chicago Press, Chicago.

Tanner, A. B. “Radon migration in the ground: supplementary review.” (1980): 5–56. In: Gesell, T.F., Lowder, W.M. “Proceedings natural radiation environment III,” National Technical Information Service, Washington

Thermo Scientific (2007) The modular system for radioactivity measurements, FH 40 G/GL Digital Survey Meter and FHT 6020 Display Unit. Thermo Scientific, 16 pages (http://www.thermo.com/eThermo/CMA/PDFs/Product/productPDF_2635.pdf). (Last accessed 1 June 2015)

Thornton, I. "Metal Contamination of Soils in Urban Areas." *Soils in the Urban Environment"*. Ed. P. Bullock and P.J. Gregory. British Society of Soil Science. Blackwell Scientific Publications, Oxford, 1991.

Trevisi, R. Risica, S. D'Alessandro, M. Paradiso, D. Nuccetelli, C. "Natural Radioactivity in Building Materials in the European Union: A Database and an Estimate of Radiological Significance." *Journal of Environmental Radioactivity* 105 (2012): 11–20.

Tukey, J.W. Exploratory Data Analysis. (1977) Addison-Wesley.

Tye, M. Hodgkinson, E. S. Rawlins, B. G. "Microscopic and Chemical Studies of Metal Particulates in Tree Bark and Attic Dust: Evidence for Historical Atmospheric Smelter Emissions, Humberside, UK." *Journal of environmental monitoring* 8 (2006): 904–912.

Unscear. "Exposures from Natural Radiation Sources." (2000): 84–141.

UNSCEAR (United Nations Scientific Committee on the Effects of Atomic Radiation), "Annex B, exposures from natural radiation sources. In: Sources and Effects of Ionizing Radiation, Report to the General Assembly with Scientific Annexes. UNSCEAR, New York" (2000): 83-156.

Vidmar T "EFFTRAN – A Monte Carlo efficiency transfer code for gamma-ray spectrometry" *Nuclear Instruments and Methods in Physics Research* 550 (2005): 603–608.

Vidmar, T. Kanisch, G. Vidmar, G. "Calculation of true coincidence summing corrections for extended sources with EFFTRAN" *Applied Radiation and Isotopes* 69 (2011): 908–911.

Völgyesi, P. Kis, Z. Szabó, Zs. Szabo, Cs. "Using the 186-keV Peak for ^{226}Ra Activity concentration determination in Hungarian coal-slag samples by gamma-ray spectroscopy." *Journal of Radioanalytical and Nuclear Chemistry* 302 (2014a): 375–383.

Völgyesi, P. Jordan, G. Zacháry, D. Szabó, Cs. Bartha, A. Matschullat, J. "Attic dust reflects long-term airborne contamination of an industrial area: A case study from Ajka, Hungary." *Applied Geochemistry* 46 (2014b): 19-29.

Wong, C. S. C, Li, X. Thornton, I. "Urban Environmental Geochemistry of Trace Metals." *Environmental Pollution* 142 (2006): 1–16.

Yudovich, Y.E. Ketris, M.P. "Arsenic in coal: a rewiev." *International Journal of Coal Geology* 61 (2005): 141–196.

Yücel, H. Solmaz, A.N. Köse, E Bor, D. "Spectral interference corrections for the measurement of ^{238}U in materials rich in thorium by a high resolution γ-ray spectrometry" *Applied Radiation and Isotopes* 67 (2009): 2049-2056.

Zacháry, D. Jordan, G. Szabó, Cs. "Geochemical study of urban soils in public areas of an industrialized town (Ajka, Western Hungary)." *Geophysical Research Abstracts* 14 (2012): EGU 2012-4762.

Zacháry, D. Jordan, G. Völgyesi, P. Bartha, A. Szabó, Cs. “Urban geochemical mapping for spatial risk assessment of multisource potentially toxic elements - a case study in city of Ajka, Hungary” *Journal of Geochemical Exploration* (submitted)

Zhang, C. Qiao, Q. Appel, E. Huang, B. “Discriminating Sources of Anthropogenic Heavy Metals in Urban Street Dusts Using Magnetic and Chemical Methods.” *Journal of Geochemical Exploration* 119-120 (2012): 60–75.

Zheng, N. Liu, J. Wang, Q. Liang, Z. “Heavy Metals Exposure of Children from Stairway and Sidewalk Dust in the Smelting District, Northeast of China.” *Atmospheric Environment* 44 (2010): 3239–3245.

Žibret, G. “Organic compounds in the urban dusts in Celje area.” *Geologija* 56 (2013): 087‑096. http://www.geologija-revija.si/dokument.aspx?id=1175 (Last accessed 15 July 2015)

Weblinks (Last accessed 15 July 2015):

Link 1: http://research.science.mq.edu.au/u-series-research-group/ADosseto/research.html

Link 2: https://www.flickr.com/photos/mitopencourseware/3707241882

Link 3: http://www.tankonyvtar.hu/hu/tartalom/tamop412A/2010-0017_60_magfizika/ch03s03.html

Link 4: http://rad-decay.software.informer.com/

Link 5: http://www.betonopus.hu/notesz/fogalomtar/12-gazbeton/12-gazbeton.htm

Link 6: (Webpage of the Hungarian Meterological Service):

http://www.met.hu/en/eghajlat/magyarorszag_eghajlata/altalanos_eghajlati_jellemzes/szel/

Link 7: http://english.mal.hu/Engine.aspx

Link 8: http://atomfizika.elte.hu/muszerek/hpge/Detektor/

Link 9: http://atomfizika.elte.hu/muszerek/index.php?oldal=9

Link 10: (NuDat database, Brookhaven National Laboratory) http://www.nndc.bnl.gov/

Link 11: http://www.worldcoal.org/

Appendices

Appendix 1. Back diffusion of radon in a sample (Tanner, 1980)

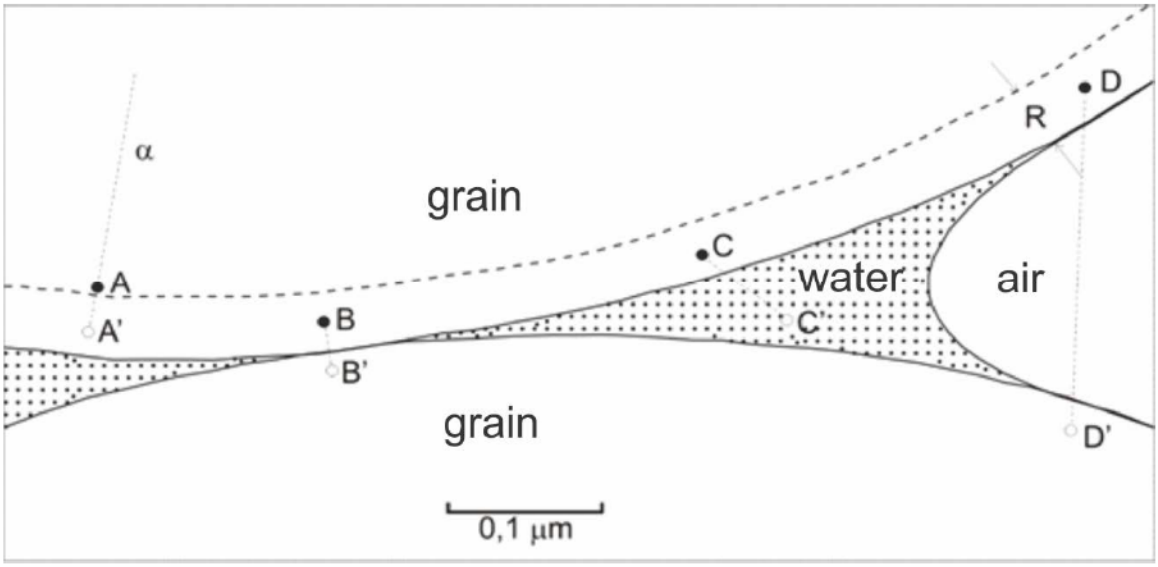

(A = recoiling Rn does not escape host grain: B = recoil directly into adjacent grain; C = recoil into water, leaving Rn in pore space /direct-recoil/: D = recoil into air, leaving Rn embedded in adjacent grain /indirect-recoil/)

Appendix 2. Main properties of Arsenic. Most of the data were summarized based on the database published by Salminen et al. (2005) and references therein.

Element	As
Atomic number	33
Main oxidation states	-3, +3, +5
Stable isotope	^{75}As
Geochemical property	Chalcophile
Main minerals	arsenopyrite (FeAsS), realgar (AsS), orpiment (As_2S_3)
Median upper continental crust (mg kg $^{-1}$)	4.8
Median topsoil (mg kg $^{-1}$)	7.03
Chemistry	Arsenic minerals and compounds are soluble in water, but As migration is limited due to strong sorption by hydroxides, clays and organic matter. The main control of both As^{3+} and As^{+5} solubility in soils is sorption to Fe (oxy) hydroxides. Arsenite (As^{3+}) is more toxic and mobile in soils than arsenate (As^{5+}). In aerobic mineral soils, As is primarily associated with iron (oxy) hydroxides, whereas As sulphide minerals may precipitate in anaerobic conditions.
Anthropogenic sources	Coal combustion, geothermal power plants, smelting, use of arsenical sprays, and pig and poultry sewage. At least 60% of the atmospheric global inputs of As are derived from natural sources.
Health	Essential for some organisms, *e.g.* 12 to 25 µg per day is required by humans, but is toxic depending on its valency and speciation. Chronic exposure increases the risk of cancer and skin pigmentation.
Notes	Global production of As was estimated as 53.5 kt in 2008. Arsenic concentration in soils, contaminated by industrial activities, may reach several percent. Large-scale risks to ecosystems and human health arise not only from industrial activities, but more recently also from the use of As-contaminated water as a source of drinking water, as in Hungary and e.g. Southeastern Asia and Latin America (Abejón and Garea, 2015)

Appendix 3. Main properties of Cadmium. Most of the data were summarized based on the database published by Salminen et al. (2005) and references therein.

Element	Cd
Atomic number	48
Main oxidation state	+2
Stable isotopes	^{106}Cd, ^{108}Cd, ^{110}Cd, ^{111}Cd, ^{112}Cd, ^{113}Cd, ^{114}Cd, ^{116}Cd
Geochemical property	Chalcophile
Main minerals	greenockite (CdS), octavite (CdCO3), monteponite (CdO)
Median upper continental crust (mg kg $^{-1}$)	0.09
Median topsoil (mg kg $^{-1}$)	0.15
Chemistry	In surface environments, Cd is most mobile under oxidising conditions at pH levels below 8. Cadmium in soils is almost invariably present in soil in the Cd^{2+} oxidation state. In all soil types, Cd activity is strongly affected by pH; it is more mobile in acidic soil within the pH range of 4.5 to 5.5, and organic matter and sesquioxides largely control its solubility. In addition, Cd forms complexes in solution with halides, cyanides and ammonium species.
Anthropogenic sources	Electroplating and battery, paint, ink and plastic manufacture, P-fertilizers, sewage sludge, Cd mining, production, use and disposal.
Health	Cadmium has no essential biological function, it is toxic to humans through the inhalation of dust, causing lung damage, and may cause cancer from long-term exposure; it is also teratogenic and embryocidal. The maximum tolerable intake of Cd is regarded as 25 μg kg^{-1} $month^{-1}$ of body weight. The chronic Cd intoxication induced tubular dysfunction of the kidney, leading to increased excretion of Ca and of low molecular weight proteins and finally to osteomalacia (softening of the bones).
Notes	The global production of Cd was 20.8 kt and world annual consumption was about 18 kt in 2008. Diffuse Cd sources, notably P-fertilizers and atmospheric depositions have increased soil Cd concentrations by about 0.1–0.3 mg Cd kg^{-1} above pre-industrial levels and actions have been taken worldwide to limit Cd emissions or Cd exposure to humans. Emissions of Zn–Cd smelters have been cut in numerous places but residual soil Cd contamination is still present.

Appendix 4. Main properties of Copper. Most of the data were summarized based on the database published by Salminen et al. (2005) and references therein.

Element	Cu
Atomic number	29
Main oxidation states	+1, +2
Stable isotopes	^{63}Cu, ^{65}Cu
Geochemical property	Chalcophile
Main minerals	chalcopyrite ($CuFeS_2$), covellite (CuS), malachite ($Cu_2CO_3(OH)_2$), native copper
Median upper continental crust (mg kg $^{-1}$)	28
Median topsoil (mg kg $^{-1}$)	13
Chemistry	Copper is mobile under oxidizing, acidic conditions, especially at pH values in the range 5.0 to 6.0. Copper mainly occurs in its divalent state (Cu^{2+}) and has high affinity for binding to organic matter. The solid-liquid partitioning of Cu in soil is largely controlled by the soil pH and organic matter content. Except for acidic soils, most (>90%) of the dissolved Cu in soil is complexed with dissolved organic matter.
Anthropogenic sources	Copper mining and smelting, the electrical industry, agriculture, sewage sludge, fertilizers, pesticides, steel works, traffic: trail transport (corrosion of overhead wires) and road transport (brake and tire wear).
Health	Copper is an important essential element for all living organisms, humans can tolerate levels up to 12 mg per day, and deficiency in plants and ruminants occur in soils with low available Cu. The recommended daily intake of Cu for humans is 1–2 mg Cu per day. Elevated soil Cu concentrations cause toxic effects in all terrestrial organisms (plants, invertebrates and micro-organisms).
Notes	World Cu production was 15.7 Mt in 2008, and the total global demand for Cu in 2007 was approximately 24 Mt. More than 95% of all Cu ever mined and smelted has been extracted since 1900.The widespread use of Cu has resulted in significant anthropogenic inputs to topsoils through atmospheric deposition and agricultural practices (fertilizers, pesticides, sewage sludge etc.).

Appendix 5. Main properties of Mercury. Most of the data were summarized based on the database published by Salminen et al. (2005) and references therein.

Element	Hg
Atomic number	80
Main oxidation states	+1, +2
Stable isotopes	^{196}Hg, ^{198}Hg, ^{199}Hg, ^{200}Hg, ^{201}Hg, ^{202}Hg, ^{204}Hg
Geochemical property	Chalcophile
Main minerals	cinnabar (HgS), cordeorite ($Hg_3S_2Cl_2$), livingstonite ($HgSb_4S_8$), native mercury
Median upper continental crust (mg kg $^{-1}$)	0.05
Median topsoil (mg kg $^{-1}$)	0.037
Chemistry	Mercury occurs in natural water in several forms including elemental Hg (Hg^0), which is rare in unpolluted waters, ionic Hg (Hg^+ and Hg^{2+}) and methylated Hg (CH_3Hg^+, CH_3Hg). In soils, Hg occurs as various forms of Hg^{2+}, generally strongly bound to organic matter and sulphides. The Hg content is generally higher in organic-rich soils than in mineral soils.
Anthropogenic sources	Main anthropogenic sources are fossil fuel combustion, mining, cement production, smelting and solid waste combustion.
Health	All chemical forms of Hg are toxic to humans and animals, methyl Hg in particular. Chronic exposure to dietary methylmercury and Hg vapour leads to the typical neurotoxic symptoms associated with Hg poisoning, including disruption of the nervous system, damage to brain functions, DNA and chromosomal damage and negative reproductive effects, such as sperm damage, birth defects and miscarriages.
Notes	The global annual Hg production in 2008 was 0.95 kt. The extensive use of Hg has resulted in significant contamination of soils locally and regionally and sometimes to human and animal exposure at toxic levels. Human use of Hg started already in antiquity and reached a maximum around 1975. Since then the major applications have been strongly reduced in many countries.

Appendix 6. Main properties of Nickel. Most of the data were summarized based on the database published by Salminen et al. (2005) and references therein.

Element	Ni
Atomic number	28
Main oxidation states	+2, +3
Stable isotopes	^{58}Ni, ^{60}Ni, ^{61}Ni, ^{62}Ni, ^{64}Ni
Geochemical property	Siderophile
Main minerals	pentlandite (Ni, Fe)$_9$S$_8$, nickeline (NiAs), ullmannite (NiSbS)
Median upper continental crust (mg kg $^{-1}$)	47
Median topsoil (mg kg $^{-1}$)	18
Chemistry	In natural water, Ni may exist in one of three oxidation states (+2, +3 and +4), although the free ion Ni predominates. In soil, Ni is strongly related to Mn and Fe oxides but, especially in surface soil horizons, occurs mainly in organically bound forms. Nickel is highly mobile under acidic, oxidizing conditions.
Anthropogenic sources	Fertilizers, steel works, metal plating and coinage, fuel combustion and detergents.
Health	Nickel is essential in certain bacteria, plants, and domestic animals, however, whether it is essential for humans is still not very clear and the toxicity and carcinogenicity of high doses of Ni are well documented. The World Health Organisation recommends a daily intake of 10 μg for humans. Nickel deficiency retards growth and impairs iron uptake. Extreme excesses of Ni are both toxic, causing dermatitis and gastric irritation, and carcinogenic illnesses.
Notes	Global Ni production was estimated to be 1.614 Mt in 2008. In recent decades, the large release of Cr and Ni by industrial activities, mainly the manufacture of stainless steel, as well as the use of sewage sludge as soil amendment in agricultural soils, have caused an impressive increase in the levels of these two metals in the pedosphere and other environmental matrices.

Appendix 7. Main properties of Lead. Most of the data were summarized based on the database published by Salminen et al. (2005) and references therein.

Element	Pb
Atomic number	82
Main oxidation states	+2, +4
Stable isotopes	^{204}Pb, ^{206}Pb, ^{207}Pb, ^{208}Pb
Geochemical property	Chalcophile
Main minerals	galena (PbS), anglesite ($PbSO_4$), cerussite ($PbCO_3$)
Median upper continental crust (mg kg $^{-1}$)	17
Median topsoil (mg kg $^{-1}$)	22.6
Chemistry	Lead is generally present in the aqueous environment as Pb^{2+} below pH 6, but it also forms complexes with organic anions, chloride and hydroxide, and insoluble or poorly soluble compounds with sulphide, sulphate, hydroxy carbonate and phosphate anions. Natural lead is particularly strongly bound to humic matter in organic-rich soil and to iron oxides in mineral soil, and is rather immobile in the soil unless present at very high concentrations.
Anthropogenic sources	Vehicle exhausts (tetraethyl Pb), metalliferous mining (especially sulphide ores), metallic detritus, Pb-bearing glass and pottery glazes, batteries, old lead-based paints, the corrosion of lead pipes in areas of soft water and sewage sludge.
Health	Lead is neither essential nor beneficial for any living organism. It can cause mental impairment in young children, causing neuropathy and hypertension in adults and may be lethal at high levels, *e.g.*over 25 μg kg^{-1} of body weight.
Notes	The global production of Pb in 2008 was 3.8 Mt. The global atmospheric Pb-emission at the end of the last century was estimated as 332 kt year^{-1}. Lead is a particularly dangerous element, as it can accumulate in individual organisms, but also in entire food chains. Lead is among the elements that have been most extensively used by man over time. This has led to extensive pollution of surface soils on the local scale, mainly associated with mining and smelting of the metal and addition of organic Pb compounds to petrol. Soil is an important pathway of human lead exposure, in particular to children engaged in hand-to mouth and pica behavior.

Appendix 8. Main properties of Zinc. Most of the data were summarized based on the database published by Salminen et al. (2005) and references therein.

Element	Zn
Atomic number	30
Main oxidation state	+2
Stable isotopes	^{64}Zn, ^{66}Zn, ^{67}Zn, ^{68}Zn, ^{70}Zn
Geochemical property	Chalcophile
Main minerals	Sphalerite (ZnS), smithsonite ($ZnCO_3$), zincite (ZnO)
Median upper continental crust (mg kg $^{-1}$)	67
Median topsoil (mg kg $^{-1}$)	52
Chemistry	Zinc mobility in the environment is the greatest under oxidizing, acidic conditions and more restricted under reducing conditions. Zinc is mostly present in the +2 oxidation state in soil. Although Zn is very mobile in most soils, clay fractions and soil organic material are capable of holding Zn quite strongly, especially in neutral and alkaline pH regimes.
Anthropogenic sources	Mining, coal and waste combustion, and steel processing. A major use of Zn is as an anti-corrosion coating. It is also used as a constituent of brass, as a white pigment (ZnO) in paint and rubber products, and in the manufacture of dry batteries.
Health	Zinc is an essential trace element for humans, animals and higher plants. A recommended intake of 11.4 mg per day is suggested for adults. Symptoms of deficiency include growth retardation, dermatitis and slow wound healing, defective immune system and, in extreme cases, birth defects. In general, Zn toxicity is not so much a problem as deficiency, although excess Zn can still cause health problems such as stomach cramps, skin irritations.
Notes	Global production of Zn in 2008 was 11.3 Mt. The world's Zn production is still rising, and industrial applications tend to disperse Zn widely in the natural environment, leading to levels above pre-industrial concentrations in air, soil and water.

Appendix 9. Attic dust field sheet

Attic Dust Field Sheet

ATTIC DUST ID _____ Date _____ Time _____ Sampler _____
Country _____ Organization _____

SAMPLE SITE LOCATION REGION _____ MAP SHEET _____
COORDINATES
National grid Easting _____ Northing _____
Decimal Degrees Longitude _____ Latitude _____
Altitude (m) _____

SAMPLING CONDITIONS (ATTIC)
Roof Type Slate □ Tile □ Corrugated Iron □ Asbestos □ Other _____
Sampling Surface Concrete beam □ Wood beam □ Fiberglass Envelope □ Floor □ Air Conditioner □ Corner □ Area in proximity of a vent □ Other _____
Mass of the sample _____ Number of sub-samples __ Location of sub-samples _____
Description of the sample _____
Notes _____

HOUSE CHARACTERISTICS
Type of the House Detached □ Semi-detached □ Terraced house □ Condominium □ Other ___
Construction Materials Wood □ Cement □ Brick □ Slag □ Ytong □ Other _____
Date of Construction _____
History of Renovations _____
House orientation _____
Condition of paint _____

SURROUNDINGS

Near-site
Garden condition grass □ cultivated □ non-cultivated □ tractors, oil □ Other _____
Local Development History _____

Far-site
Wind Direction _____
Surrounding Industry _____
Landscape _____
Land use Agriculture □ specify crop _____ Pasture, grassland, fallow field □ Wetland □
Forest: Deciduous □ Coniferous □ Mixed □ Non-cultivated, moorland, etc. □ Parkland □ Other □

GAMMA RADIATION (ATTIC) Total _____
Instrument _____

NOTES _____

SKETCHES:

Appendix 10. The nuclear data of the γ-rays used in the calculations

Energy_lit (keV)	Nuclide	Intensity (γ/100 decays)	Unc_abs intensity	Spectral interference	Chain 2	Branching in chain 2	Intensity (γ/100 decays)	Unc_abs intensity	Comments
186.211	^{226}Ra	3.55	0.019	^{235}U	^{235}U	1	57.2	0.3	two decay chains: ^{238}U, ^{235}U
241.997	^{214}Pb	7.27	0.022	no or negl.					
295.224	^{214}Pb	18.4	0.036	^{210}Tl	^{238}U	0.0004	79	10	secular eq. supposed
351.932	^{214}Pb	35.6	0.07	^{211}Bi	^{235}U	1	13	0.19	two decay chains: ^{238}U, ^{235}U
609.312	^{214}Bi	45.5	0.19	no or negl.					
665.453	^{214}Bi	1.53	0.007	no or negl.					
768.356	^{214}Bi	4.89	0.016	no or negl.					
806.174	^{214}Bi	1.26	0.006	no or negl.					
934.061	^{214}Bi	3.10	0.01	no or negl.					
1001.026	^{234m}Pa	0.847	0.008	no or negl.					
1120.287	^{214}Bi	14.9	0.03	no or negl.					
1155.190	^{214}Bi	1.64	0.007	no or negl.					
1238.110	^{214}Bi	5.83	0.014	no or negl.					
1280.960	^{214}Bi	1.44	0.006	no or negl.					
1377.669	^{214}Bi	3.97	0.011	no or negl.					
1401.500	^{214}Bi	1.33	0.007	no or negl.					
1407.980	^{214}Bi	2.39	0.008	no or negl.					
1509.228	^{214}Bi	2.13	0.01	no or negl.					
1661.280	^{214}Bi	1.05	0.009	no or negl.					
1729.595	^{214}Bi	2.84	0.01	no or negl.					
1764.494	^{214}Bi	15.3	0.05	no or negl.					
1847.420	^{214}Bi	2.03	0.012	no or negl.					
2118.550	^{214}Bi	1.158	0.005	no or negl.					
2204.210	^{214}Bi	4.913	0.023	no or negl.					
2447.860	^{214}Bi	1.548	0.007	no or negl.					

Energy_lit: Literature value of energy
Unc_abs: Uncertainty of the absolute intensity
negl: negligible
eq: equilibrium

Appendix 11. Major and toxic element concentrations in the studied attic dust samples

		Toxic elements (mg/kg)							Major elements (g/kg)		
		As	**Cd**	**Cu**	**Hg**	**Ni**	**Pb**	**Zn**	**Fe**	**Ca**	**S**
Attic dust	**1**	11.5	0.531	41.6	0.076	17.5	42.9	199	25.2	78.3	29.0
	2	16	0.691	27.1	0.648	19.1	61.4	147	12.7	76.4	80.7
	3	9.96	0.383	14.1	0.058	12.1	50.3	179	9.89	46.4	47.6
	4	16.4	1.15	38.1	0.611	27.1	88.1	261	17.3	65.5	54.2
	5	12.8	1.09	31.3	0.66	17.8	85.2	200	15.3	68.5	39.3
	6	14.7	1.80	128	0.249	32.6	130	422	18.9	65.9	15.8
	7	14.3	1.54	65.0	0.306	23.4	178	326	17.8	48.8	20.6
	8	19.4	0.565	28.8	0.524	22.5	58.2	92.7	16.2	84.6	58.4
	9	21.7	0.437	29.0	0.775	26.3	56.2	90.2	26.2	87.0	57.8
	10	10.1	1.64	48.7	0.565	22.3	100	276	15.7	93.2	50.8
	11	10.3	1.3	48.5	0.29	30.8	118	364	22.5	105	15.9
	12	15.0	4.6	40.5	0.179	43.1	107	309	23.6	73.6	14.0
	13	13.3	1.51	47.7	0.236	25.5	88.8	174	19.6	73.5	47.0
	14	15.4	0.846	40.4	0.574	25.1	57.4	114	21.0	70.8	26.2
	15	10.7	1.51	42.7	0.089	21.5	205	323	13.9	61.8	12.9
	16	19.4	2.02	50.0	0.328	26.4	166	746	23.2	81.6	50.6
	17	17.1	11.7	63.4	0.125	28.2	425	760	23.6	86.2	30.6
	18	15.0	2.66	98.4	0.229	23.9	231	919	21.3	57.3	23.0
	19	34.5	1.62	32.5	0.340	17.0	38.8	588	11.0	117	89.4
	20	15.1	0.984	42.2	0.685	14.3	42.5	159	12.9	50.7	19.0
	21	10.4	1.08	31.5	0.945	13.8	54.3	307	14.5	47.0	19.6
	22	18.4	0.628	31.5	0.488	20.0	96.1	113	14.2	93.5	52.3
	23	7.02	1.11	49.7	1.97	15.8	81.0	202	7.93	69.8	55.1
	24	9.79	1.33	63.9	0.791	24.2	71.2	857	23.0	131	35.1
	25	18.4	1.76	44.0	0.631	37.5	84.1	251	29.2	142	41.8
	26	28.9	1.61	38.2	0.184	38.4	881	404	27.4	114	29.6
	27	13.0	1.67	27.0	0.13	38.6	149	524	21.4	122	41.9
Coal waste dump	**1**	10.2	0.137	10.7	0.080	17.5	4.52	11.0	12.2	120	27.9
	2	3.08	0.077	5.79	0.559	8.75	2.94	8.06	5.71	209	24.9
	3	5.47	0.107	9.27	0.033	18.2	5.38	21.9	12.3	161	39.5
Waste heap of PP	**1**	9.22	0.217	26.1	0.004	52.5	7.64	24.3	36.3	150	12.6
	2	8.25	0.144	18.1	0.002	35.1	6.64	13.7	23.9	161	13.4
	3	12.5	0.234	20.0	0.002	37.6	11.1	20.0	26.0	177	16.3
	4	13.3	0.26	22.3	0.003	39.8	11.2	27.8	24.9	188	15.8
Red mud	**1**	88.0	0.825	54.4	1.84	210	116	114	199	64.2	10.6
	2	70.7	0.585	38.3	0.737	127	87.6	88.1	161	61.8	9.1
	3	78.5	0.865	51.9	1.62	210	117	118	210	57.5	9.38
	4	100	0.813	61.6	2.73	268	147	128	253	50.0	6.67
	5	114	0.944	63.5	2.96	276	154	129	262	51.4	6.24
	6	90.8	0.923	49.3	3.59	227	130	115	217	60.3	5.67
	7	104	0.962	51.3	1.69	220	128	121	219	53.9	7.09
	8	101	1.02	45.6	1.73	220	129	125	204	54.1	7.29
	9	85.6	0.803	39.9	1.08	162	93	104	156	52.2	6.15
	10	97.5	0.961	46.9	1.57	211	120	126	203	54.5	6.43